Early Stage Fouling Effects Prediction for Yacht Design

A grey-box model approach using operational voyage data

MT54035: MT MSc Thesis

By,

M. de Haas (4711378)

FEADSHIP

TUDelft

Early Stage Fouling Effects Prediction for Yacht Design

A grey-box model approach using operational voyage data

MT54035: MT MSc Thesis

by

M. de Haas

Performed at

Feadship, De Voogt Naval Architects

to obtain the degree of Master of Science in Marine Technology
in the specialization of Ship Design
at the Delft University of Technology,
to be defended publicly on Tuesday July 5, 2022 at 10:00 AM.

Student number:	4711378	
Project number:	MT.21/22.034.M.	
Project duration:	November 8, 2021 - July 5, 2022	
Thesis committee:	Dr. A.A. Kana,	Delft University of Technology (Supervisor)
	Ing. A.A. El Mouhandiz,	Feadship - De Voogt Naval Architects (Supervisor)
	Dr. A. Coraddu,	Delft University of Technology (Assistant Supervisor)
	Ir. N.D. Charisi,	Delft University of Technology (Committee)
	Dr. M.L. Baptista,	Delft University of Technology (Committee)

TUDelft *FEADSHIP*
ROYAL DUTCH SHIPYARDS

Preface

Coming from a family with a long history in the shipping business, I have always been around boats and the water. From this followed my own passion for ships, together with an eagerness to learn new things and solve problems. The combination of this lead to my choice for the Bachelor Marine Technology when I started in Delft. Enjoying everything I had learned so far, I followed this up with the Master in Marine Technology. During this program I participated in courses in the specializations of Maritime Operations and Management, Marine Engineering, and Ship Design together with the Masters main courses. Free electives were taken in Introductions into Offshore & Dredging together with Ports & Waterways and Scientific Writing. As a final step, a Ship Design thesis with a main focus on the problem of marine biofouling has been written in the past 8 months preparing for graduation.

This thesis would not have been possible without the help and support of a number of people. First of all, I want to thank Feadship and De Voogt Naval Architects for offering me a graduation intern position, together with additional guidance and support. Giedo Loeff, thank you for helping me in the early stages of the project and welcoming me at de Voogt. I want to give a special thanks to Abdel-Ali El Mouhandiz for the excellent guidance throughout this thesis. In our weekly meetings you always gave me your critical opinion and helped me making the next steps and pushing the boundaries. Not only did this help a lot, I also really enjoyed working with you and learned a lot from your experience.

From the Delft University of Technology I especially want to thank Austin Kana for his outstanding help during my thesis. Working with you on my Bachelor Final work was something I enjoyed together with getting to know you. Thank you for the time invested in the project and for guiding me to reach my goals. Your clear feedback and research approach has elevated my project to a higher level. Andrea Corradu, thank you for assisting in the project and sharing your knowledge on both marine biofouling, ship propulsion and data-driven modeling.

Ultimately, I want to thank everyone around me for their love and support. This includes my family and friends, for both distraction and support in my time at the TU Delft. Last, special thanks to my girlfriend Danique, who is my biggest support.

Matthew de Haas
Delft, June 2022.

Summary

Marine biofouling is known as the undesired adverse effect of living organisms growing on submerged surfaces. Biofouling creates roughness on the hull and propeller and thus additional frictional resistance and loss of propeller efficiency, also referred to as an additional sea margin for ships due to biofouling. The International Maritime Organization (IMO) identified marine biofouling as one of the primary problems from both economic and ecologic points of view. Biofouling threatens the ecological balance of world seas by transferring invasive aquatic species and causes a reduction in hydrodynamic performance of ships, which in turn increases fuel costs and greenhouse gas (GHG) emissions. Superyachts are especially heavily exposed to fouling, as they are stationary longer than commercial vessels, often staying in ports or being anchored across sea and in high tropical temperatures.

In this thesis focus is put on predicting marine biofouling growth together with its effects on ship performance to improve ship design, together with operation and maintenance. This is done together with Feadship, the largest superyacht builder in the Netherlands. To do so, a grey box approach has been applied, combining white box with black box models. White box models are first principle and either physics or experimental based, and easily interpretable. On the other hand, black box models are trained on given data, with no prior knowledge about a system. While white box can be applied for all predictions, black box can often perform better on data within the range its trained for on hard to understand problems. With grey box modeling, advantages and disadvantages from both can be combined into a working model.

For the white box modeling, first the ship resistance with a smooth hull was predicted. This was done with the calm water resistance based on ship speed, combined with a contribution from wind, waves and temperature difference. After this, marine biofouling growth was predicted with help of a experimental based model. With this model, a prediction can be made on the level of roughness present on the ship. Next, the roughness can be used to find and increase in frictional resistance and loss of propeller efficiency. Last, these are combined to make a power prediction for a fouled ship in a given condition.

The grey box model uses the white box fouled ship power prediction and its used data, together with anchorage and sailing days since clean ship. Furthermore, average anchorage temperature and sailing speed is also taken into account together with ship motions. To capture the problem, a deep extreme learning machine was used, which uses a feedforward neural network. With use of deep learning principles, the model can learn as more data is presented and start to find patterns. Finally, it was found that with this data-driven model, predictions could be made over a 2-year dataset with an accuracy of around 91.4% $\pm$ 0.2%. In comparison, on this same dataset, white box predictions gave an accuracy of around 85.3% $\pm$ 0.3%, using the mean absolute percentage error to determine both. With a margin missing on the smooth ship power, the accuracy of predictions was later increased to 89.4% $\pm$ 0.3%. Last, a black box configuration was worked out, not making use of the white box prediction. Here, an accuracy of 89.8% $\pm$ 0.2% was found. In conclusion, it was found that the grey box model showed the highest prediction accuracy.

With the developed model, relevant questions have been answered from both a research and industry perspective. For Feadship, the developed model was applied for their yachts to give insight in power increase, fuel increase, maintenance increase, speed loss, range loss and added cost due to biofouling. Next to this attention was payed to fouling resistance for regions with higher and lower flow, together with a comparison of different antifouling coatings available.

With implementation of the proposed grey box and white box models, predictions can be made for ships varying in all ranges of available data. With an indication of ship profile and parameters, biofouling and its resulting sea margin can be estimated with high accuracy in early stage ship design.

Contents

List of Figures

List of Tables

Problem Introduction & Exploration

In the first part of this report, an introduction to the problem will be given in chapter 1. Next in chapter 2, a deeper problem analysis will be presented. In chapter 3, the method to be used for this research will be explored. After this, the chosen methodology will be worked out in detail in Part II.

<div align="right">

1

</div>

<div align="right">

Introduction

</div>

Marine biofouling is known as the undesired adverse effect of living organisms growing on submerged surfaces. Biofouling creates roughness on the hull and propeller and thus additional frictional resistance and loss of propeller efficiency. This is also referred to as an additional sea margin for ships due to biofouling. The International Maritime Organization (IMO) identified marine biofouling as one of the primary problems from both economic and ecologic points of view (Castro, 2013). The IMO states that the problem of marine biofouling threatens the ecological balance of the world seas by transferring invasive aquatic species and causes a reduction in hydrodynamic performance of ships, which in turn increases fuel costs and greenhouse gas (GHG) emissions. Especially superyachts are heavily exposed to fouling, mainly due to their operational profile. Superyachts are stationary longer than commercial vessels, often staying in ports or being anchored across sea (Chambers et al., 2006). Within the fleet of superyacht builder Feadship, many vessels only sail around 10% of the time (Feadship, personal communication, 2022).

The global yacht fleet is increasing over the last years and is expected to grow onward, as shown in Figure 1.1. With an increasing yacht fleet, the importance of yacht design and their environmental footprint is starting to grow. For this reason, sustainable yachting is developing with more green ways to sail. As one of the industry leaders, Feadship has already build yachts powered hybrid diesel-electric (Feadship, 2015; 2020; 2021b), and is currently developing yachts powered by methanol and hydrogen, moving towards zero-emission yachting.
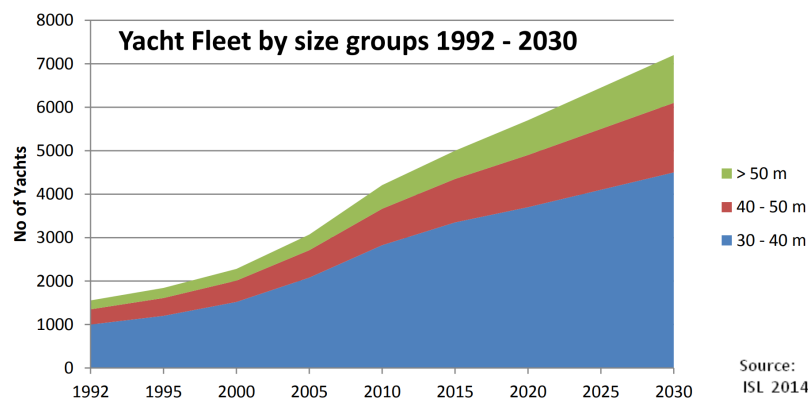
Figure 1.1: Growing yacht fleet worldwide, from Lindstad et al. (2015).

Not only is the superyacht industry working towards more sustainable yachting, the entrance of environmental policies concerning superyachts are also starting to take shape. With the Paris Agreement in 2015, the goal has been set to limit global warming to well below 2 degrees Celsius (United Nations, 2016). However, it is important to mention that the Paris Agreement depends on National Determined Contributions (NDCs), and does not set specific targets for sectors. For this reason the IMO set the goal

for GHG emissions from shipping to reduce 40% by 2030 and 70% by 2050 (MEPC, 2018). It must be mentioned that this is mainly focused on shipping and the CO_2 emissions per transport work. Here, the main ambition was the decline of the carbon intensity of the shipping industry through implementation of further phases of the energy efficiency design index (EEDI). To meet specifically with yacht design, the Yacht Environmental Transparency Index (YETI) has recently been developed to clearly indicate a yachts impact on the environment (Letschert, 2020). A system that is not only supported by policy but also by the industry, giving yacht designers and builders the opportunity to make a distinction with their ship when it comes to sustainability. This also helps to add more qualification to the eco-friendly level of yachts, with the 'green' card currently being overplayed and blurry lines on what constitutes green yachting credentials (SuperyachtNews, 2019).

With already 66 yachts worldwide over 100 meters, yacht size is also increasing and these types of ships are no longer neglectable (Superyacht Times, 2022). An increase in fleet size, yacht dimensions and yacht environmental policies & goals strengthen the importance for study on yacht design. With an increase in industry size and movement towards more sustainable yachting, vessel optimization is essential. It is noteworthy to mention that yachts have different operational profiles than other vessels, which opens possibilities for yacht research. The operational profile of each superyacht can be very different and change over time, which increases the complexity for the problem of marine biofouling on yachts. However, researching marine biofouling for the field of superyachts, with different sailing times, locations and parameters can give important new insight to this problem.

To give a better description of the problem and its background, first the problem of marine biofouling will be addressed in section 1.1. Next, in section 1.2 antifouling and fouling mitigation measures will be presented. In section 1.3, the development of antifouling systems is further outlined. After this, in sections 1.4 and 1.5, prediction methods and modeling trends within the maritime industry will be discussed. In section 1.6, Feadship & De Voogt Naval Architects shall be introduced. Next, in section 1.7, the literature consulted for this research is presented. In section 1.8, the research questions shall be presented. Last, in section 1.9, the research outline and main scope is presented.

1.1. Marine Biofouling

Marine fouling is the accumulation of micro and macro-organisms on immersed surfaces (Bressy and Lejars, 2014). According to Bressy and Lejars, more than four thousand fouling organisms have been identified worldwide. Among them, bacteria, diatoms, and algae spores are the main micro-organisms which settle on ship hulls. Barnacles, tubeworms, bryozoans, mussels, and algae are the most common macro-organisms. These micro- and macro-organisms grow on ships when in water, which can be seen as an inevitable process. This not only includes the ship hull but also the propeller and sea-water intakes. The attachment on ships of marine biofouling not only has negative influences on vessel performance, but also gives the possibility for organisms to change locations and thus ecosystems. This way, organisms can arrive in waters where they have little to no natural enemies, with the risk of losing the ecological balance of world seas (Alghamdi and Quijada Cordova, 2019).

Traditionally, the fouling process can be separated into four general stages, which starts the growth from microfouling to macrofouling (Yebra et al., 2004). In the first minute the water causes the submerged surface of the clean hull to be covered with a conditioning film of organic polymers. A process that Yebra and others describe and is essentially governed by physical forces such as Brownian motion, electrostatic interaction and van der Waals forces. In the next 24 hours, this first layer of film allows bacteria and diatoms to get attached to the hull, initiating the form of biofilm and microfouling. In the next week, the biofilm basis allow secondary colonizers as spores of macroalgae and protozoa to grow. After two to three weeks, macrofouling has started to grow as the tertiary colonizer. An overview of this process is shown in Figure 1.2.

The growth of these organisms depends on a lot of variables, making marine biofouling a complex problem.

> "The settlement of marine fouling organisms is influenced by several factors including salinity, pH, temperature, nutrient levels, flow rates and the intensity of solar radiation. These

factors vary seasonally, spatially and with depth" (Bressy and Lejars, 2014, p. 12).

All these variables presented by Bressy and Lejars only add to the difficulty of the problem, making it harder to understand and make possible predictions. With dependency on temperature and solar intensity, one can see that the climate at a certain location can have a large impact on the level of fouling. The problem of biofouling is site-, season and substratum-specific and the control methods effective at a given geographical location may not hold good elsewhere (Flemming et al., 2009). Accumulation of marine biofouling is faster when a vessel is frequently stationary or in high-temperature tropical waters, a combination that is often applicable for yachts (Stevens, 1937). Flemming and others state that antifouling measures are taken all over the world with very unequal levels of success. The authors conclude that there is no such thing as an universal solution to the biofouling problem.

			macrofouling
	microfouling		*tertiary colonizers* ~~~~~~~~~~~~~~~~~~~~~~~
		secondary colonizers **	
	primary colonizers //		
organic film +++			
Substrate ###			
1 min	*1 - 24 h*	*1 week*	*2 - 3 weeks*
adhesion of organic particles (e.g. protein)	**bacteria** *(e.g.Pseudo monas putrefaciens, Vibrio alginofyticus)* **diatoms** *(e.g. Achnantes brevipes, Amphiprora paludosa. Amphora coffeaeformis, Licmophora abbreviata Nifzschia pusilla)*	**spores of macroalgae** *(e.g. Enteromorpha intestinalis, Ulothrix zonata [Chlorophyta])* **protozoa** *(e.g. Vaginicola sp., Vorticella sp., Zoolhamnium sp., [CiliataJ)*	**larvae of macrofoulers** *(e.g. Balanus amphitrite [Crustacea] Electra crustulenta [Bryozoa] Laomedia flexuosa [Coelenterata] Mytilus edulis [Mollusca] Spirorbis borealis [Polychaeta] Styela coriacea [Tunicata])*

Figure 1.2: Temporal structure of settlement, from Abarzua and Jakubowski (1995).

1.2. Antifouling & Fouling Mitigation Measures

Currently, shipping companies try to mitigate the problem of hull and propeller fouling by applying antifouling paints on the underwater ship and by regularly cleaning the hull and propeller(s) (Lam and Lai, 2015). Within this process, a trade off is often made between the extra maintenance cost to keep the ship clean compared to the additional operational cost of sailing with a fouled hull. However, the hull and propeller are often cleaned when other maintenance is scheduled, which does not ensure optimal cleaning schedules (Kjær et al., 2018). This is mainly due to the high cost of either dry-docking or lifting a vessel (Figure 1.3) or placing it on a ship slipway, together with sometimes limited time or availability at different shipyards. Furthermore, the ship must sail to the yard and has downtime, this is mainly a costly process for commercial and service vessels. For the hull cleaning of the vessel, it is important that the fouling and antifouling that comes off the vessel is filtered and does not go back into the ocean, river or sewage.
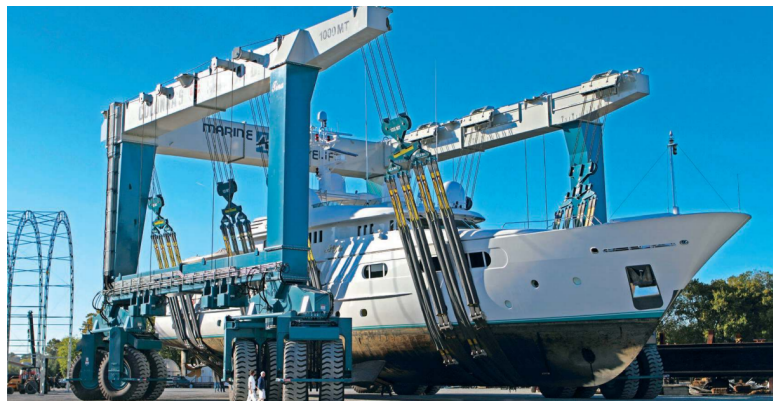
Figure 1.3: Yacht out of the water for hull cleaning and antifouling application, from Marine Travelift (2022).

Apart from getting the vessel out of the water for maintenance, divers or special machines can also clean the hull with the vessel still in the water (Fleet Cleaner, 2022; HullWiper, 2022). For underwater cleaning, the use of hard coatings is preferable, which can last for at least 10 years and may even extend the life of the hull. Hard coatings can be cleaned underwater and are neutral to the ocean because the waste generated by cleaning does not contaminate the marine environment (Morrisey and Woods, 2015). It should be noted that manual hull cleaning is commonly performed on small ships. Concluding in Figure 1.4, an overview is given between all parameters that influence marine antifouling systems.
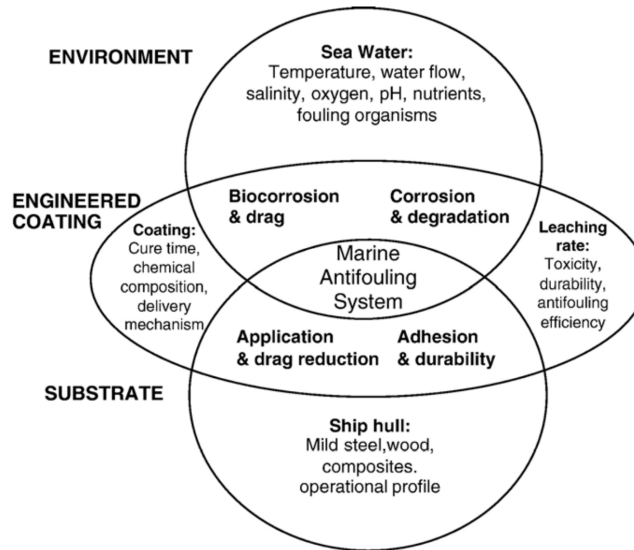
Figure 1.4: Key interactive parameters affecting an antifouling coating system, from Chambers et al. (2006).

For antifouling coatings, different paints are present on the market. Operators often apply biocidal self-polishing types, chemical substances that kill or deter microorganisms responsible for biofouling and prevent the formation of biofilm. If desired to use less toxic antifoulings, fouling release paints can also be used. These paints are silicon or hydrogel based, and improve possible fouling detachment at higher ship speeds. However, it should be noted that this type of antifouling coating also changes the texture of the ship hull. For example, while ship lifting and docking is no problem, a ship slipway is not advised with the risk of the ship not keeping its position. Not only is the type of antifouling coating decisive for ship performance, it also determines how reapplication can be done. Some paints can more easily be cleaned of the hull than others, and with some it is more difficult to clean the fouling off. This process is also important to prepare a clean hull so that new antifouling can be applied. Ship owners could also look at different levels and sorts of antifouling for different sections of the vessel. For example, more could be invested into locations with high Reynolds numbers and sections close to the propeller. An extra investment could also be done with ultrasonic antifouling systems, where transducers are mounted in the ship to send ultrasonic waves through the hull to the surrounding water, killing micro-organisms that form the initial fouling sequence. In Table 1.1, a small overview is created for different measures, their effectiveness, applicability and cost. For antifouling paints and dry cleaning, it can be noted that these two go hand in hand and require dry-docking or placement of the vessel onshore, which is a costly and time consuming process. This is dependent on close by yards, their facilities, their occupation, the local economy/currency, and ship type & size.

Method	Effectiveness	Applicability	Cost
Antifouling paints	Dependent on ship operation & surrounding climate, helps significantly with decrease of fouling growth.	Ship needs to be docked or taken onshore, hull preparation dependent on type of previous antifouling coating applied.	$100 - $1000 per 5L material cost + man hours (International Marine, 2022c).
Dry cleaning	Clears fouling from ship, important to do periodic together with new antifouling application.	Ship needs to be docked or taken onshore.	High pressure cleaner + man hours.

Periodic underwater cleaning	Effectiveness depending on method, important that quality of antifouling stays intact and only fouling is removed.	Can be performed at every location, more difficult with large ship.	Cost of diver for smaller ships or underwater cleaning device.
Ultrasonic system	Well proven effectiveness, but avoiding the growth of marine biofouling is complex. Can assist on import locations.	Large applicability, only initial investment and locations for transducers required.	Investment in power control and transducers placed in the ship.

Table 1.1: Antifouling & fouling mitigation measures.

The table above does not make a differentiation in types of antifouling coatings. For this reason, a case study performed by Feadship is provided, that gives insight in the cost of antifouling coatings over a 10 year basis. Within this case study, biocidal, silicone release coating, hydrogen release coatings and hard coating antifoulings have been taken into account from different suppliers. This case study is especially beneficial since most research papers often do not give insight into overall cost for antifouling paints. Getting insight into overall cost for a product over a lifetime requires longtime experience, something the ship and yacht industry has and can help with. For the case study, biocide antifouling by Micron99 was taken as the starting point since it was applied at the moment. For privacy reasons, the first application of biocide antifouling is selected as the nominal price of 100% to plot the results. This way, internal cost calculations and quote prices are remained secret while differences in application cost and fuel cost reductions are clearly visualized. It is important to mention that docking/lifting costs are not yet taken into the equation, as they heavily depend on ship size, location and yard facilities. However, it can be assumed that docking costs for superyachts are high and would show effect in total cost calculation for different antifouling options. Furthermore, the following considerations have been made for this case study (Feadship, personal communication, 2022):

- Material and application cost are based on supplier information.
- Fuel cost estimations are based on sailing profile of reference vessel, vessel engine performance diagrams and average MGO price.
- Sea margin predictions are based on a two year mean value for various Feadships, which will be discussed in the next section. Sea margins for alternative systems are judged by Feadship based on supplier information.
- Docking/lifting cost are very significant when required solely for cleaning and application of the anti-fouling system.
- Cleaning cost of e.g. hard coating could be significantly reduced when conducted by the crew itself.

In Figure 1.5, the result of the case study is presented to see how antifouling coating costs relate to each other together with their influence on fuel costs.
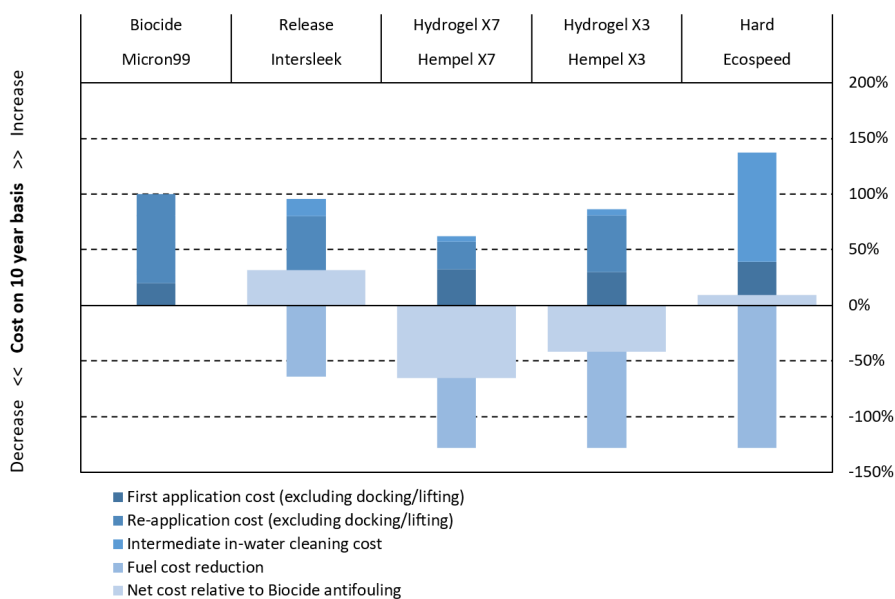
Figure 1.5: Antifouling cost case study performed by Feadship.

It is important to mention that the case study presented in the previous figure was build upon very rough fouling predictions and supplier information. With better modeling for specific vessels, a better overview could be given on most optimal antifouling paints. With fouling having a large influence on both vessel operation and maintenance cost, assessing and predicting the sea margin with high accuracy to determine best antifouling measures and ship operation is very important.

1.3. Development in Antifouling Strategies

With possible antifouling systems clear, it is important to explain the historic development of antifouling systems and current trends, as industry and research need to work towards better protective and more environmental friendly antifouling systems. Since ships have sailed the oceans, people have been encountered to the problem of biofouling, resulting in strategies on how to deal with this problem. For example, Christopher Columbus also experienced the problem of biofouling, and added the following (ABS, 2011):

> "All ships' bottoms were covered with a mixture of tallow and pitch in the hope of discouraging barnacles and teredos, and every few months a vessel had to be hove-down and graved on some convenient beach. This was done by careening her alternately on each side, cleaning off the marine growth, repitching the bottom and paying the seams."

Over time, antifouling approach has come from use of lead and copper, to use of TBT coatings, towards more environmentally friendly and fouling release paints. An overview of this is shown in Table 1.2, where major events are identified.

Timeline	Major events
1500-300 BC	Use of lead and copper sheets on wooden vessels
1800-1900s	Heavy metals (copper, arsenic, mercury) incorporated into coatings
1800s-present	Continued use of copper in AF coatings
1960s	Development of TBT conventional coatings
1974	Oyster farmers report abnormal shell growth
1977	First foul release AF patent
1980s	Development of TBT SPC coatings allowed control of biocide release rates
1980s	TBT linked to shell abnormalities in oysters (Crassostrea gigas) and imposex in dogwhelks (Nucella lapillus)
1987-1990	TBT coatings prohibited on vessels <25 m in France, UK, USA, Canada, Australia, EU, NZ and Japan
1990s-present	Copper release rate restrictions introduced in Denmark and considered elsewhere e.g. California, USA
2000s	Research into environmentally friendly AF alternatives increases
2001	International Maritime Organisation (IMO) adopts "AFS Convention" to eliminate TBT from AF coatings from vessels through: 2003 – prohibition of further application of TBT 2008 – prohibition of active TBT presence
2008	IMO 'AFS Convention' entered-into-force

Table 1.2: Historical development of the antifouling strategies, from Demirel et al. (2013).

The presented trends are important, as it can be seen that fouling is a hard to handle problem with constant development on how to approach it. Furthermore, fouling is handled by placing toxic products on the ship to kill and prevent organism growth. However, this also means that antifouling products can be bad for the environment. While TBT coatings showed the most optimal performance against biofouling accumulation, research later showed that these paints had toxic effects towards, oysters, molluscs and marine organisms, through which they could also enter the food chain (Alzieu et al., 1986; Gibbs and Bryan, 1986; Okay, 2004). As a consequence, TBT paints have been banned from 2003 for application and since 2008 for operation by the IMO with the International Convention on the Control of Harmful Anti-fouling Systems on Ships (IMO, 2001). Nevertheless, it can be seen that it has often been replaced with other toxic biocidal products, with similar problems as TBT coatings and less protection. Towards the future, the goal will be to develop better protective and more environmental friendly antifouling systems.

1.4. Importance of Accurate Prediction Methods

Gaining new insight into biofouling and its added sea margin can help considerably with yacht design, maintenance and operation. It can be noted that biofouling has a large influence on the required power of ships, and that small

reductions can have significant impact on power consumption. Hence, providing accurate information on added sea margin due to fouling can help decision making for initial yacht design and later maintenance. Furthermore, if prediction methods are improved, these can also be used by others within the maritime industry, since this problem is not only limited to yachts. Therefore, it can also help shipping companies and possibly policy makers into improving decision making when it comes to the problem of marine biofouling. Investing more in keeping ships clean could save large amounts in fuel cost, greenhouse gas emissions and propulsion maintenance (Coraddu et al., 2019).

Making accurate predictions when vessels are still being designed can take this one step further. With better insight in the problem of fouling beforehand, choices can be made to invest more in mitigation measures and keep low sea margin during operation. Not having additional fouling sea margins of 35% and over could result in alternative propulsion systems becoming more feasible for ships. This is due to the fact that all alternative propulsion systems require either more space or weight in the vessel compared to current used fuels (Sui et al., 2020). For this reason, keeping the required power from the propulsion system as low as possible is an important factor in accelerating the implementation of alternative propulsion systems in ships and yachts.

Currently, yacht and vessel owners do not have enough insight into biofouling growth and its consequences for one ship. Even though averages within the industry are well known, predictions are not done for specific vessels. Big steps could be taken for yacht builders and designers, an industry where every vessel is a one of a kind with different operational profiles and climates they sail in. Currently, Feadship takes into account an average sea margin for their yachts over time (Feadship, personal communication, 2021). In Figure 1.6, a prediction for the added sea margin over time across 4 Feadship yachts is provided. In this figure, it is also directly visible that within the Feadship fleet, large differences are present between different yachts. This conclusion can be drawn from a small study of the datasets acquired from the Feadship fleet. With differences in fuel use over time clearly visible for different yachts, conclusions can be drawn that biofouling has at least a large influence. With clear differences between different vessels, study could be done into this data to get a deeper understanding on the problem of biofouling.

First results based on a multi-year data set for 4 Feadships. This trend will be updated when more data becomes available. The trend shows a 30-day average sea margin. Fouling days are the days since last hull and propeller cleaning and application of anti-fouling.
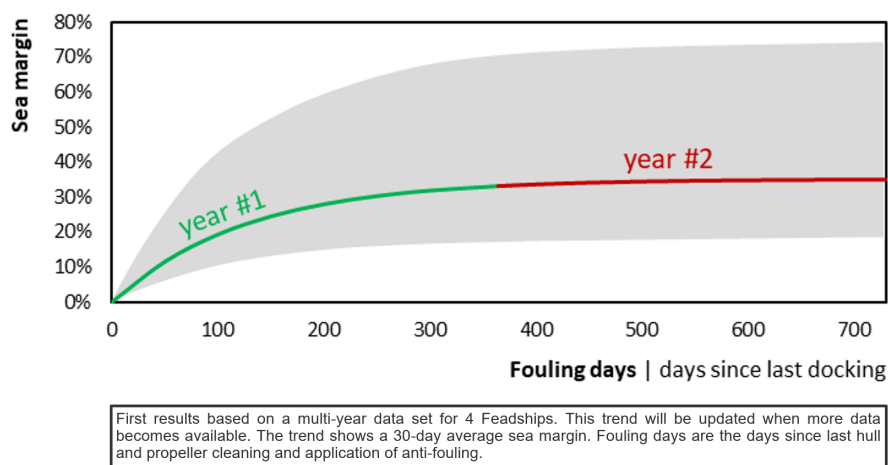
Figure 1.6: Estimation of added sea margin due to marine biofouling for 4 Feadship yachts based on fuel use trends over time.

Gaining insight into marine biofouling growth for current and new designed yachts could help significantly with customised hull and yacht maintenance. Last, it is important to mention that the level of marine biofouling itself cannot be measured directly on the hull when operational, and only when out of the water. For this reason, it is important that research is done into the problem, predictions are made, and that these are also validated when ships go into dock.

1.5. Modeling Trends within the Maritime Industry

Marine biofouling and its added sea margin are very difficult to predict and there is currently no accurate and universal method for doing so (Propulsion Committee of the 28th ITTC, 2017). The standard approach for estimating the speed loss can be carried out by applying ISO 19030 (ISO 19030-2, 2016). This approach prescribes methods for measuring changes in hull and propeller performance to give an indication for hull and propeller efficiency. However, this lacks a clear method on how to predict added sea margin due to fouling for ship design. As such, only low-fidelity analytical expressions exist recommended by the Propulsion Committee of the 28th ITTC, having an average error of around 20%. Therefore, making reliable predictions can only be done by gathering data and studying a large variety of ships.

Using principles as black box modeling and machine learning, can help with improving traditional maritime models to make predictions. Artificial intelligence has been used to improve white box model resistance methods, reducing a relative error ranging from 17.9% to 28.1%, to a relative error in the range of 1.6% to 2.7% (Pedersen and Larsen, 2009). Odendaal (2021), Zwart (2020) and Bakker (2021) have shown great potential with combining white box and black box models into grey box models with significant increase in prediction accuracy's to improve early stage ship design and ship operation. Here theory and physical relations/findings are combined with data-driven models. The white box ensures prediction accuracy outside of the data that the black box is trained with, since the black box is better at interpolation but can lack extrapolation capacity, due to no actual knowledge on the problem.

Last, it can be noted that black box models are especially beneficial when a system's behaviour is not fully understood or when white box models lack either predictability or accuracy (Leifsson et al., 2008), as is the case with modeling of biofouling and its sea margin. For example, more research is focused on the effects of fouling on ship performance rather than making biofouling growth predictions for ships. For different ships and situations, both towing tank test, mathematical models, and Computational Fluid Dynamics (CFD) calculations have been performed to asses added resistance for different fouled ships and plates. However, this is always focused on a given ship and a given fouling situation and is not flexible. Making marine biofouling growth predictions would take this one step further. But even then, fouling changes during sailing are still not taken into account, as predictions are limited to static modeling rather than dynamic. It can be noted that both are very complex problems depending on many variables. However, this does make it interesting for grey box modeling, since new insight based on data can be achieved. For this reason and also others, it is the hypothesis that grey box modeling can in many ways assist in solving this problem.

1.6. Feadship & De Voogt Naval Architects

The research outlined in this report will be done in cooperation with Feadship and Delft University of Technology. Here, Feadship and De Voogt Naval Architects will share both their ideas, key knowledge, and extensive amounts of yacht data to help answer the research questions. In this section, first an introduction to Feadship and De Voogt Naval Architects will be given. Next, their experience with the problem of biofouling and internal business case will be discussed.

1.6.1. Company Introduction

As one of the industry leaders, Feadship Dutch Royal Shipyards is specialized in custom built superyachts. *"Over the years, the name Feadship has become synonymous with the finest quality luxury motor yachts"* (Boat International, 2022). Feadship is a cooperative venture between De Vries Shipyards and Royal van Lent Shipyards, with de Vries having their main yards located in Aalsmeer and Makkum and van Lent having their main yards located in Amsterdam and de Kaag. De Voogt Naval Architects is owned by both companies, and is the main naval architect and marine engineer on all projects for the Feadship group located in Hoofddorp. In Figure 1.7, De Vries Shipyard in Makkum and the Royal van Lent Shipyard in Amsterdam are shown.

(a) De Vries Shipyard, Makkum location.

(b) Royal van Lent Shipyard, Amsterdam location.

Figure 1.7: Illustration of one of the yards for both Feadship families, from Feadship (2021a).

De Voogt Naval Architects (Figure 1.8) is not only the main naval architect and marine engineer on all Feadship projects, Research & Development together with Knowledge & Innovation for the Feadship group are also operated from De Voogt Naval Architects. Feadship does research into numerous yacht topics to design better and more sustainable yachts. Feadship sees this as both social responsibility as an opportunity to stay competition ahead.

Figure 1.8: De Voogt Naval Architects, Hoofddorp, from Feadship (2021a).

1.6.2. Business Case

As mentioned in the previous sections, marine biofouling is a problem that the full maritime industry has to deal with. Each company has its experience with it, and tries to make more informed decisions to mitigate the problem. Here it is important that the problem of fouling does not have one solution, and has many variables that influence the problem. Hence, information on the problem and deeper understanding can be very valuable to make better sea margin predictions in ship design and improve so-called condition based maintenance.

Feadships De Voogt Naval Architects Knowledge & Innovation team does all kind of research to develop yacht design and broaden knowledge within the organization. One of the projects is the development of its 7SEAS Portal, an initiative that tries to collect data from the full fleet. Within 7SEAS, all AIS data from the vessels is collected, including wind, weather, resistance and ship parameters. This way the operational profiles can be captured for research and predictions. One thing that is missing within the platform is ship specific predictions for marine biofouling. Currently, assumptions are made based on known patterns, such as shown in Figure 1.6, where the trends for added sea margin due to marine biofouling were plotted. To improve this model, the goal is to develop a ship, environment and operation specific method that can predict a ships marine biofouling level over time. Furthermore, this model should also give insight into what yacht crew and owner can expect, so that custom advice can be given.

Within this thesis the method will developed for Feadship and their 7SEAS Portal. Not only is integration important, the model must also be evaluated to see what this means for Feadship yachts specific. To do so, a business case is developed and several questions can be outlined that are important for Feadships business case:
- Which type of antifouling should be applied for which yacht?
- What is the difference between the influence of salt and fresh water on the marine biofouling growth?
- How does anchor location relate to the problem of biofouling?
- How influential is the propeller to the problem of fouling and how/when should it be treated?
- Should vessels be cleaned and provided with new antifouling prior to yacht transits?
- Can it be useful to use more antifouling on some regions of the ship than others, e.g. regions with higher Reynolds numbers?

To answer these questions and others, the different parameters outlined should be covered within the model. Since these questions cannot directly be answered with research currently done, it can be seen that the outcome will be both beneficial to Feadship and to the field of maritime and marine biofouling research.

1.7. Literature Retrieval

For this research, databases of the Delft University of Technology Library have been taken as a starting point to find relevant sources covering the main research question (Delft University of Technology, 2022). This helped with identifying relevant work done, and a possible research gap. In this process, papers closest to the proposed research have been taken as a reference to what is currently known and unknown in science when it comes to the problem of marine biofouling and its added sea margin. Furthermore, Google Scholar has been used to find the more recent and often cited work (Google, 2022). Keyword combinations like *Marine Biofouling*, *Marine Biofouling Resistance Prediction*, *Data-Driven Fouling Prediction*, *Yacht Fouling* and *Fouling Resistance Methods* have been used to get a first understanding of the topic and its key challenges.

However, knowledge on the topic is not only limited to papers published by various authors. With help of both Feadship and Delft University of Technology, different experts have leaned on in their view of the problem to share their knowledge and expertise. From the side of Feadship, this has helped with getting a better image on how this

problem relates directly to yachts and is handled within the industry. From Delft University of Technology, this has helped with getting a clearer view on the science behind marine biofouling, understanding of theories developed and potential research gaps. With help from both industry and science, the believe is that a good overview can be created on the problem, with confidence for possible improvements. Since Feadship is a larger organisation, the plan is to not only talk with research and design employees, but also plan meetings with their refit & services section for a more field view of this problem. The main goal is to listen to as many angles as possible for this problem, to get the best possible view on how to answer the research question and deliver significant improvement to both Feadship and the scientific community.

1.8. Research Questions

To get greater insight into the added sea margin from marine biofouling for yachts, the following main question must be answered:

> *"How can Feadship use in-house & onboard sensor data to accurately predict the added sea margin as a result of marine biofouling over time for yacht design, operation & maintenance?"*

To help answer this question, different sub questions can are set to find and develop an accurate prediction method:
- What are the current methods, both white box and black box, to predict added sea margin due to marine biofouling?
- What are the method requirements to model the effects of fouling?
- What methods are suitable to meet the method requirements, and if suitable how can machine learning and grey box modeling assist in solving the problem?

Once a prediction method is developed and the literature for this problem is studied, different sub questions can be answered:
- Does the model show difference in added sea margin for different antifouling systems, and can this form a basis for antifouling system selection?
- How much do vessel parameters, operational profile and location influence marine biofouling growth?
- How accurate is the model compared to the current sea margin predictions used in Feadship and general ship design, and if required should adaptions be made?

The questions presented above are both important for marine engineers, ship designers and Feadship. The overall goal is to give new insight on the problem of marine biofouling for improvement of ship design, operation & maintenance.

1.9. Research Scope & Outline

The report outline consists for the first part in the current introduction and exploration of the problem. The second part of the report contents the main methodology. After this, the third part contains the model validation, application and the business case. The last part contains the conclusion and discussion. Overall, it should be noted that the report is written from a Ship Design perspective. Main focus is put on model results and how they can influence and improve current ship design practices. Furthermore, focus is set on improvement from a production and operation perspectives. This also means that in the report, simplifications and assumptions will be made to come to best educated guesses so that modeling can be improved and modeling tools can be used in a practical way. An overview of the outline is shown in Figure 1.9.
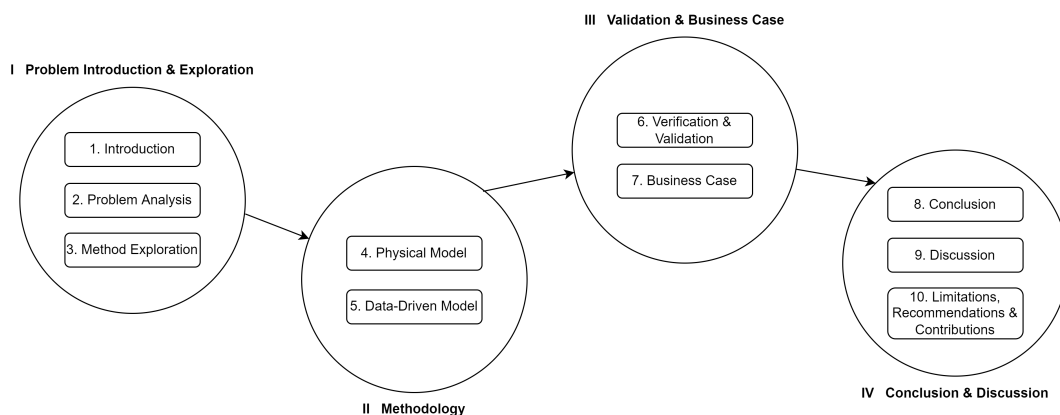
Figure 1.9: Research outline.

2

Problem Analysis

With the problem of the added sea margin from marine biofouling for yachts introduced, this chapter will give a deeper analysis of the problem. First in section 2.1, marine biofouling and its place within ship & yacht design will be discussed. Next, current methods to predict the added sea margin from marine biofouling will be presented in section 2.2. However, the added sea margin from marine biofouling is not only a result of added hull resistance. For this reason, section 2.3 shall go deeper into the effects of marine biofouling on the ship propeller. In section 2.4, some recent research into black box modeling with marine engineering applications is studied. After this, the data available by Feadship will be presented in section 2.5. With data available and current methods known, in section 2.6, the method requirements will be set up for this research.

2.1. Marine Biofouling within Ship & Yacht Design

When a contract is signed to design a new ship, naval architects often pass through various steps to work out a concept and later deliver a more detailed design. Within this process, a greater picture of the yacht is created together with its looks and performances. In Figure 2.1, the design approach for Feadship is shown with the role of De Voogt Naval Architects highlighted.
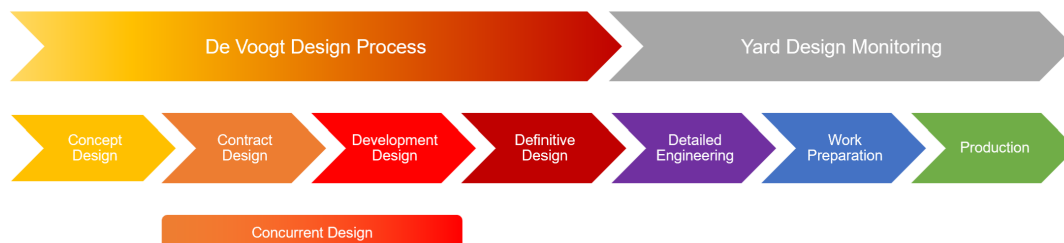
Figure 2.1: De Voogt Naval Architects design approach, from Odendaal (2021).

The approach used by De Voogt Naval Architects is inline with the traditional design spiral approach as shown in Figure 2.2. In both figures it becomes visible how all aspects of the design are repeated multiple times, with its level of detail increasing over time. Added in the design spiral are the different aspects of design covered numerous time. When it comes to marine biofouling, this can be seen as both an operational & maintenance problem as a design problem. It occurs during operation, is fixed when in maintenance, and should be taken into account and mapped when a ship or yacht is designed.

When it comes to marine biofouling for ship design, this problem can be taken into account either within hydrodynamics or within powering requirements of the vessel. This mainly depends on the level of detail of the assessment that is made for the problem of biofouling. When only an average sea margin is taken into account, it can be seen that this is likely done within powering calculations. Nonetheless, in a more detailed approach, future roughness and added frictional resistance is modelled in hydrodynamic calculations, while loss of propeller efficiency due to fouling is taken into account in power requirements.

With the current research the goal will be to use hydrodynamic calculations together with ship parameters and operational profile, to predict future marine biofouling growth and added sea margin. With this overview of sea margin over time for vessels, better powering estimations can be done. This way there can be a better assurance

that vessels do not only meet their design requirements with initial sea trails, but also during lifetime operation. Furthermore, better vessel maintenance and operation instructions can be presented to the client after ship launch.
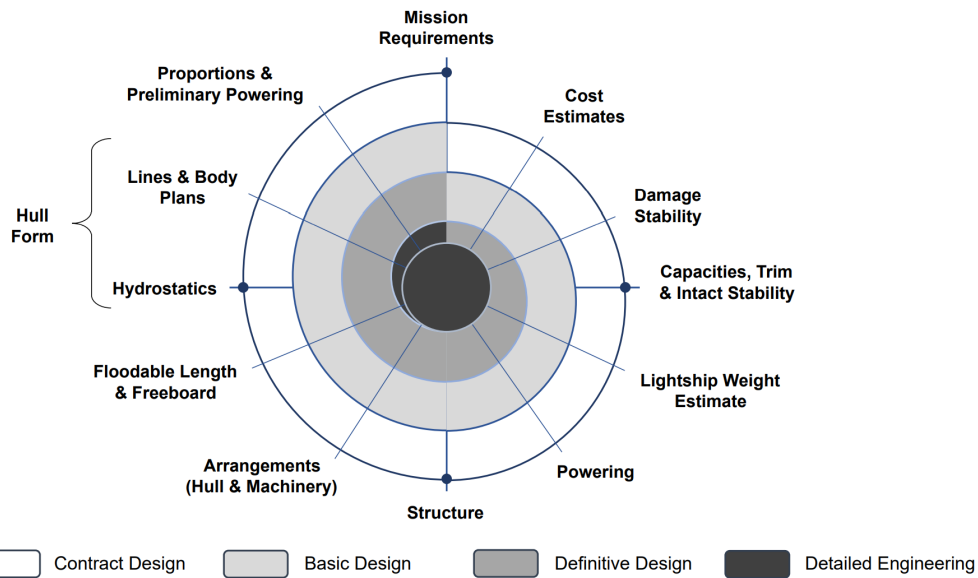
Figure 2.2: Traditional design spiral approach used by De Voogt Naval Architects, from Evans (2009).

With marine biofouling and its added resistance assessment also being part of early stage design, it can be seen that this adds extra weight on the decision making process. In this phase, little knowledge is yet available and many decisions and choices must be made. However, for the problem of marine biofouling, insight in planned operational profile by the client, overall vessel parameters and ship shape & powering can already give data to work with when it comes to making predictions. This little amount of data is not enough for developing a new tool, but can be used with a model already in place powered by reference vessels and their data. This is also why research on current ships is important for ship design. As shown in Figure 2.3, within the early stages of design a lot is still unknown while a lot of costs are committed early in the process. This makes models & tools based on previous ships & data very valuable. This is also the case for Feadship, building models on vessel data and their profiles can significantly help with future yacht design. This is not only the case for marine biofouling but also for other hard to predict and important problems.
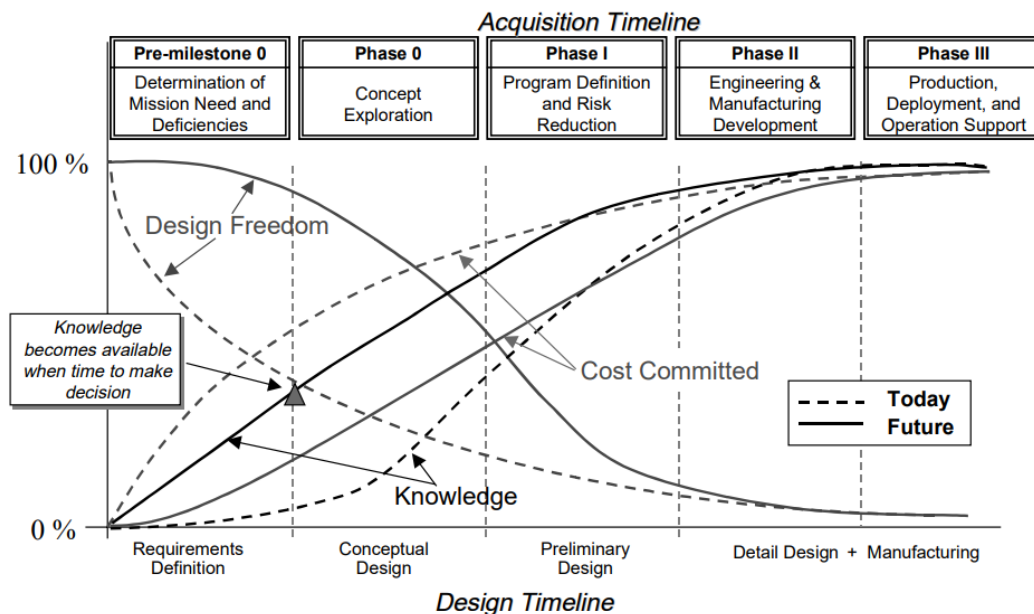
Figure 2.3: Relationship of design freedom, knowledge, and committed cost, from Mavris and DeLaurentis (2000).

2.2. Added Ship Resistance & Marine Biofouling Modeling

Marine fouling generates surface roughness which increases the frictional resistance of a ship moving through water and consequently increases fuel consumption and emission of greenhouse gases (Bressy and Lejars, 2014). It is known that fouling can lead up to an additional sea margin of up to 35% with a fully fouled hull (Uzun et al., 2019). This is a problem widely known within the maritime industry. Furthermore, extensive amounts of research have been done into the problem with attempts to improve fouling predictions and antifouling systems selection. However, within research fouling is also known as a very complex problem. With dependencies on a lot of variables, marine biofouling growth can be different in every case.

In Table 2.1, some of the relevant research is shown together with their method, accuracy, applicability and last the number of citations based on Google Scholar (2022). After introduction of this, the different available methods will be discussed together with their pros and cons based on the current papers.

Source	Method	Accuracy	Applicability	Citations
Data-driven ship digital twin for estimating the speed loss caused by the marine fouling (Coraddu et al., 2019)	Data-Driven	Significant improvement compared to conventional ISO 19030 method.	Method largely applicable, requires non-indifferent amount of data from ship to be investigated.	49
Practical added resistance diagrams to predict fouling impact on ship performance (Demirel et al., 2019)	First-Principle Experimental Based	Noteworthy margin of error, model limited to frictional resistance and flat plate modeling.	Comprehensive applicability, model using surface condition, ship length and ship speed. However, fouling condition is an input rather than an output.	24
A CFD model for the frictional resistance prediction of antifouling coatings (Demirel et al., 2014)	CFD	Frictional resistance increase predicted within 0.14% to 2.5%.	Model limited to frictional resistance increase and fixed biofouling conditions.	94
Time-Dependent Biofouling Growth Model for Predicting the Effects of Biofouling on Ship Resistance and Powering (Uzun et al., 2019)	First-Principle Experimental Based	Ability to predict change in required effective power within a 4% range of validation ship. However, not all fouling conditions represented and sailing process not taken into account.	Highly applicable due to input parameters for both fouling simulation and resulting additional resistance & power.	20
Predicting the effect of biofouling on ship resistance using CFD (Demirel et al., 2017)	CFD	Total resistance coefficient estimated within 1.17% with a numerical uncertainty of 0.74%. Larger deviation for required effective power.	Gives greater insight into problem under the effect of a rotating propeller. However, CFD computations are based exclusively on the vessel & fouling case imported.	134

Table 2.1: Literature for added ship resistance & marine biofouling modeling.

When it comes to predicting the added sea margin due to fouling, research has been done for first-principle experimental based models, more extensive Computational Fluid Dynamics (CFD) calculations and even data-driven modeling. Here it should be noted that these predictions can be split up in two processes: the prediction of marine biofouling growth and its following added sea margin. When it comes to CFD research, it is important to mention that this research is focused on a fouling case as a starting point, and the modeling of its additional resistance as main part of the research.

First-principle experimental based models are more friendly to use when obtained and are more practical to compute expected fouling and added sea margin. Furthermore, using and studying these models give greater insight into the physical phenomenons behind fouling. However, in these more conventional methods approximations are often made. An example can be found in modeling the added sea margin as a result of fouling by computing the added frictional resistance of a flat plate as discussed by Demirel et al. (2019). Moreover, Uzun et al. (2019)

confirm this and explain how in conventional models not all fouling situations can be represented and models are often limited to static growth of fouling, not change in fouling that occurs when sailing.

On the other hand, CFD methods could be used to determine the added sea margin of the researched fouling condition with high accuracy. Demirel and others (2014, 2017) have shown promising results with only few percentages deviation between predicted resistance and power compared to verified results. However, the results are limited to the chosen ship hull, and working out CFD computations for all possible fouling conditions is close to impossible and insufficient. Additionally, doing a large variety of CFD computations can be considered very expensive.

As with CFD, data-driven models show great potential to predict added sea margin for marine biofouling. This relatively technique can help with giving new insights and accounting all variables without simplifications, it is also a lot cheaper than performing extensive CFD calculations for new vessel design (Coraddu et al., 2019). With data-driven modeling, the system is trained to find patterns between data input and output. This also means that the model is not built on physical knowledge, which can be seen as both a pro and a con. While the disadvantage is that the user has less insight in the problem and obtained solution, a clear advantage is that the model can cover the full problem. This including parts that current theory finds hard to cover. Boundary conditions for data-driven methods are their requirement for a large and accurate data collection and its lack of extrapolation predictions.

It is important to emphasize that while many research is done on the problem of fouling, little models exist that are able to capture and predict marine biofouling growth for ships. Models often use different types of fouling, barnacle type, height and coverage as a starting point. By doing so, most models and papers available focus on added resistance as a result of marine biofouling for ships, rather than predicting the biofouling growth itself. Furthermore, studies into marine biofouling itself are often more detailed and focusing on specific characteristics to get a deeper understanding of the complex fouling problem, with so many variables and different sorts of fouling. For an ideal biofouling growth model, function 2.1 can be consulted with all parameters that have an influence shown (Babin et al., 2008):

$$BG = f_1(SST, psu, pH, v, I, S, t, m_t, \sigma, \theta_c, R_t, \eta_c) \tag{2.1}$$

Where:

BG	=	Biofouling growth
SST	=	Seawater surface temperature
psu	=	Salinity (dissolved salt content of the water)
pH	=	Acidity
v	=	Speed of the water flow
I	=	Light intensity
S	=	Concentration of nutrients
t	=	Time of exposure to the water
m_t	=	Micro-texture of the surface
σ	=	Surface potential
θ_c	=	Contact angle (measure of wettability)
R_t	=	Roughness parameter
η_c	=	Antifouling coating performance parameter

However, generating a model with all the parameters is difficult, especially with the complexity of the problem. Even the ideal model may not capture all parameters, and it is currently not known how all these parameters relate to each other. For now, only which variables play a role, how much, and how they influence biofouling growth positively or negatively is known. For this reason, current research is focused on models that rather use the most dominant parameters of the fouling problem. With simplifications, it becomes easier to make predictions and also to verify and validate model accuracy. Models can only be based on experiments and obtained data, rather than using first-principle physical relations.

2.3. Ship Propeller & Marine Biofouling

Ship propulsion and vessel speed is mainly dependent on the ship hull, propeller and engine (Atlar et al., 2018). The added sea margin due to marine biofouling, is mainly the result of both added hull resistance and decreased propeller efficiency. In the previous section, different methods to determine added hull resistance as a result of marine biofouling were discussed. In this section, the relation between the ship propeller and marine biofouling will be presented.

Some of the different methods available when it comes to marine biofouling & ship propellers are shown in Table 2.3, in which the type of method, accuracy, applicability and numbers of citations are indicated for each source.

Source	Method	Accuracy	Applicability	Citations
The impact of biofouling on the propeller performance (Farkas et al., 2020a)	CFD	Accurate change in open water efficiency predictions for researched cases with help of CFD. Proven to have relatively low numerical uncertainties.	Gives greater insight into flow around fouled propeller in open water condition. Investigation of biofilm and hard fouling for propeller performance investigated separately for different surface conditions.	7
Performance prediction method for fouled surfaces (Farkas et al., 2020b)	First-Principle Experimental Based	Simulation uncertainties ranging up to 5%.	Model is applicable for different ship types and surface conditions. Model uses propeller characteristics together with drag and lift coefficients to determine roughness effects on open water characteristics based on initial roughness values.	6
Investigating the effect of biofouling on propeller characteristics using CFD (Owen et al., 2018)	CFD	High accuracy between validation experiment and CFD results.	Model limited to both fouling condition, ship type and chosen PPTC propeller. However, model does give good insight into results of different levels of fouling with high accuracy of results.	57
Penalty of hull and propeller fouling on ship self-propulsion performance (Song et al., 2020a)	CFD	Simulation uncertainties mostly around 1%.	Model limited to used ship hull and propeller. Greater insight is achieved by investigating combinations between clean and fouled hull and propeller scenarios for different surface conditions.	40

Table 2.3: Literature for ship propeller & marine biofouling.

Both hull cleaning and propeller polishing are performed to remove unwanted fouling particles and increase vessel efficiency. However, the effect of fouling on a propeller is not given as much attention as hull fouling, resulting in a lack of material on this subject (Owen et al., 2018). One possible reason is that it might be difficult to study using model-scale experiments incorporating all different fouling types (Korkut, 2012). For this reason, most work on this topic is done in recent years with help of CFD. By using CFD, flow around a fouled propeller can be visualized properly, as shown by Farkas et al. (2020a) in Figure 2.4.

Overall, modeling with help of CFD increases fidelity and accuracy of results. However, this also means that results are always limited to the imported hull and/or propeller and fouling condition. On the other hand, a first-principle experimental based model as the one proposed by Farkas et al. (2020b) decreases fidelity but increases applicability.
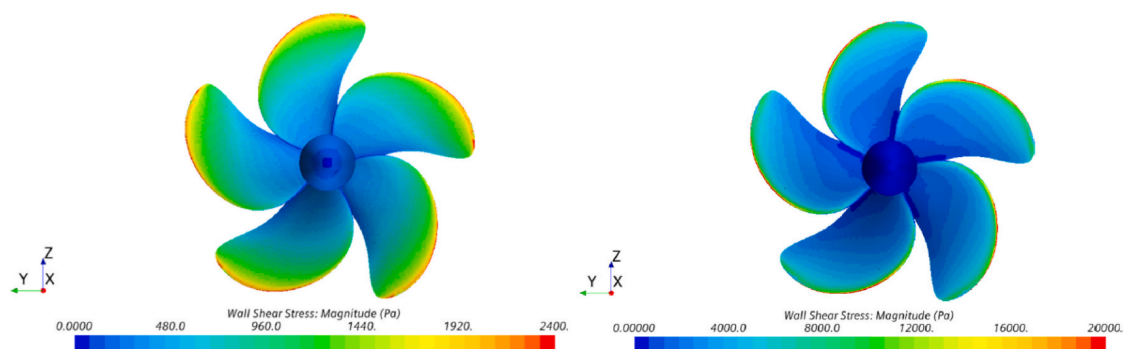
(a) Wall shear stress distribution for smooth (left) and fouled (right) KP505.

(b) Vorticity magnitude for smooth (upper) and fouled (lower) KP505.
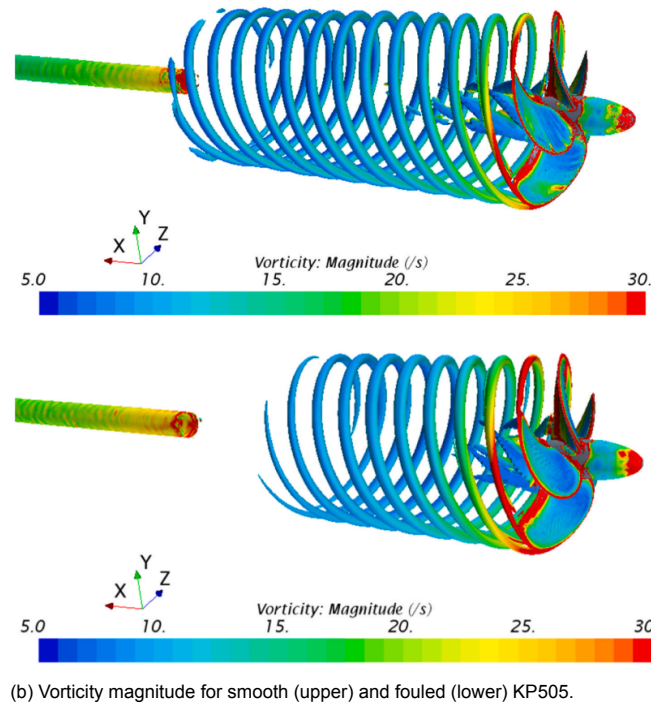
Figure 2.4: Illustration of differences in vorticity and shear stress for smooth and fouled propeller, from Farkas et al. (2020a).

2.4. Black Box Modeling

Making use of black box models is a recent development for predictions within the maritime industry. It is found that black box models powered by machine learning principles can help by improving prediction accuracy and covering complex problems. With potentials shown, different types of regression techniques could be used. In the table below, some relevant papers are provided that show the use of black box modeling techniques within the maritime research field related to propulsion and ship performance.

Source	Methodology	Research Problem	Citations
Prediction of Full-Scale Propulsion Power using Artificial Neural Networks (Pedersen and Larsen, 2009)	Artificial Neural Network	Use of propulsion power, ship speed, wind and sea & air temperature to predict propulsion power with high accuracy. Hull and propeller fouling mentioned but not accounted in method due to complexity.	57
Statistical modelling for ship propulsion efficiency (Petersen et al., 2012)	Gaussian Processes & Artificial Neural Network	Investigation and comparison of both Gaussian processes and artificial neural networks to model fuel efficiency in ship propulsion. White box modeling trends applied to account for fouling.	85
Physics-based shaft power prediction for large merchant ships using neural networks (Parkes et al., 2018)	Artificial Neural Networks	Shaft power prediction of large merchant ships in different weather conditions based on large data collection of multiple vessels over a 27 month period, making use of artificial neural networks. Biofouling not mentioned within paper.	20
Data-driven ship digital twin for estimating the speed loss caused by the marine fouling (Coraddu et al., 2019)	Deep Extreme Learning Machine	Digital vessel twin is developed with data shortly after leaving dock. Difference in ship speed over time is later evaluated and predicted due to biofouling.	49

Table 2.4: Literature for black box modeling within maritime industry for propulsion and ship performance.

2.5. Available Data

Within this research, a large amount of data with different sources will be provided by Feadship. This gives the opportunity for detailed modeling and possible new insight into the problem. In Table 2.5, an overview of the available data is shown. It can be noted that this available data is in line with data presented in a recent Master Thesis by Odendaal (2021). However, it should be mentioned that after contact with Feadship, small adaptions have been made. The available data contains ship design specifications, various captain logs, and maintenance, engine, motion, voyage report and auxiliary power data. Outlining this data and evaluating which data is available and which is not, is essential to set up method requirements.

Data Type	Data Source	Description
Ship design specifications	Inhouse design department databases	Ship design parameters: hull shape information (L, B, C_b, C_p) design loading conditions (T, v_s, range), LCG, LCB, propulsion systems, engine specifications, propeller selection, general arrangements.
Maintenance data	In house maintenance and shipyard databases	State of the hull and propeller fouling, date of last hull cleaning
Engine and motion data	Sensor monitoring	Main engine and generator power (shaft power), tank levels (consumption), ship motions (pitch and roll).
Voyage report data	7SEAS Portal Initiative	Onboard feedback monitoring: ship speed and heading, wave conditions (height, period and directions), wind conditions (speed and direction) and corresponding measured operational profiles from Feadship fleet. Also includes all weather related parameters associated to past, present, and future climate conditions.
Auxiliary power data	Influx database format	Additional hotel load system feedback monitoring: recorded total auxiliary loads (incl. sampling rates), AC power (voltage, amperage, and fan speed), air and sea temperature, and exterior relative humidity.
Voyage logs	Captain logs from different vessels	Relative feedback on yacht performance, travel logs & functioning of systems onboard.

Table 2.5: Available dataset types, locations and descriptions, adapted from Odendaal (2021).

2.6. Method Requirements

With the problem of marine biofouling and its added sea margin for yachts identified, a model is proposed to make accurate predictions in early stage design and ship operation. The goal is to evaluate the Feadship fleet and its collected data, and find both patterns and outcomes to make forecasts. Furthermore, the goal is to combine existing white box models will be combined with a newly set up black box model powered by Feadships data. Before the model selection will be done in the next chapter, first the method requirements have been set as stated below:

MR.1   A white box model that predicts marine biofouling growth overtime.
MR.2   A white box model that predicts added hull resistance as a result of marine biofouling.
MR.3   A white box model that predicts reduced propeller efficiency as a result of marine biofouling.
MR.4   A black box model that successfully captures ship-specific and environmental phenomena.
MR.5   A black box model that improves approximations and knowledge gaps of white box model.
MR.6   A black box model that successfully extracts level of marine biofouling from ship dataset.
MR.7   A grey box model that combines the white and black box models.
MR.8   A method that is based on available data within Feadship & De Voogt Naval Architects.
MR.9   A method that is based on various vessels within Feadship fleet.
MR.10 A method that can filter out errors in voyage data.

3

Method Exploration

In this chapter the main methodology for the model and current research will be explored. The goal is to formulate a method that will give accurate fouling and fouling effect predictions and will fit to the method requirements, as set up in section 2.6 and referenced by MR and their number. In this chapter, first in section 3.1, the white box model will be selected. Next, in section 3.2, the black box model will be selected. In section 3.3, the configuration for the grey box model will be presented. Finally, in section 3.4, the method requirements as proposed in section 2.6 will be evaluated.

3.1. White Box Modeling

With the problem analysis performed and different available methods and research known, first method selection will be done for the white box. Here, the different methods presented in the previous chapter will be assessed for the current research. For the white box modeling, the goal is to split the computation up into two models. Inline with MR.1, a model will be developed to predict marine biofouling growth. This model will be presented in subsection 3.1.1. Inline with MR.2 and MR.3, a white box model will be developed to predict the added sea margin as a result of marine biofouling. This model will be presented in subsection 3.1.2. By dividing the white box up into two models, both different physical processes that are occurring can be separated. This way a better overview of what is happening in and around the yacht is created and higher fidelity calculations can be used. Last, in subsection 3.1.3, the level to which the problem is covered by the white box model will be assessed. Based on this assessment, the parts of the problem that are not yet covered can be identified. This gives the opportunity to cover the last open points with the black box. As mentioned, black boxes can be very successful to cover complex problems and when a systems behaviour is not fully understood. Combining both white box and black box model will provide a powerful and accurate grey box model.

3.1.1. Marine Biofouling Growth

In the previous chapter different methods to predict ship roughness due to fouling were presented. With fouling conditions known, added hull resistance and loss of propeller efficiency can be predicted. In section 2.2 and section 2.3, different methods were discussed to predict added resistance and loss of propeller efficiency due to marine biofouling. Multiple of these recent papers show the great potential of using Computational Fluid Dynamics (CFD) to predict vessel performance with fouling conditions. Separate from this, first-principle experimental based models where also discussed together with data-driven methods.

For the current proposal, data-driven modeling will be used in the black box configuration, which will be discussed in section 3.2. This leaves both CFD modeling as well as using a first-principle experimental based model open for the current white box. CFD requires more work and computation time, in return the user achieves higher fidelity and a more precise answer. However, the current model will be developed to run for a large variety of vessels, operations, locations and datasets. Therefore, it is important to create a model that can do lots of computations while working with changing variables. Furthermore, the model should also serve as an early stage design tool. To compute CFD calculations, a detailed model is required as input. Inline with that, this research supposes that more can be gained by using a first principle based modeling rather than using a CFD model. Here it is important to mention that the white box model will be integrated with the black box model, with the expectation of increasing model accuracy and problem coverage. Overall, the goal of the model is to create a deeper understanding of marine biofouling growth, and give predictions of marine biofouling and its effects for different yachts and operational profiles. To select the most useful method for the current method, a trade off is made based on the different papers

discussed in section 2.2, of which an overview is presented in Table 3.1, together with the pros and cons of each method. Here the usefulness is indicated with positive, neutral, or negative sign.

Source	Usefulness[1]	Pros & Cons
Data-driven ship digital twin for estimating the speed loss caused by the marine fouling (Coraddu et al., 2019)	◒	Paper covers both marine biofouling growth and effect on ship speed. However, this is a data-driven model rather than a white box model, and thus more applicable for section 3.2.
Practical added resistance diagrams to predict fouling impact on ship performance (Demirel et al., 2019)	◒	Added resistance diagrams could be used as a start point for fouling resistance predictions. However, model does not predict fouling. Resistance diagrams lack fidelity and are not custom to yachts, their environment and operational behaviour.
A CFD model for the frictional resistance prediction of antifouling coatings (Demirel et al., 2014)	⊖	A CFD model is considered unpractical for the current research. The goal is to compute fouling and resulting resistance for multiple yachts in a lot of situations, rather than detailed calculations for only little situations. With many iterations required, a first-principle model is preferred over CFD.
Time-Dependent Biofouling Growth Model for Predicting the Effects of Biofouling on Ship Resistance and Powering (Uzun et al., 2019)	⊕	Best model for current research to the authors knowledge. Covers both marine biofouling growth predictions in a first-principle experimental based model as the computation of the added resistance resulting from this.
Predicting the effect of biofouling on ship resistance using CFD (Demirel et al., 2017)	⊖	A CFD model is considered unpractical for the current research. The goal is to compute fouling and resulting resistance for multiple yachts in a lot of situations, rather than detailed calculations for only little situations. With many iterations required, a first-principle model is preferred over CFD.

Table 3.1: Model selection for added ship resistance & marine biofouling modeling (MR.1 & MR.2).

To predict marine biofouling growth over time, the model used will be based on the time dependent biofouling growth model by Uzun, Demirel, Corradu and Turan (2019). This model is one of the newer and more advanced models to make predictions for biofouling growth in different regions, with an increasing frictional resistance parameter due to biofouling as a result.

The basis for the model of Uzun et. al (2019) are fouling measurements performed for different types of fouling over time. This includes measurements for slime, non-shell organisms and calcareous fouling. With these measurements, a Gaussian fit type was found that corresponds best to the data and growth patterns. This was done by applying a half-bell curve to satisfy the saturation phase at maximum fouling point. Extensive field test data was provided by a paint company which were conducted for over 3 years. The authors add:

> "Biofouling growth on coated and immersed plates was assessed according to ASTM D6990-05 (2011), and ASTM D3623-78a (2012) performance standards and evaluations were recorded for mainly three types of biofouling accumulations through monthly observations" (Uzun et al., 2019, p. 8).

It is important to mention that the process of fouling change when sailing is not taking into account. Uzun et al. mention that modeling is limited to static data and that with detachment it is not realistic to reach the required shear stresses in order to overcome the adhesion strengths of biofouling organisms on biocidal antifouling coatings (Uzun et al., 2019; Oliveira and Granhag, 2016). However, this also means that the model is less representative for coatings where fouling detachment is possible at certain speeds. Since this will also be evaluated within this research, this is a point that partly needs to be covered by the black box. As mentioned, shortcomings of the white box will be listed at the end of this section.

Since the model tests were only performed around the Equator and Mediterranean region, the authors propose to inter- and extrapolate the results as a function of water temperature. To do so, Uzun et al. make use of a function that can approximate the surface water temperature based on the latitude degree of a ships location. This way the found patterns can be computed for all regions around the world, assuming water temperature as the most dominant fouling parameter. Last, the authors go into detail on the high added resistance when more barnacles

---

[1]Reflecting on usefulness in regard to practicality for the current model, not functioning as a review to the paper.

are attached to the hull. For this reason, the authors present a logarithmic function that can determine the area covered by calcareous fouling. Based on how high this level is, a selection can be made on whether fouling rating or calcareous surface coverage is the dominant fouling parameter.

With the accumulative fouling rating formula, growth predictions for calcareous fouling, non-shell organisms and slime can be done. Here again attention can be paid to the growth process of biofouling, as discussed in section 1.1. It was presented how first slime is formed around the hull, followed by non-shell organisms and finally the more heavy calcareous fouling. This can all so be seen back in different fouling diagrams that can be made. In Figure 3.1, calcareous fouling growth predictions for both the Equatorial region and the Mediterranean region are presented. For the Mediterranean region, it can be seen that it takes over a year for both slime and non-shell organisms have settled around the ship, and growth of macrofoulers can start.
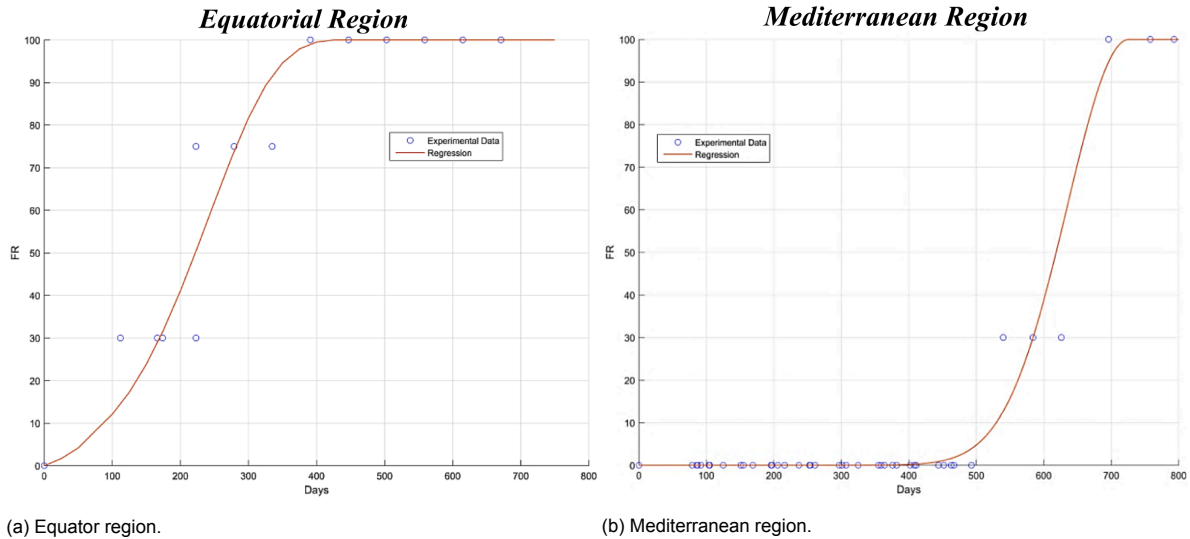
(a) Equator region.

(b) Mediterranean region.

Figure 3.1: Calcareous fouling growth shown over 800 days with a maximum fouling rating of 100, from Uzun et al. (2019).

With insight in fouling rating and calcareous surface coverage, the equivalent sand roughness height (k_s) can now be computed. This parameter will be determined in micrometers, and represents the roughness thickness present on the ship surface. The equivalent sand roughness height is often used in marine biofouling studies to quantify the biofouling present on the ship, and translate this it added hull roughness. It can be noted that with this, the marine biofouling growth can now be determined at any point and time for any location with roughness as a result. As a next step, roughness present on the ship can be computed to added sea margin. With this, the method exploration for the marine biofouling growth process is now finished. In the next chapter, the methodology selected will be presented in detail. However, first the other methods must be selected to form the model.

3.1.2. Added Sea Margin as a Result of Marine Biofouling
In the previous section it was determined how marine biofouling growth predictions can be made, with the equivalent sand roughness due to biofouling (k_s) as a result. Next, in this section the added sea margin as a result of the predicted marine biofouling will be calculated.

Added Hull Resistance
To start with vessel resistance, first it is important to mention the relation between the required effective power (P_E), total ship resistance (R_T) and ship speed (V_S), as shown in Equation 3.1. Next, in Equation 3.2, it can be seen how the total resistance can be split up into its different factors, including frictional resistance (R_F), increase in frictional resistance due to biofouling (ΔR_F), residual resistance (R_R) and air drag resistance (R_{AA}).

$$P_E = R_T V_S \tag{3.1}$$
$$R_T = R_F + \Delta R_F + R_R + R_{AA} \tag{3.2}$$

In the function above, the residual resistance includes wave resistance, the viscous pressure resistance, and the additional resistance due to the form or curvature of the hull. This means that this parameter is also dependent on weather condition, something that has to be accounted for and has an influence on the total sea margin of the ship. To account for both still water resistance and resistance in different weather conditions, Feadships initial design calculations, resistance measurements and VoogtWAVE & 7SEAS Portal will be used. With use of this model,

all different weather conditions can be taken into account and evaluated. Here it can be noted that VoogtWAVE method makes use of the regular wave height, incoming wave direction and other parameters to compute the added resistance as a result of the wave. This is embedded in 7SEAS Portal, where predictions based on wind and weather conditions are made. With this method, all other factors that play a role in the resistance of the ship are taken into consideration, so that the additional contribution from biofouling can be identified and later validated. Based on the previous function, the added frictional resistance due to fouling could be calculated, as shown in the equation below.

$$\Delta R_F = \frac{1}{2}\rho S \Delta C_F V_S^2 \tag{3.3}$$

To find the added frictional coefficient due to biofouling (ΔC_F), the resulting equivalent sand roughness height from the marine biofouling growth model can be used. For this conversion, three different methods were studied and evaluated:

- Experiments performed by Schultz (2007), conversion of equivalent sand roughness (k_s) height into roughness function (ΔU^+). Use of Granvilles (1987) similarity law to find the added friction resistance coefficient due to biofouling (ΔC_F).
- Experiments performed by Farkas et al. (2018), model based on equivalent sand roughness height (k_s) and diatoms surface coverage (SC) to find roughness function (ΔU^+). Use of Granvilles (1987) similarity law to find the added friction resistance coefficient due to biofouling (ΔC_F).
- Model by Townsin (2003) that directly computes the added frictional resistance coefficient due to biofouling (ΔC_F) based on the equivalent sand roughness height (k_s), ship length (L_{WL}), and Reynolds number (Re).

The first method would combine multiple steps including reading out a figure instead of using a function, which is not preferred for the current method. Furthermore, it can be noted that this method also applies only for certain surface coverage conditions (Schultz, 2007). It can be noted that the functions of the second option are based on diatoms surface coverage, a microfouling. This is not inline or close to the calcareous surface coverage fouling predicted within the current model. Therefore, this method would heavily under predict the roughness and thus resistance due to biofouling for this model. The last and most optimal method to the authors knowledge is the function proposed by Townsin (2003). This function has a direct approach to the problem and is also recommended by the ITTC (2014) as the performance prediction method to calculate added frictional hull resistance due to biofouling roughness.

With the additional frictional resistance coefficient due to biofouling (ΔC_F) now able to be determined, it can be used to compute added frictional ship resistance as explained and the loss of propeller efficiency.

Loss of Propeller Efficiency
Similar to the models for added resistance and marine biofouling, a trade-off will also be made to select the best fit model for the modeling of ship propeller & marine biofouling. In Table 3.2, the papers presented in section 2.3 are evaluated and a comparable overview as above is presented. Based on this evaluation, the performance prediction method for fouled surfaces by Farkas, Degiuli, Martić and Ančić (2020b) will be used as a basis for modeling of propeller efficiency loss.

Source	Usefulness[2]	Pros & Cons
The impact of biofouling on the propeller performance (Farkas et al., 2020a)	(dark circle)	This model is a follow up on Performance prediction method for fouled surfaces (Farkas et al., 2020b). this paper gives good insight into propeller performance due to biofouling but uses CFD rather than a first-principle relations.
Performance prediction method for fouled surfaces (Farkas et al., 2020b)	(+)	Best model for the current research to the authors knowledge. Gives practical formulas to calculate change in open water efficiency as a result of difference in lift and drag propeller coefficients due to fouling.
Investigating the effect of biofouling on propeller characteristics using CFD (Owen et al., 2018)	(−)	A CFD model is considered unpractical for the current research. With many iterations required, a first-principle model is preferred over CFD.

---

[2]Reflecting on usefulness in regard to practicality for the current model, not functioning as a review to the paper.

Penalty of hull and propeller fouling on ship self-propulsion performance (Song et al., 2020a)		Model does give great insight into differences in clean/fouled hull and propeller and combinations. This helps with understanding of hull and propeller interaction when it comes to fouling. However, a CFD model is considered unpractical for the current research.

Table 3.2: Model to predict reduced propeller efficiency as a result of biofouling (MR.3).

As with added frictional resistance, the loss of propeller efficiency will also be computed based on the predicted roughness. By calculating changes in lift (identified with subscript L) and drag (identified with subscript D) for the propeller due to fouling, the new open water efficiency can be computed from smooth (identified with subscript S) to rough condition (identified with subscript R). In order to do so, Equations 3.4 and 3.5 will be used (Farkas et al., 2020b). These function are based on the added frictional resistance coefficient (ΔC_F) for the propeller and different propeller characteristics. It should be noted that the added frictional resistance for the propeller is not yet predicted, since it is dependent on the propeller plate length. According to Farkas et al., the plate length can be taken as the chord length at $0.75R$ and will be implemented into Townsins function. For propeller characteristics, original design parameters from Feadship and their yacht propellers will be used to find the new operation points.

$$K_{TR} = K_{TS} - \Delta K_{TD} - \Delta K_{TL} \tag{3.4}$$
$$K_{QR} = K_{QS} - \Delta K_{QD} - \Delta K_{QL} \tag{3.5}$$

With changes in propeller performance due to biofouling now computable, the new open water efficiency can be calculated. In order to do so, Equations 3.6 and 3.7 can be used (Klein Woud and Stapersma, 2002).

$$J = \frac{v_a}{nD} \tag{3.6}$$
$$\eta_O = \frac{J}{2\pi} \frac{K_T}{K_Q} \tag{3.7}$$

Resulting Added Sea margin due to Biofouling
The open water efficiency of the propeller is important for power transfer from propeller to effective power. As shown by Klein Woud and Stapersma, the effective power is a result of the number of propellers (k_p), multiplied by the power from each propeller (P_P) factored by the open water (η_O), hull (η_H) and relative rotative (η_R) efficiencies. Based on this function for the fouling condition, the rough effective power ($P_{E,R}$) at a given speed or the rough ship speed ($V_{S,R}$) at a given power output can be determined. These two follow from an increase in resistance, decrease is propulsion efficiency and given ship power or speed. By selecting ship speed and finding rough power consumption compared to the smooth situation, added cost in fuel can be found and trade-offs can be made between this and investing in clean ships.

With this last step, the white box model is complete and a white box model is proposed that predicts marine biofouling growth overtime (MR.1), added hull resistance due to biofouling (MR.2) and reduced propeller effiency due to biofouling (MR.3). For this method available data from Feadship & De Voogt Naval Architects will be used as outlined in section 2.5. Here, it is important to mention that all other relevant data concerning ship resistance and propeller characteristics are already available for the yachts. For this reason, only computing changes due to biofouling for resistance and propeller is satisfactory. With this model, predictions will be made for multiple yachts within the Feadship fleet, inline with method requirements MR.8 and MR.9. Last it is important that all data entering the white box is checked to filter out errors in voyage data. This will be done by applying Chauvenet's criterion. With Chauvenets criterion, the dataset is filtered to find errors that have to large deviation, based on a Gaussian distribution and the standard deviation of the dataset for each variable.

Next to filtering errors with help of Chauvenet's criterion, other filtering might also be applied. For example, a minimum speed of $v_s > 2kts$ can be applied to filter noise out for clear anchoring / mooring AIS data compared to yacht sailing. However, this will depend on data accuracy and patterns once the dataset will become familiar. With implementations of functions for filtering errors out of voyage data, MR.10 is met. In chapter 4, this selected method will be explained in detail.

3.1.3. White Box & Problem Coverage
Within this subsection, the proposed white box will be assessed to check its ability to capture the complex problem of marine biofouling. The goal is to identify the gaps that are difficult to cover with current theory, and use this as follow up for the black box model in section 3.2. This way, fleet data can be used to predict hard to capture

phenomena and successfully cover the problem in a grey box model, which will be presented in section 3.3. Based on the current section, with help of the developed white boxes the model can now compute:

- Marine biofouling growth predictions based on regional and environmental parameters resulting in equivalent sand roughness height.
- Convert growth predictions into added frictional resistance coefficient with help of the Reynolds number, ship length and equivalent sand roughness height.
- Use increase in frictional resistance biofouling coefficient to predict added ship resistance due to biofouling.
- Use increase in frictional resistance biofouling coefficient to derive change in drag & lift coefficient to predict reduction of open water efficiency due to biofouling.

However it can be noted that the problem is not yet fully covered with the proposed model. Even though the model can now predict added sea margin due to marine biofouling, still several assumptions and simplifications have been made. These need to be mapped and properly covered where required. The following assumptions and shortcomings can be listed:

- The marine biofouling growth predictions are based on logarithmic functions developed from field lab data performed only within the Mediterranean and Equator regions, and several simplifications have been made compared to the ideal biofouling growth model to increase practicality. A black box model could improve prediction accuracy and expand region coverage.
- Marine biofouling growth predictions are derived from field lab data for SPC coating. However, for the case study and research it is desired to study effects of different antifouling measures. Using this as a parameter in the black box could show potentials and effects of different systems. Results obtained can improve maintenance and operation choices based on a cost benefit analysis.
- While biofouling growth is predicted, the fouling process when vessels sail is not covered within the current model. For this reason, this fouling process must be predicted for different antifouling coatings with help of the black box model.
- Hull & propeller interaction within fouling situation is not yet clear or taking into account. Currently both systems are covered separately. However, biofouling also changes water flow to the propeller and possible other propeller performance as discussed by Song et al. (2020a).

Based on the shortcomings listed above, it can be seen that the white box model does not successfully cover the full problem. However, with first-principle models, it is often difficult to capture all parameters that have an influence on the problem, as model simplifications are often done for practicality. In return, the current method is good for both understanding and extrapolation. Using a grey box model would give the opportunity to attack the problem from another angle and give different coverage of the theory.

The current list will form a basis to fulfill MR.5: *A black box model that improves theoretical parts with assumptions, approximations or knowledge gaps of white box model.* Based on this, MR.5 can be identified as follows:

MR.5.1 A black box model that can predict marine biofouling growth, taking into account full effect on ship performance for different antifouling systems.

MR.5.2 A black box model that can predict marine biofouling during sailing, taking into account full effect on ship performance for different antifouling systems.

With MR.5.1, marine biofouling growth predictions can be improved, while antifouling systems can be taken into account together with possible hull & propeller interaction effects. With MR.5.2, marine biofouling detachment predictions can be made, while antifouling systems can be taken into account together with possible hull & propeller interaction effects.

3.2. Black Box Modeling

A black box can be viewed as a system which gives outputs based on inputs, without clarity of what happens inside the system and without the system having any physical knowledge. For this reason, black boxes are based on data-driven modeling as they require large data input and need to be trained to give correct data output. By doing so, the black box starts to recognize patterns and increase its intelligence about the system, also called artificial intelligence. This way the system becomes a program that can sense, reason, act and adapt. The discussion of black boxes and artificial intelligence often comes hand in hand with the term machine learning. Machine learning is a part of artificial intelligence, where algorithms improve over time as they are exposed to more data.

With machine learning principles, various prediction & modeling methods have been improved for different fields of research. Instead of trying to model all phenomena and physics involved with this problem, the black box simply uses and compares data to give predicted output, without any physical understanding of either ships, water, resistance or powering. This has both its benefits and its downsides. Using a black box can improve modeling

accuracy significantly. However, it is difficult to assess which patterns the system has found as one cannot see or understands what happens within the black box. Since all patterns are found within the range of trained data, it should also be mentioned that the black box can lack extrapolation accuracy. This means that both white box and black box modeling are important in the field of research to come to better results and learn more.

For data-driven models, deep learning represents the state-of the art technique (Coraddu et al., 2019). Here, the word 'deep' refers to the use of multiple layers within the method, instead of a single layer model. With use of multiple layer neurons, deep learning attempts to simulate the human brain to 'learn' from large amounts of data (IBM Cloud Education, 2020). In Figure 3.2, an overview of deep learning within machine learning & artificial intelligence is given. Before machine learning principles or even deep learning can be used, first models have to selected to overcome the different problems identified.
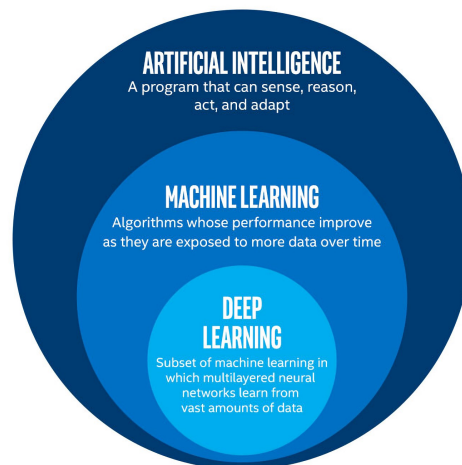
Figure 3.2: Artificial Intelligence, Machine Learning & Deep Learning, from Bansal (2019).

3.2.1. Learning Machine Selection

Based on the defined problem and available data, a model must be selected. As mentioned, data-driven modeling will be used to give predictions on parts that are difficult to cover with the white box model, which were highlighted in subsection 3.1.3. The goal is to use machine learning algorithms so that it can learn from the data that it is provided with. With large quantity of data available and the goal of data-driven modeling, using a deep learning technique would be optimal for this case. However, there are many different models and an appropriate model must be selected.

Selecting the best model is difficult, even advanced practitioners and researchers often fail to perform model selection and error estimation in the correct way (Oneto, 2018). Oneto argues that model selection and error estimation will always be necessary since there will never be a golden learning algorithm able to solve all data related problems in the optimal way. While model selection contains both the selection of a learning machine and hyperparameters, first the type of machine must be selected. With the focus on deep learning, obvious choice could be to make use of artificial neural networks (ANN). These can be seen as one of the most applied methods within the maritime industry. Pedersen and Larsen (2009) were one of the first to train an ANN to predict propulsion power for container vessels. Parkes (2018) modelled shaft power prediction of shipping vessels with high accuracy. Next to this, Petersen et al. (2012) compared ANN with Gaussian Process (GP) for the modeling of ship propulsion efficiency. Nonetheless, when attention is paid at the closest case compared to the current research, instead of most research within the maritime industry, it can be found that a Deep Extreme Learning Machine (DELM) can successfully predict ship speed loss due to fouling effects. Corradu et al. (2019) showed this with Extreme Learning Machines (ELM) that make use of feedforward neural networks. This overcomes problems posed by backward-propagation training algorithm with potentially low convergence rates, critical tuning of optimization parameters, and presence of local minima that call for multi-start and re-training strategies (Huang, 2014; 2015; Ridella et al., 1997; Rumelhart et al., 1986). With some of these advantages outlined, and a DELM already applied to biofouling modeling, this machine is selected in the first stage of model selection. This way multiple hidden layers with neurons can be used to train the model for accurate and fast predictions for marine biofouling and its effects. An overview of the trade off is shown in Table 3.3, where the papers presented in section 2.4 are evaluated.

Source	Usefulness[3]	Pros & Cons
Prediction of Full-Scale Propulsion Power using Artificial Neural Networks (Pedersen and Larsen, 2009)	⊖	Paper does give insight into application of ANN for capture of ship data. However, fouling process not taken into account since it was hard to capture.
Statistical modelling for ship propulsion efficiency (Petersen et al., 2012)	⊘	Papers shows differences between ANN and GP for ship specific problem. Furthermore, fouling was modelled in a simplified way so that paper gives additional insight for modeling choice.
Physics-based shaft power prediction for large merchant ships using neural networks (Parkes et al., 2018)	⊖	Papers shows again possibilities of ANN for modeling ship data and characteristics. However, fouling is not covered within the model making it less representative for the current case.
Data-driven ship digital twin for estimating the speed loss caused by the marine fouling (Coraddu et al., 2019)	⊕	Closest model to current case. Model uses DELM to build digital ship twin and find relation in speed loss overtime as a result of marine biofouling. With this paper and black box selection as a proven method for marine biofouling capture within data, this method is the best choice to the authors knowledge.

Table 3.3: Evaluation of applied black box models within maritime industry.

It can be seen that in this case, the last layer of the DELM makes use of supervised learning., which tries to model relations between the variable and the input parameters, using labeled datasets. This means that before the training process, part of the modeling is labeling all input and output parameters. Doing so, the model can measure its accuracy and learn over time. On the other hand, unsupervised learning uses algorithms to analyze and cluster unlabeled datasets. Tissera and McDonnel (2016) have shown that supervised learning can significantly improve network training time and memory usage for Extreme Learning Machines.

The first Extreme Learning Machine was built as a single layer feed-forward neural network, called Shallow ELM (Huang et al., 2006). Later, the configuration of multiple layers was added to present the DELM. Both extreme learning machines are presented in Figure 3.3.

(a) SELM structure.   (b) DELM structure.
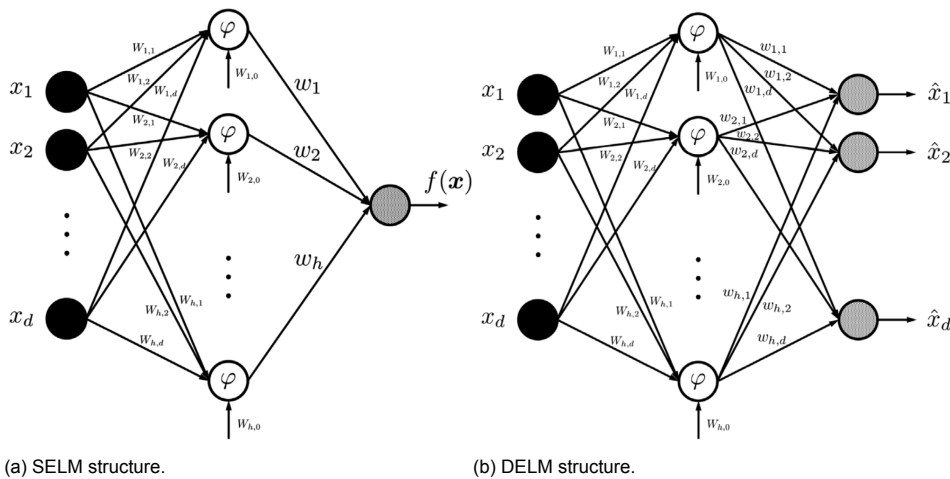
Figure 3.3: Extreme Learning Machines, from Coraddu et al. (2019).

3.2.2. Model Application

The black box model will be specifically programmed to improve the white box model shortcoming as discussed in subsection 3.1.3. This means that both MR.5.1 & MR.5.2 must be met, so that these shortcomings are covered. In the sections below, a proposal is done for how both fouling development during anchorage and sailing can be captured.

---

[3]Reflecting on usefulness in regard to practicality for the current model, not functioning as a review to the paper.

This part of the grey box should cover MR.5.1: *A black box model that can predict marine biofouling growth, taking into account full effect on ship performance for different antifouling systems* together with MR.5.2: *A black box model that can predict marine biofouling detachment, taking into account full effect on ship performance for different antifouling systems.* To do so, it is important that the black box can find performance difference over time compared to the ships clean hull & propeller situation in different environmental conditions. Coraddu et al. (2019) solved this problem by developing a data-driven ship digital twin with help of deep learning principles. Data is used after vessel launch in different weather conditions so that the model can predict expected speed when power and other conditions are known, developing a smooth ship digital twin. Then, relations can be found between predicted speed and actual speed with a fouled hull over time. For the current research, both assessment on how to predict speed loss and increase in power will be explained, as the problem can be seen from two angles:

- Ship power stays equal and marine biofouling growth results into loss of ship speed
- Ship sails at constant speed and marine biofouling results into additional required power

Even though both are explained, increase in power will be used as the main parameter for this research. This is due to the fact when increase in required power in known, additional fuel cost can easily be estimated. Building a digital twin ship is a time consuming process, and in this case a lot of relevant data is already available within Feadship. Since the goal is not to develop an all data-driven/black box model but rather to fill gaps with a black box model, the choice will be made to use Feadship data for ship power prediction in non-fouled condition. This choice has also been made since sensor data with clean ship is not always available. With a smooth ship prediction, calculated predictions can be made on expected power in a fouled situation, providing the black box with a full white box prediction and all data for fouling predictions.

With relevant data on ship condition, weather and water conditions, and vessel speed compared to power, fouling relations can be found over time. With given speed and outside conditions, for each situation the expected smooth power can be predicted. The real power then shows the difference due to biofouling. According to Calder (1992), the main engine degrades very slowly in time and related effects are only noticeable after years of operations apart from regularly maintenance. On the other side, fouling effects are visible within months of operation. To this extent, it can be assumed that almost all change in power within a short period of time follows from fouling effects. This can also be validated by comparing data prior and after hull & propeller treatment. The goal is to find to what extent different parameters, as some of the presented above, weigh on total biofouling growth, so that future marine biofouling margin can be predicted. With this black box proposal, MR.5.1 and MR.5.2 can be met. More information on how the black boxes will be set up will be discussed in chapter 5.

3.2.3. Black Box & Problem Coverage

With the following steps taken the black box model is now fully explained. With the selection of the DELM, a black box model that can capture ship-specific and environmental data is selected, inline with MR.4. Furthermore, the black box model will be specifically programmed to improve the white box shortcoming as discussed in subsection 3.1.3. With this MR.5 will be fulfilled. This is done with proposal of a black box that can predict marine biofouling growth (MR.5.1) and fouling change during sailing (MR.5.2) while taking into account full effect on ship performance and antifouling systems. For MR.6, it was important that the black box model could extract the level of marine biofouling from the ship data set. With both marine biofouling development during anchorage and sailing available, predictions can be made on future power increase over time. Being able to predict this added sea margin over time gives insight into the marine biofouling growth over time. With this, MR.6 is met. Next, it can be noted that the black box model will be based on available data within Feadship & De Voogt Naval Architects (MR.8) and that the model is based on various vessels within the Feadship fleet (MR.9). Last, it is important that all data used for the model is checked to filter out errors in voyage data. To do so the same function(s) will be used as for the white box model, inline with MR.10.

3.3. Grey Box Modeling

With both the white box (section 3.1) as the black box (section 3.2) discussed, last the the grey box model will be discussed. The grey box is where both models have to be combined to come to the final model, able to fulfill all method requirements and give all required output. Grey box modeling is a technique used more and more within the maritime industry to combine classical white box models with new vessel data and improve models and predictions with both strong inter- and extrapolation. For example, Leifsson and others (2008) simulated operational optimization of ocean vessels. Yang et al. (2019) modelled fuel consumption of ships towards sustainable shipping with a grey box model. As part of Delft University of Technology, fellow researchers and recent graduates have also shown promising results when it comes to grey box modeling. Trim optimization for ships in service has been optimized by Zwart (2020), a reference-based design approach has been developed by Bakker (2021) and early stage energy consumption predictions have been made by Odendaal (2021).

To combine both white box and black box models, either a parallel and series configuration can be chosen, as shown in Figure 3.4. Series configuration uses data computed by one box to partly power the other. Parallel configuration adds different results of both boxes or finds a desirable average.

(a) Serial configuration.

(b) Parallel configuration.
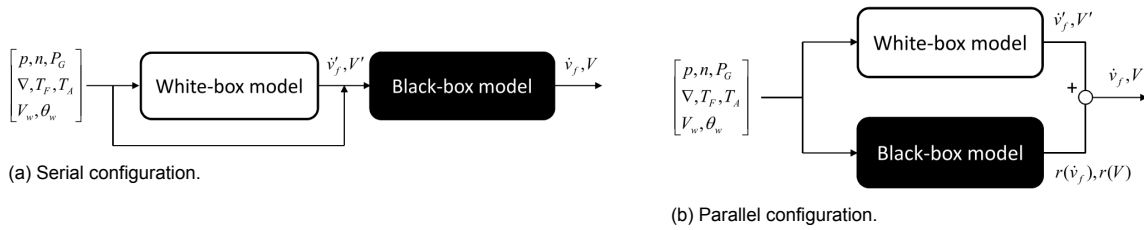
Figure 3.4: Grey box modeling, from Leifsson et al. (2008).

For the current case, a serial configuration will be used. This means that all the data that is used in the model is both applied to the black box and white box. However, white box predictions are not final, as these are used as extra input for the black box, making the model grey. As discussed in subsection 3.1.3, the white box does not cover all aspects of the complex problem of biofouling or all aspects. In the white box, first the equivalent sand roughness height is computed as discussed in subsection 3.1.1. Next, the added frictional resistance is calculated together with the loss of propeller efficiency to find the added sea margin due to biofouling growth, as discussed in subsection 3.1.2. The black box can make predictions for changes in fouling for both anchorage and sailing. Next, white box predictions are used as additional input to give a better prediction for ship fouling sea margin. Overall, this will result into the grey box as shown in Figure 3.5. With the flow of white box and all data into the black box, the requirement to make this a grey box model (MR.7) is satisfied.
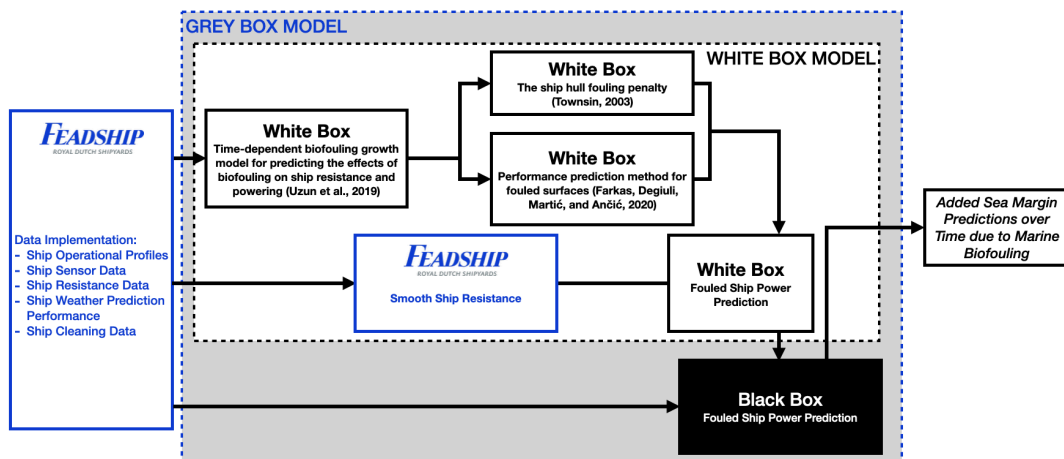
Figure 3.5: Proposed grey box model.

3.4. Method Requirement Assessment

As a last step, in Table 3.4, each method requirement is reviewed to check if it integrated into the final solution. As can be seen in the table, the final grey box model corresponds to all method requirements set in the problem analysis. With this, the main goal of the method exploration is met.

		White Box	Black Box	Grey Box
A white box model that predicts marine biofouling growth overtime.	MR.1	✓		✓
A white box model that predicts added hull resistance as a result of marine biofouling.	MR.2	✓		✓
A white box model that predicts reduced propeller efficiency as a result of marine biofouling.	MR.3	✓		✓

A black box model that successfully captures ship-specific and environmental phenomena.	MR.4		✓	✓
A black box model that improves approximations and knowledge gaps of white box model.	MR.5		✓	✓
A black box model that can predict marine biofouling growth, taking into account full effect on ship performance for different antifouling systems.	*MR.5.1*		✓	✓
A black box model that can predict marine biofouling detachment, taking into account full effect on ship performance for different antifouling systems.	*MR.5.2*		✓	✓
A black box model that successfully extracts level of marine biofouling from ship dataset.	MR.6		✓	✓
A grey box model that combines the white and black box models.	MR.7			✓
A method that is based on available data within Feadship & De Voogt Naval Architects.	MR.8	✓	✓	✓
A method that is based on various vessels within Feadship fleet.	MR.9	✓	✓	✓
A method that can filter out errors in voyage data.	MR.10	✓	✓	✓

Table 3.4: Method requirements assessment.

II
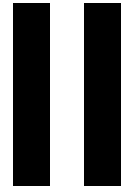
Methodology

Within the methodology, the grey box that was proposed as part of the problem introduction and exploration in Part I will be presented in detail. In chapter 4, the physical model to find the fouled ship power is presented. Here, the method to find the smooth ship resistance is explained, together with marine biofouling growth and its resulting added sea margin, which contains the hull resistance increase and the propeller efficiency loss. In chapter 5, the data-driven model is presented, which contains the black box for marine biofouling development during both anchorage and sailing. Here the white box prediction is added as an initial input to make the model grey. For clarity, an overview of this is shown in Figure 3.6, which is based on Figure 3.5. After the methodology, the model outcome will presented and will be used for the business case in Part III.
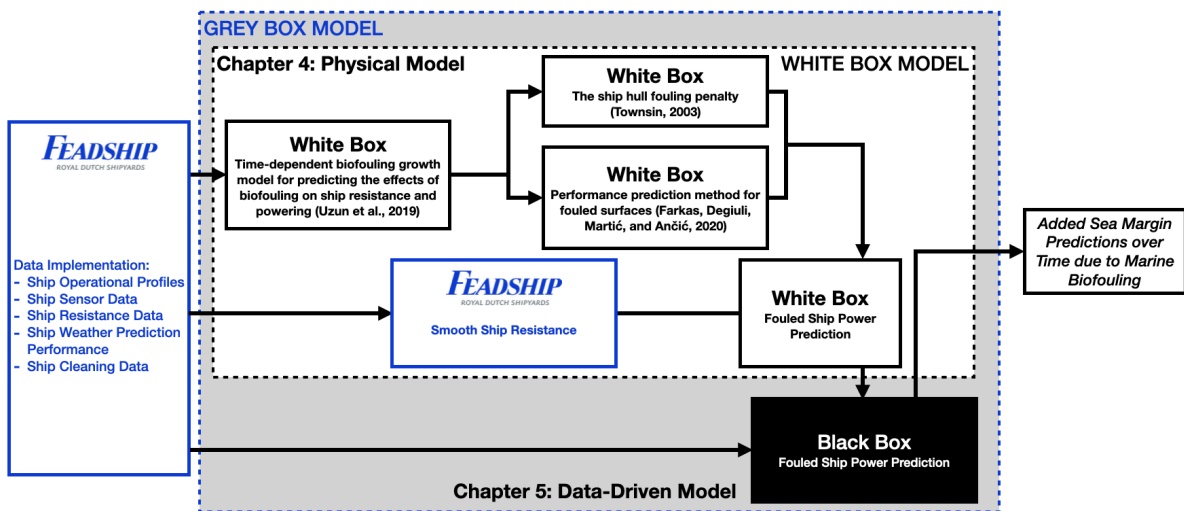
Figure 3.6: Methodology coverage for chapters 4 & 5.

4
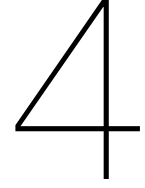
Physical Model

Within the previous chapter, the method to answer the main research questions have been explored. As a result, first a white box prediction will be made to find the fouled ship power. In section 4.1, the ship resistance is predicted based on a given condition for a smooth ship. Next in section 4.2, the model to predict marine biofouling growth will be discussed. After this, in section 4.3 the models to predict added sea margin due to the biofouling growth are presented. Last in section 4.4, the fouled ship power is predicted.

4.1. Smooth Ship Resistance

With the chosen grey box approach, first a white box prediction has to be made for the fouled ship power. Therefore, first the resistance for a smooth ship will be determined. Combining expected power in a smooth condition with additional fouling effects will then give a fouled ship power prediction. To make this prediction, Feadship yacht data and the calm water resistance will be used as a basis. After this, environmental conditions will be taken into account to compute resistance changes. With this, the smooth ship resistance will contain the following elements:

- Calm water resistance
- Wind resistance
- Wave resistance
- Resistance change due to water temperature difference

4.1.1. Calm Water Resistance

As a basis for the resistance prediction in any given condition, the calm water resistance is computed based on the ship speed. Here it is important that the speed over water is taken, rather than the speed over ground as measured with AIS. To find the speed over water, ship heading and speed is used together with the water current heading and speed, as shown below:

$$V_{S,x} = V_G \cdot \cos(\theta_G) + V_C \cdot \cos(\theta_C) \tag{4.1}$$

$$V_{S,y} = V_G \cdot \sin(\theta_S) + V_C \cdot \sin(\theta_C) \tag{4.2}$$

$$V_S = \sqrt{V_{S,x}^2 + V_{S,y}^2} \tag{4.3}$$

$$\theta_S = \arctan\left(\frac{V_{S,y}}{V_{S,x}}\right) \tag{4.4}$$

Where:

$V_{S,x}$	=	Ship speed in x-direction	[m/s]
$V_{S,y}$	=	Ship speed in y-direction	[m/s]
V_G	=	Ground speed	[m/s]
θ_G	=	Ground heading	$[rad]$
V_C	=	Current speed	[m/s]
θ_C	=	Current heading	$[rad]$
V_S	=	Ship speed	[m/s]
θ_S	=	Ship heading	$[rad]$

With the speed over water known, the calm water resistance (R_{calm}) can be determined based on the ship data, where the resistance at each speed is known for the given vessel. The calm water resistance forms the main body

for the resistance prediction. As an example, the calm water resistance relation is displayed in Figure 4.1 for one of the Feadship yachts.
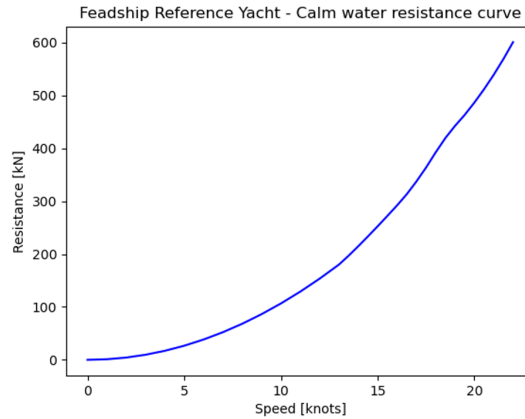
Figure 4.1: Calm water resistance for one of the Feadship yachts, only displaying relation and not values for privacy reasons.

4.1.2. Wind Resistance

To determine the added resistance due to wind, the wind resistance coefficient (C_X), area of maximum transverse section exposed to wind (A_{XV}), air density (ρ_A) and relative wind speed (V_{WR}) are used (ITTC, 2014). Here, the relative wind speed is based on the ship speed (V_S), wind speed (V_W) and wind direction (θ_W) (Aijjou et al., 2020). To compute the relative wind speed, Equation 4.6 can be used. To find the total air drag resistance, Equation 4.5 can be used.

$$R_{AA} = \frac{1}{2} \cdot C_X \cdot A_{XV} \cdot \rho_A \cdot V_{WR}^2 \tag{4.5}$$

$$V_{WR} = \sqrt{V_S^2 + V_W^2 + 2 \cdot V_S \cdot V_W \cdot \cos(\theta_W)} \tag{4.6}$$

4.1.3. Wave Resistance

To determine the added wave resistance, Feadship partly uses their privately developed VoogtWAVE method together with the Jonswap Spectral Density. VoogtWAVE gives a prediction of the added thrust in waves (taw) based on ship speed, heading, length, displacement and waterplane coefficient of the foreship. This method is based on the SPAWAVE method and adjusted for Feadship yachts (Grin, 2015). To maintain confidentiality, VoogtWAVE is not further presented and SPAWAVE will be introduced briefly to understand how the added thrust waves (taw) is formed for the Jonswap Spectral Density. Added resistance due to waves is induced by radiated waves as a result of ship motions, together with reflected waves as a result of incoming waves reflecting against the ships hull. On short and long waves, the following can be noted (Burger, 2017):

  • Short waves do not influence the motion of the vessel as the wave height of short waves is limited. Wind waves are generally short waves and give the largest contribution to wave reflection.
  • Long waves or swell waves provide the largest contribution to wave radiation. For wave radiation calculations it is important to take into account the loading condition as this determines the motion response.

In Figure 4.2, the parameters that influence the non dimensional added thrust in waves are shown. For more information, the paper by Grin (2015) can be consulted.
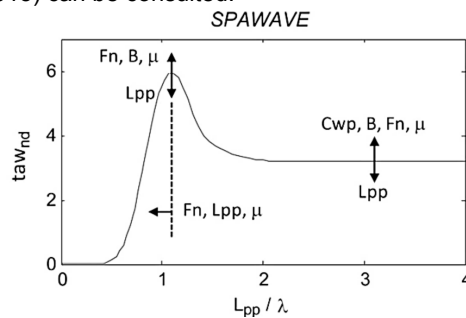
Figure 4.2: Influence of length between perpendiculars (Lpp), width (B), Froude number (Fn), waterline coefficient (Cwp), ship heading (μ) and wave length (λ) on the non dimensional added thrust in waves taw_{nd} in SPAWAVE, from Grin (2015).

With the added thrust in waves known, next the added wave resistance must be found. An actual sea state is normally described by a wave spectrum such as the Pierson-Moskowitz (1964). To allow for flexible spectrum shapes, the spectrum is multiplied with the peak enhancement factor (γ), defining the JONSWAP spectrum as expressed below (Hasselmann et al., 1973):

$$S = \frac{\alpha g^2}{\omega^5} \exp\left[\frac{5}{4}\left(\frac{\omega_p}{\omega}\right)\right] \gamma^{\exp\left[\frac{(\omega-\omega_p)^2}{2\sigma^2-\omega_p^2}\right]} \tag{4.7}$$

For the added wave resistance, it is important to notice that irregular waves can be represented as linear superposition of the components of regular waves. This resistance can be elaborated as follows:

> 'The mean resistance increase in short crested irregular waves (R_W) is calculated by linear superposition of the directional wave spectrum (E), and the response function of mean resistance increase in regular waves (R_{wave})' (ITTC, 2014, p. 8).

Here, the directional wave spectrum (E) is found by multiplying the JONSWAP spectrum (S) with the angular distribution function (G). Overall, the wave added resistance can be written as displayed in function Equation 4.8.

$$R_W = 2\int_0^{2\pi}\int_0^\infty \frac{R_{wave}(\omega,\alpha,V_S)}{\zeta_A{}^2}E(\omega,\alpha)d\omega\,d\alpha \tag{4.8}$$

The method proposed is largely inline with the ITTCs advice for the added wave resistance, with detailed computation of regular wave thrust (taw) and extension of JONSWAPS peak enhancement factor.

4.1.4. Displacement & Temperature Difference Resistance Change

Last, a correction can be accounted for difference in resistance due to change of temperature ($\Delta R_{\Delta T}$) and change of displacement ($\Delta R_{\Delta D}$) of the ship, caused by a change in water properties. This approach is taken since the predicted resistance is build upon the ships calm water resistance, rather than computing all factors of the ships resistance. With the ship resistance known at a certain water temperature, density and salinity condition, the resistance changes for the current condition must be taken as a correction. The approach taken is based on the change in density of the water (ρ, ρ_0, C_{T0}) and change of frictional resistance coefficient for given water temperature and salinity (C_F, C_{F0}), as displayed below (ITTC, 2014; 26th ITTC Specialist Committee on Uncertainty Analysis, 2011):

$$\Delta R_{\Delta D} = R_{T0}\left(\frac{\rho}{\rho_0} - 1\right) \tag{4.9}$$

$$\Delta R_{\Delta T} = R_F\left(\frac{C_{F0}}{C_F} - 1\right) \tag{4.10}$$

Within these equations, the total resistance for the reference water temperature and salt content (R_{T0}) and the frictional resistance for actual water temperature and content (R_F) can be determined as follows:

$$R_{T0} = \frac{1}{2}\rho_0 S V_S{}^2 C_{T0} \tag{4.11}$$

$$R_F = \frac{1}{2}\rho S V_S{}^2 C_F \tag{4.12}$$

For the frictional resistance (R_F), two things must be considered:
- Frictional resistance is also covered in the white box approach (subsection 4.3.1) together with the approximation of the frictional resistance coefficient (C_F, subsection 4.3.2)
- Difference in this section compared to the white box is that numbers for a clean hull are used rather than already taking into account an added resistance factor (ΔR_F), since the goal is to compare predicted clean hull performance to actual rough hull performance

4.2. Marine Biofouling Growth

In this section, further elaboration will be given on how the marine biofouling growth is computed over time.
- **Model basis:** Uzun, D., Demirel, Y., Coraddu, A., & Turan, O. (2019). Time-dependent biofouling growth model for predicting the effects of biofouling on ship resistance and powering. *Ocean Engineering*, *191*. https://doi.org/10.1016/j.oceaneng.2019.106432.
- **Goal:** Using anchor locations and time to find the increase in biofouling roughness on the ship.

The chosen model makes use of two main principles: a fouling rating and the fouling surface coverage for barnacles and calcareous fouling. The fouling rating forms a basis for the model, combining slime, non-shells organisms and calcareous fouling into one overall fouling rating. Overall, this gives a good indication on the level of fouling present on the ship and its resulting roughness. However, when calcareous fouling is present on the ship, its level of surface coverage can be a dominant factor. Due to this, the calcareous surface coverage was introduced by the authors as an additional parameter. Based on the levels for these two parameters, the roughness thickness present on the ship can be determined, which is modelled with the equivalent sand roughness height. An overview of this process is shown in Figure 4.3. For all functions, variables, and a detailed formulation of the model, Appendix A can be consulted.
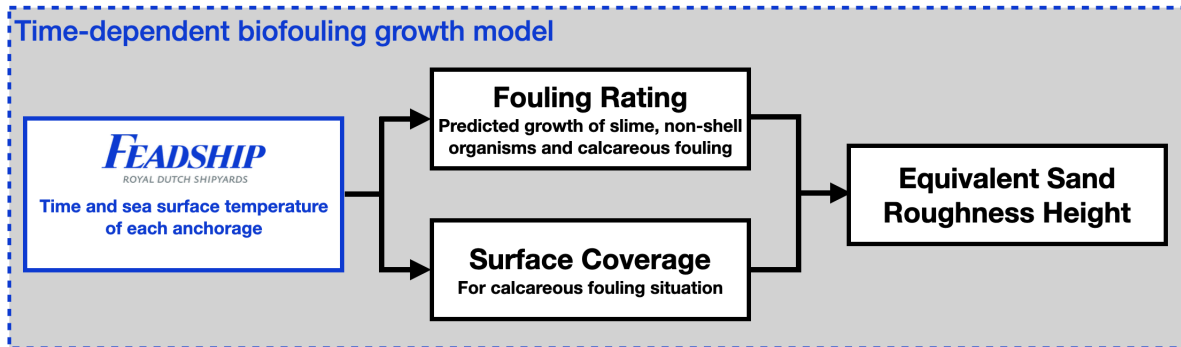
Figure 4.3: Marine biofouling growth & resulting equivalent sand roughness height determination, illustrative overview of model by Uzun et al. (2019).

4.2.1. Model Usage & Limitations

In the introduction of this section, it was shown how roughness is a found by either using fouling rating or surface coverage. However, in between these two, there is a gap, as they do not connect. It can be found that the fouling rating can be used until a fouling rating of 70, which leads to a total equivalent sand roughness height of 1,000.2 micrometers. The calcareous surface coverage can only and must be used when this value passes the 5%, and results in a equivalent sand roughness height of 1003.1 micrometers. With only a small difference in roughness between them and enough time, interpolation to connect both was used. An overview of the suggested interpolation for both regions is shown in Figure 4.4.
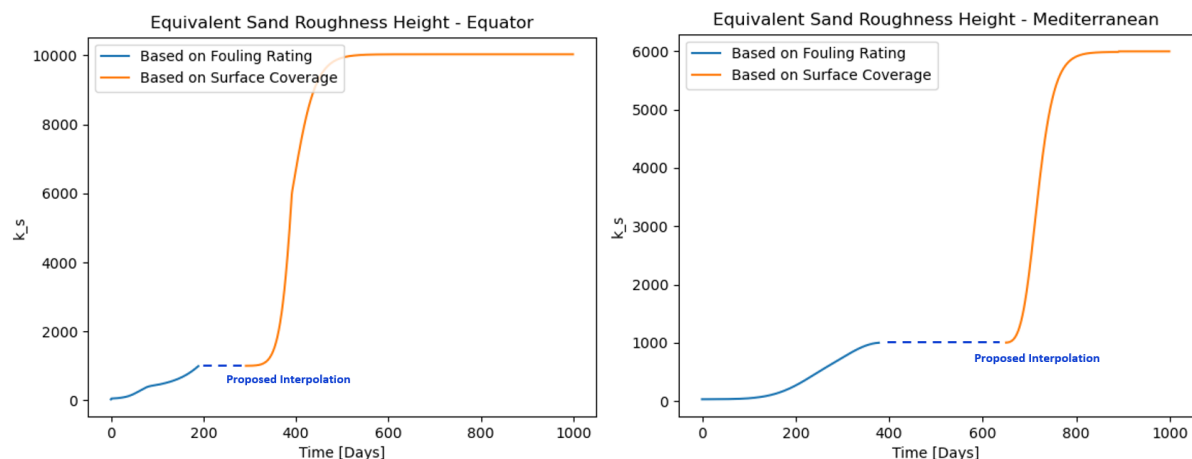
(a) Equator.

(b) Mediterranean.

Figure 4.4: Equivalent sand roughness height based on Uzun et al. (2019) together with proposed interpolation for missing values.

Since the data is limited to the Equator and Mediterranean regions, the authors suggest to interpolate and extrapolate found patterns based on sea surface temperature as the dominant fouling parameter. In case only ship location is known, Equation 4.13 is introduced. The function can be used to compute the Sea Surface Temperature (SST) for any location, where it is important to note that differences in temperature due to longitude changes were neglected as these differences are relatively small compared to latitude changes (Uzun et al., 2019; Pielke, 2012).

Interpolation and extrapolation can then be done with Equation 4.14, where the sea surface temperatures and antifouling performance parameters are used from locations x and y are used. With help of this function, biofouling growth trends found for the Equator and Mediterranean can be inter- and extrapolated for all locations. Last, the authors also propose to scale all logarithmic constants for the calcareous surface coverage curves. However, doing so results into strange and unrealistic curves. For this reason, the curves are first formed based on the constants and are then interpolated and extrapolated based on sea surface temperature.

$$SST_a = 12.5 + 15 \left(cos \left(\frac{latitude\ degree}{28.64} \right) \right) \tag{4.13}$$

$$\eta_{ca}(\Delta SST) = \frac{\eta_{cy}(SST_a - SST_x) + \eta_{cx}(SST_y - SST_a)}{SST_y - SST_x} \tag{4.14}$$

With marine biofouling predictions now available for all locations, last it is important how these anchorage studies can be combined over ships operational time. The current model is based on static measurements over a longer period, thus lacking information of fouling changes during sailing. With a SPC coating for the current model, the assumption has been made by the authors that marine biofouling detachment is not occurring, as it is not realistic to reach the required shear stresses in order to overcome the adhesion strengths of biofouling organisms on biocidal antifouling coatings (Uzun et al., 2019; Oliveira and Granhag, 2016). This also means that the model is less suitable for use with coatings that rely on fouling detachment processes, as corrections should be accounted for sailing periods. Nevertheless, in the method exploration of this study, it was determined that fouling changes during sailing can be found within the grey box model.

For the current model, no fouling changes during sailing means that the ship will go into a new anchor location with the same fouling rating and surface coverage as in the previous region. For the current model, it is important that when a new region is entered, it is obtained at which day in the growth process the biofouling currently is in this new region. This is an important step since a year in the Equator does not result into a year in the Mediterranean. Thus when a new region is reached, this means that the ship is at a different day in the growth process for this region.

For the current research the steps explained above are taken. In case a more simple approach is desired, users could also obtain roughness curves for both regions first (as shown in Figure 4.4), and then interpolate and extrapolate accordingly. Last it is important to mention that when a vessel is cleaned and antifouling is reapplied, both surface coverage and fouling rating are set back to zero. With ability of combining marine biofouling growth during anchorage intervals over a ships operational time for all locations, the resulting equivalent sand roughness height can now be computed for each ship. Overall, the most important model limitations can be summarized as follows:
- Model is based on Equator and Mediterranean fouling measurements, with interpolation and extrapolation recommended based on only sea surface temperature, making the model less applicable for regions colder than the Mediterranean.
- Measurements taken over a longer period throughout different seasons, which are not filtered or identified.
- Model based on salt water, it is known that salinity has a substantial effect on fouling growth. Furthermore, different species grow and live in salt water then in sweet water, making the model less applicable for sweet water locations.
- Model based on SPC coating, fouling changes during sailing not taken into.

4.3. Added Sea Margin due to Biofouling
Within this section, the computation of added hull resistance and loss in propeller efficiency will be explained. As part of resistance changes, some attention is also given to change wave making resistance due to fouling. The approaches taken is based on the choices made within the method exploration.
- **Model basis resistance:** Townsin, R. (2003). The ship hull fouling penalty. *Biofouling*, *19*(S1), 9–15
- **Model basis propeller:** Farkas, A., Degiuli, N., Martić, I., & Ančić, I. (2020b). Performance prediction method for fouled surfaces. *Applied Ocean Research*, *99*. https://doi.org/10.1016/j.apor.2020.102151
- **Goal:** Compute the added hull resistance and loss of propeller efficiency based on the equivalent sand roughness height, to find the increasing sea margin as a result of marine biofouling growth over time.

4.3.1. Added Resistance
The total resistance of a ship can be seen as a combination of frictional, residual and air drag resistance, as shown in the equation below.

$$R_T = R_F + R_R + R_{AA} \tag{4.15}$$

Here, the residual resistance can mainly be divided into the wave making resistance and to the viscous pressure resistance. By using the form factor $(1 + k)$, viscous pressure and friction resistance can be combined. It can

be seen that an increase of biofouling will result into an increase of the frictional resistance due to biofouling. Therefore, the equation can be written as followed (Demirel et al., 2017,Oliveira et al., 2018):

$$R_T = (1 + k)R_F + \Delta R_F + R_W + R_{AA} \tag{4.16}$$

Added Frictional Resistance
The added resistance as a result of marine biofouling can mainly be captured in increase in frictional resistance. To do so, the increase in frictional resistance coefficient will be computed, as shown in Equation 4.17. Here the change in frictional resistance coefficient (ΔC_F) is calculated based on the equivalent sand roughness height (k_s), the ship waterline length (L_{WL}) and the Reynolds number (Re).

The determination of the Reynolds number is shown in Equation 4.18, where u is the flow speed and ν is the kinematic viscosity (Klein Woud and Stapersma, 2002). Here, the viscosity is dependent on water temperature for either fresh or salt water (26th ITTC Specialist Committee on Uncertainty Analysis, 2011). The flow speed is taken as a average number across the hull. In subsection 4.3.3, an approach will be discussed into dividing the flow speed and the frictional resistance coefficient across different regions of the ship. With this approach, answers within the business case that was mapped out can be answered to estimate the weight of different ship sections in the total added frictional resistance.

$$\Delta C_F = 0.044 \left[\left(\frac{k_s}{L_{WL}} \right)^{\frac{1}{3}} - 10 \cdot Re^{-\frac{1}{3}} \right] + 0.000125 \tag{4.17}$$

$$Re = \frac{uL_{WL}}{\nu} \tag{4.18}$$

Next, the added frictional resistance coefficient can be computed to the increase in frictional resistance, as shown in Equation 4.19 and outlined in the method exploration.

$$\Delta R_F = \frac{1}{2}\rho S \Delta C_F V_S^2 \tag{4.19}$$

It is known that the total ship resistance is a combination of frictional resistance, air drag resistance and residual resistance, where the latter includes wave resistance, viscous pressure resistance, and the additional resistance due to the form or curvature of the hull. Not only does biofouling have an influence on frictional resistance, also the wave making resistance can change as a result of biofouling.

Change in Wave Resistance
Although marine biofouling mainly has an influence on the frictional resistance of the ship, it can be noted that it also has effects on the wave resistance. One of the key findings by Demirel et al. (2017) is the decreasing wave resistance with an increasing surface roughness. This trend was later also found by Oliveira et al. (2018), Song et al. (2020b), and Kanninen et al. (2022). It is important to mention that these findings go against the traditional view that wave-making resistance is not affected by hull-roughness (Institution and of Ships, 1952):

> "The findings by Demirel et al. agree well with other numerical studies that demonstrated viscous effects on wave patterns, namely that the boundary layer thickness (which is increased by hull roughness) changes the stern pressure field, leading to dampening of the stern wave system" (Oliveira et al., 2018, p. 8).

In Figure 4.5, the changes in wave pattern for a smooth and heavy calcareous fouled hull are presented. In these figures, the characterised damping of the stern wave system in the fouled situation is clearly visible.

(a) Smooth condition.

(b) Heavy calcareous fouling condition.
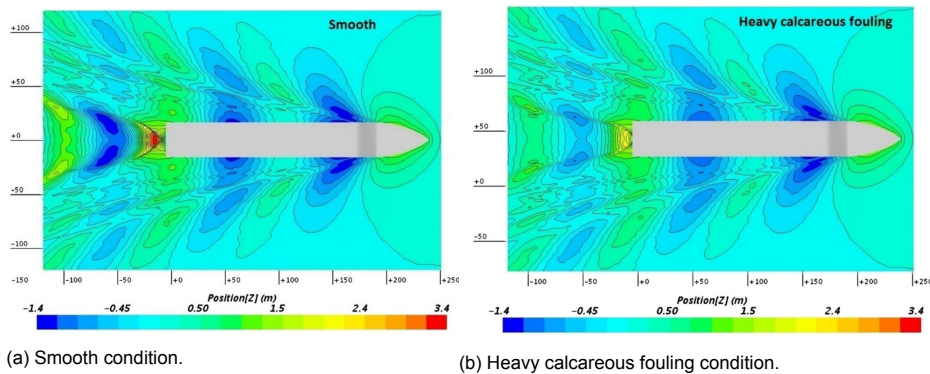
Figure 4.5: Wave patterns for smooth and heavy calcareous fouling condition ($V_s = 24$ knots), from Demirel et al. (2017).

Oliveira et al. re-analyzed the results by Demirel et al. to determine the extent to which the form of the hull can affect the penalty due to hull roughness. This was done for speeds of 19 knots and 24 knots, for 7 different fouling scenarios. With little additional research yet done in this field to the authors knowledge, the found changes in resistance wave coefficient can be used as a basis in case the added wave resistance must be computed with fouling present on the hull. It can be noted that this part is not fundamental to find an overall sea margin for calm water resistance, but can improve calculations for ship performance with fouling in waves. It is proposed to interpolate and extrapolate between both speeds and fouling to get an average percentage correction for wave coefficient (ΔC_W). The corrections used are shown in Table 4.2.

Equivalent Sand Roughness Height (k_s)	19 knots	24 knots
0 (μm)	-	-
30 (μm)	-1	-1
100 (μm)	-7	-10
300 (μm)	-12	-15
1,000 (μm)	-17	-22
3,000 (μm)	-22	-27
10,000 (μm)	-18	-30

Table 4.2: Percentage change in ΔC_W at 19 and 24 knots, from Oliveira et al. (2018).

Oliveira et al. show that as fouling increases along the ship, the wave resistance continuously decreases. It can be seen that this effect is larger for a higher velocity, which can be attributed to the fact the contribution of the viscous effects becomes more important on lower speeds.

It needs to be emphasized that the chosen approach is a very rough approximation of the change in wave resistance due to biofouling. However, with lack of empirical models available, this gives the opportunity to account for this change without large additional steps taken, as this is not the main part of this research or a crucial step within the model. Furthermore, the change in viscous resistance is taken into account with the ship and speed specific form factor, as the other part of the residual resistance. It is the author belief that this is a better approach as not accounting for this change at all. Overall, realizing that wave resistance decreases with increase of biofouling instead of a traditional approach were no changes are identified, can be seen as an important relation and understanding.

4.3.2. Propeller Efficiency Loss

In the method exploration, the model by Farkas et al. (2020b) was selected to compute the change in thrust and torque coefficient due to biofouling, and find a new open water efficiency / operating point of the propeller. This is done by finding the change in drag and lift for both coefficients, as highlighted in Equations 4.20 and 4.21. Here subscript S and R represent the smooth and rough condition.

$$K_{TR} = K_{TS} - \Delta K_{TD} - \Delta K_{TL} \tag{4.20}$$

$$K_{QR} = K_{QS} - \Delta K_{QD} - \Delta K_{QL} \tag{4.21}$$

The chosen method makes use of the added frictional resistance due to roughness, and uses propeller characteristics as propeller pitch (P), diameter (D), number of blades (Z), chord length (c) and maximum thickness (t). Here it is important to mention that both chord length and maximum thickness are taken at radius $0.75R$. First the changes as a result of drag coefficient will be determined, as shown in the functions below:

$$\Delta K_{TD} = -\Delta C_D \cdot 0.3 \frac{P}{D} \frac{cZ}{D} \tag{4.22}$$

$$\Delta K_{QD} = \Delta C_D \cdot 0.25 \frac{cZ}{D} \tag{4.23}$$

However, in order to perform these steps, first change in drag coefficient (ΔC_D) must be computed. This can be done by taking into account drag coefficient in smooth condition (C_{DS}) and the drag coefficient in rough condition (C_{DR}) as functions of the frictional resistance coefficients for smooth (C_{FS}) and rough condition (C_{DR}).

$$\Delta C_D = C_{DS} - C_{DR} \tag{4.24}$$

$$C_{DS} = 2\left(1 + \frac{t}{c}\right) \cdot C_{FS} \tag{4.25}$$

$$C_{DR} = 2\left(1 + 2\frac{t}{c}\right) \cdot C_{FR} \tag{4.26}$$

It can be noted that at this point, the added frictional coefficient due to biofouling (ΔC_F) can be computed with help of the function of Townsin, as discussed in subsection 3.1.2, where the chord length at radius 0.75R can serve as the plate length. To compute the frictional resistance coefficient in smooth (C_{FS}) and rough (C_{FR}) state, first the frictional resistance coefficient for smooth condition (C_{FS}) must be found, which can be done by either using Schroenherrs friction line (Equation 4.27) or with the ITTC-1957 skin friciton line (Equation 4.28). To save computational time, the latter will be chosen (Farkas et al., 2020b; ITTC, 2011).

$$\frac{0.242}{\sqrt{C_{FS}}} = log(Re \cdot C_{FS}) \tag{4.27}$$

$$C_{FS} = \frac{0.075}{(log(Re) - 2)^2} \tag{4.28}$$

With the change in drag coefficient (ΔC_D) now known, changes as a result of the lift can now be found. Changes as a result of reduced value of lift coefficient (ΔC_L) can be determined for both the thrust and torque coefficient with the equations below. Here, J represents the advance coefficient, used to express propeller speed as a function of advance velocity, propeller speed and propeller diameter.

$$\Delta C_L = -1.1\Delta C_D \tag{4.29}$$

$$\Delta K_{TL} = \Delta C_L \frac{cZ}{D} \cdot \frac{0.733 + 0.132J^2}{\sqrt{1 + 0.18\left(\frac{P}{D}\right)^2}} \tag{4.30}$$

$$\Delta K_{QL} = \Delta C_L \frac{cZ}{D} \cdot \frac{0.117 + 0.021J^2}{\sqrt{1 + 0.18\left(\frac{P}{D}\right)^2}} \tag{4.31}$$

With changes as shown in Equations 4.20 and 4.21, the new propeller open water efficiency for the rough condition (η_{OR}) can now be calculated with the functions below (Klein Woud and Stapersma, 2002).

$$J = \frac{v_a}{nD} \tag{4.32}$$

$$\eta_{OR} = \frac{J}{2\pi} \frac{K_{TR}}{K_{QR}} \tag{4.33}$$

4.3.3. Non Uniform Distribution of Added Frictional Resistance

One of the goals set in the business case of Feadship (subsection 1.6.2) was to be able to see effect of regions with high flow on total fouling resistance. It is known that added roughness has a larger effect on regions with high flow and thus higher Reynolds numbers. For this reason, it could be interesting for Feadship to invest extra in high flow regions compared to low flow regions. Example could be to use different type of products for special regions. For Equation 4.17, this would mean that the equation must be split up into different regions of the yacht with different levels of flow speed. The equation can be split up into regions with different wetted surface areas with different equivalent sand roughness heights. Even though it is hard to predict how fouling growth would change with more/different antifouling coating, a different fouling level for these locations does give insight into its effect on total ship resistance. Here, it is important to note that for these different regions, the different Reynolds numbers can be taken into account as well, to get a better overview on their total weight on the added ship resistance.

Splitting up Equation 4.17 is however more complicated than it seems. The wetted surface area can easily be split and summed up for different regions. With these regions, different equivalent sand roughness heights and Reynolds numbers could be entered to compute differences. However, with waterline length powered to the one third, splitting this factor is more complicated. This is the case since the function is based on flat plate friction. Friction at the beginning and end of plates is higher than in the center. For this reason, it is powered by one third and multiple plates with shorter length weigh heavier combined to one long plate. This leaves two options to deal with waterline length in this function, as discussed below and shown in Figure 4.6.

(a) Use waterline length of each separate section for determination added frictional resistance coefficient due to biofouling, with differentiation in wetted surface area, equivalent sand roughness heights, and Reynolds number. Each section is seen as separate plate with length powered to the one third.

(b) Use waterline length of full ship and for equation and then factor by percentage of section length. This way, the different length sections summed will have an equal weight in the added frictional resistance coefficient compared to when the formula was not split up. Each section is seen as part of full waterline length of ship that is powered to the one third.
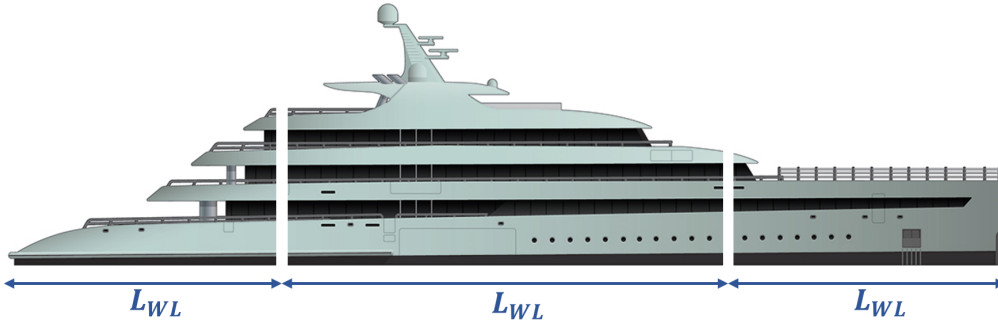
(a) Waterline length in function of Townsin based on section length, $L_{WL}^{\frac{1}{3}}$ for each section.
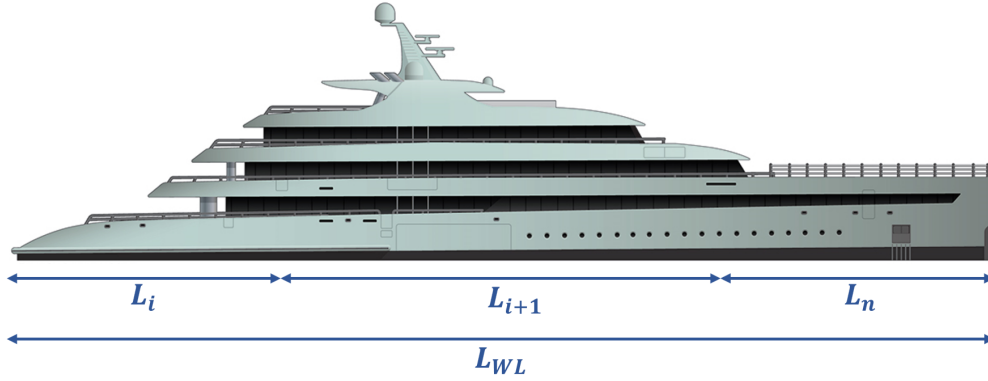
(b) Waterline length in function of Townsin based on fraction of full waterline length of ship in equation, $\frac{L_i}{L_{WL}} \cdot L_{WL}^{\frac{1}{3}}$ for each section.

Figure 4.6: Options for waterline length division in function of Townsin.

The goal for the business case is to give insight in possible changes on the total added sea margin due to biofouling, and what investments can possibly be best. This means that both functions are a best educated guess, rather than a physically correct approximation. This is the case since a powered function cannot be split up into multiple factors in a correct mathematical way. However, in this case it is most important that the formula that is split up does give equal result when same fouling and Reynolds numbers are entered into the equation, compared to the normal formula. This is a verification step that has to be taken to make sure the function keeps a correct formulation. For this reason, the second proposed option has to be chosen. Here it can be noted that when different values are entered, the formula is the best approximation for the full picture with use of Townsins function. Here it is important to mention that there is currently no function to do a comparable approximation. If there was more interest in this strategy, both towing tanks tests and CFD calculations could be performed to find more accurate answers. With limited time within this research and this point not being the main scope, the proposed formula adaption does seem like a good approximation to give some additional insight for the business case. If antifouling application plans are made later based on this function, it could be validated to what extent this approximation was true. Since this is not the main port the current research, the proposed adaption of the formula of Townsin seems sufficient to give some additional information as part of the already developed method, without doing a full new research. An overview on how the added frictional resistance due to biofouling can be approximated with ship length split up is shown below:

$$\Delta R_F = \sum_{i=1}^{n} \left(\frac{1}{2} \rho S_i V_S^2 \left(0.044 \left[k_{s,i}^{\frac{1}{3}} \cdot \frac{1}{L_{WL,i}/L_{WL} \cdot L_{WL}^{1/3}} - 10 \cdot Re_i^{-\frac{1}{3}} \right] + 0.000125 \right) \right)_i +$$

$$\left(\frac{1}{2} \rho S_{i+1} V_S^2 \left(0.044 \left[k_{s,i+1}^{\frac{1}{3}} \cdot \frac{1}{L_{WL,i+1}/L_{WL} \cdot L_{WL}^{1/3}} - 10 \cdot Re_{i+1}^{-\frac{1}{3}} \right] + 0.000125 \right) \right)_{i+1} +$$

$$\left(\frac{1}{2} \rho S_n V_S^2 \left(0.044 \left[k_{s,n}^{\frac{1}{3}} \cdot \frac{1}{L_{WL,n}/L_{WL} \cdot L_{WL}^{1/3}} - 10 \cdot Re_n^{-\frac{1}{3}} \right] + 0.000125 \right) \right)_n \quad (4.34)$$

4.4. Fouled Ship Power Prediction

With smooth ship resistance outlined and fouling growth and effects predicted, next a fouled ship power prediction can be made. First the total resistance (R_T) can be found based on the calm water resistance (R_{calm}), the air drag resistance (R_{AA}), the wave resistance including changes due to biofouling ($R_W + \Delta R_W$), friction changes due to temperature ($\Delta R_{\Delta T}$), changes due to displacement ($R_{\Delta D}$), and added frictional resistance due to biofouling (ΔR_F), as shown below.

$$R_T = R_{calm} + R_{AA} + R_W + \Delta R_W + \Delta R_{\Delta T} + \Delta R_{\Delta D} + \Delta R_F \tag{4.35}$$

Next, the fouled brake power (P_{BR}) can be predicted, with the help of the found total resistance for the fouled situation together with ship speed, hull efficiency (η_H), rough open water efficiency, relative rotative efficiency (η_R), propulsive efficiency (η_D), gearbox efficiency (η_{GB}) and shaft efficiency (η_S) (Klein Woud and Stapersma, 2002):

$$P_E = R_T V_S \tag{4.36}$$

$$\eta_D = \eta_H \cdot \eta_{OR} \cdot \eta_R \tag{4.37}$$

$$P_D = \frac{P_E}{\eta_D} \tag{4.38}$$

$$\eta_{TRM} = \eta_{GB} \cdot \eta_S \tag{4.39}$$

$$P_{BR} = \frac{P_D}{\eta_{TRM}} \tag{4.40}$$

In the function above the efficiencies are defined as follows:

η_D	=	Propulsive efficiency	[-]
η_H	=	Hull efficiency	[-]
η_O	=	Open water efficiency	[-]
η_R	=	Relative rotative efficiency	[-]
η_{TRM}	=	Transmission efficiency	[-]
η_{GB}	=	Gearbox efficiency	[-]
η_S	=	Shaft efficiency	[-]

It can be seen that in the functions above, the brake power of the engines is computed towards effective towing power for the ship, and vice-versa. Here efficiencies for the shaft and gearbox (transmission), together with the hull and propeller (propulsive) efficiency are taken into account. An overview of this process is shown in Figure 4.7, where the brake horsepower (BHP) at the engine is converted to shaft horsepower (SHP), delivered horsepower (DHP) into effective horsepower (EHP). Note that the thrust horsepower (THP) is identified rather than effective horsepower, as this forms a part of the power transfer from delivered to effective power.
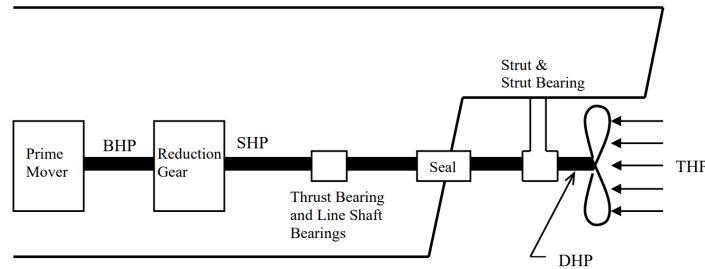
Figure 4.7: Simplified ship drive train, from United States Naval Academy (2022).

With these functions, the added sea margin as a result of marine biofouling is now clear. By finding power consumption compared to the smooth situation, added cost in fuel can be found and maintenance plans can be made to reduce cost. As shown in the function below, the mass flow of fuel is a direct result of the specific fuel consumption (sfc) and the given brake power (P_B). Note that the conversion from effective power to brake power depends on numerous factors, as the power delivered by the main engines is not equal to the effective power transferred into the water to tow the ship.

$$\dot{m}_f = sfc \cdot P_B \tag{4.41}$$

In case the speed loss due to biofouling would have to predicted, it can be seen that instead of combining measured speed and computed total resistance, a combination of measured power and total resistance could be used to find the new ship speed in a similar way. Last, in case it is desired to find the power increase due to biofouling, the same equations as above can be used. However, this time without the different fouling contributions in Equation 4.35 and with the smooth propeller efficiency rather than the rough in Equation 4.37.

5

Data-Driven Model

Within this chapter, the data-driven model as proposed in the method exploration will be presented (section 3.2). First, attention will be payed to the to be used input data for the grey box prediction in section 5.1. Next, in section 5.2, the data preparation for the model is presented. Last, the use of the Deep Extreme Learning Machine (DELM) will be further explained in section 5.3.

5.1. Grey Box Input

Before a model can be build, it should first be determined what information the grey box should be provided with, so that it can learn from this data and find a pattern. With the chosen approach, the available data is first used for a white box prediction, and then this prediction is combined with the original input data into a grey box prediction. This means that input parameters for the data-driven model include the physical model fouled ship power prediction, the variables that were used for finding the smooth ship resistance, the variables that were used for the fouling growth prediction, and variables that were used for finding the power based on these.

The smooth ship resistance prediction includes ship speed & direction, wave height, direction & period, and wind speed & direction. Next to this, additionally available motions data is used to improve the power prediction in general, including the smooth ship condition. To find fouling roughness, the average sea surface temperatures on anchorage locations were used together with the anchorage days. Therefore, in the current model both will be used as an input parameter, where the average sea surface temperature is taken over all anchorages. Next to anchorage, sailing days since clean ship and average speed when sailing are also taken into account. With the physical model lacking a prediction for fouling change during sailing, this is a part where a grey box prediction can improve accuracy to the total found power. The input information can be summarized as shown in Table 5.1.

Input variables	Output variable
White box fouled ship power prediction	
Ship speed	
Ship direction	
Wave height	
Wave direction	
Wave period	
Wind speed	
Wind direction	
Average sea surface temperature	Fouled ship power
Anchorage days since clean ship	
Sailing days since clean ship	
Average ship speed	
Mean roll	
Mean pitch	
Roll deviation	
Pitch deviation	

Table 5.1: Input and output variables for grey box model.

Currently the research will be focused on single vessels, with a data-driven model developed for specific ship predictions. However, once more vessel data becomes available, this introduces the possibility of learning relations between ships. For this reason, the important ship specific parameters can be entered into the model. From the physical model, it was learned that waterline length and wetted surface area are the main parameters that are important to determine added fouling sea margin. Furthermore, it can be seen that the type of antifouling has a very dominant influence on the level of fouling attachment and possible detachment, in case of a fouling release paint. Furthermore, this is also one of the most interesting parameters to study, as it gives insight in product scores. Last, it must be mentioned that when different ships are entered into the model, it is important that enough ships are entered, and that differences between some ships are not to big, so that relations on ship parameters on fouling growth can properly be learned by the algorithm. Summarized, when more ship data is available, the following variables can be added to the model:

- Ship length over waterline
- Ship wetted surface area
- Type of antifouling

With this chosen approach, a sailing factor could be computed separate, which could give a correction on white box predictions. This was an important step in the formation of the grey box model (section 3.3). With this, the information that goes into and out of the grey box is not determined. However, data must still be prepared and the grey box itself must still be built. This will be explained in sections 5.2 & 5.3 respectively.

5.2. Data Preparation

In section 2.5, the data available for this project was presented. This data was mainly available within three information sources:

- Marin reports: Ship design specifications clustered per ship
- Environmental database: Voyage report data clustered per ship based on AIS. Used to project speed, water temperature, waves, etc.
- Sensor datafiles: Engine and motion data for yachts equipped with sensor monitoring

The first two information sources, are available for a large part of the recent fleet and are sufficient for white box calculations, as presented in chapter 4. Once a data-driven model is built, these databases can also be used to make new predictions. However, to develop a data-driven model, the third information source is required, containing sensor data, with as most important variable the measurements of brake power of both engines. Next to integrating these data sources, data preparation consists of filtering, calculations and data scaling. An overview of this process is visualized in Figure 5.1 and explained throughout this section.
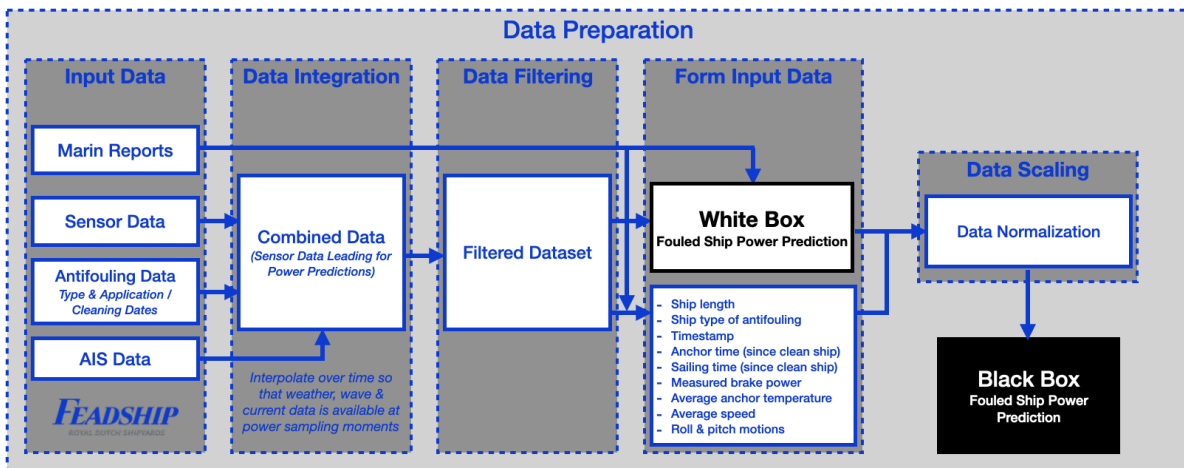
Figure 5.1: Data Preparation.

5.2.1. Input Data

Before further data preparation is presented, it is first important to get a better understanding of the data available. For this reason, some figures have been added which provide information on the ships operational profile and use. First in Figure 5.2, a logarithmic distribution is displayed for one of the yachts most frequent speeds and power used. The logarithmic scale has been chosen here since the vessel only sails roughly 15% of the time, which

would otherwise cause in only a largely visible frequency at zero speed and power.

(a) Ship speed in knots.   (b) Delivered brake power in kilowatts.
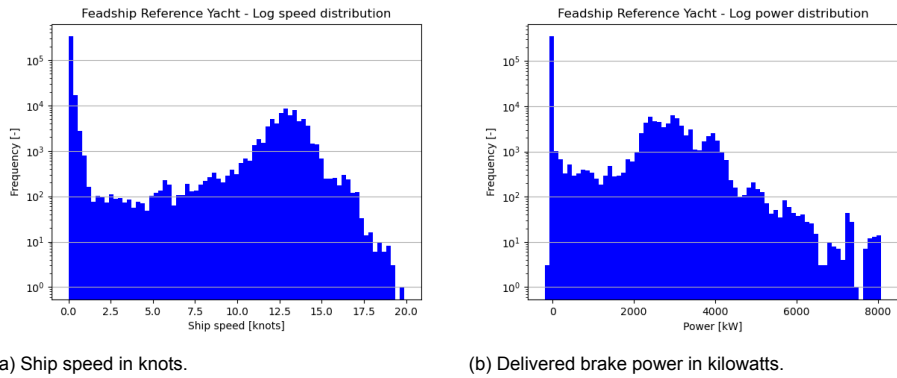
Figure 5.2: Logarithmic distribution of most frequent speeds sailed and total brake power delivered by the main engines.

To get an overview of the performance of the yacht, both the propeller speeds and ship speed are displayed for ship brake power output. In Figure 5.3, both these relations are visualized based on the sensor data available for a taken yacht. Here, a clear difference between both figures can immediately be identified. While the so-called propeller law ($P_B \propto n_p{}^3$) is very visible in the first figure, the second figure clearly shows a less standard output between ship speed and power. This output is expected as efficiencies are far more predictable within the ship rather than ship input to ship outside performance. Here, all resistance adding factors including fouling play a role.

(a) Propeller speed [rpm] against ship brake power [kW].   (b) Ship speed [knots] against ship brake power [kW].
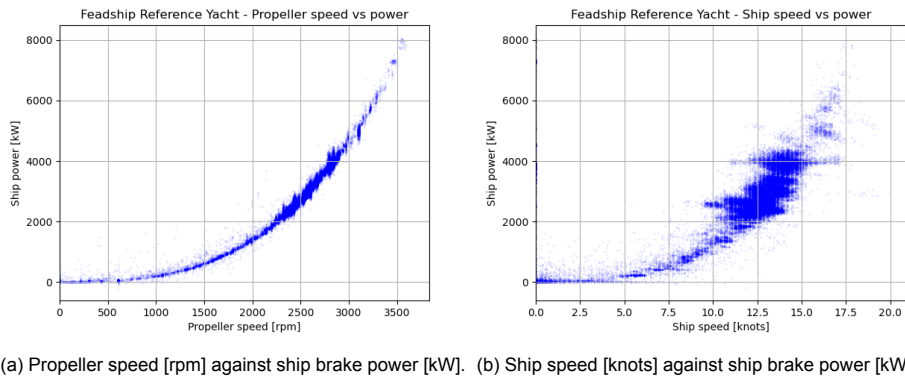
Figure 5.3: Comparison of propeller speed (left) and ship speed (right) at ship brake power.

To give some better insight into the operational profile of the displayed yacht, Figure 5.4 is added. Here, the ships speed over a 2-year period is displayed together with the measured water temperature over this time. In Figure 5.4b, it is clearly visible that ship is exposed to varying water temperatures as it moves across the globe and through different seasons, which can have large influence on the level of biofouling growth when anchoring in these locations.

(a) Ship speed [knots] over time.   (b) Water temperature [°C] over time.
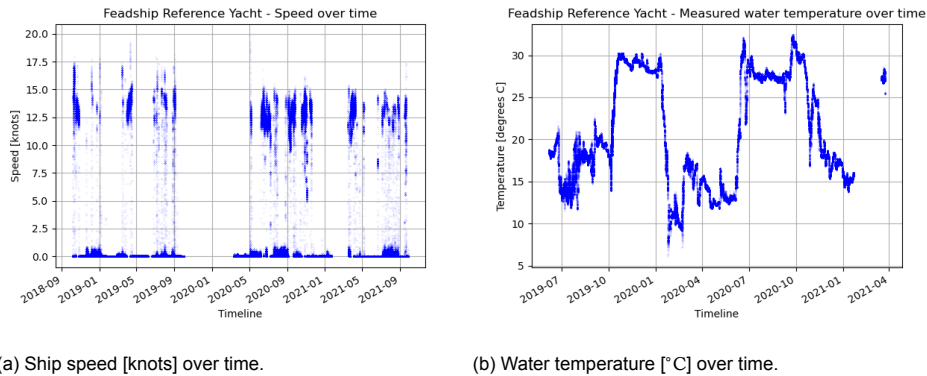
Figure 5.4: Speed and water temperature over time.

Since waves are not measured directly, ship performance in waves is a slightly more rough part of the method. Only motions data could give more accurate information on ship performance in waves. This means that the power as predicted for smooth hull is an overall good approach, but lacks some accuracy for ship wave resistance predictions. To overcome this inaccuracy, the grey box will also be provided with motion data at the time points of power predictions, so that the learning machine can better understand where possible extra margin can come from. It is expected that when ship motions are high, additional power was used. In Figure 5.5, insight is given into the most frequent roll and pitch mean motions. It can be noted that the deviation of roll and pitch motions is also available.

(a) Mean roll motion [deg].   (b) Mean pitch motion [deg].
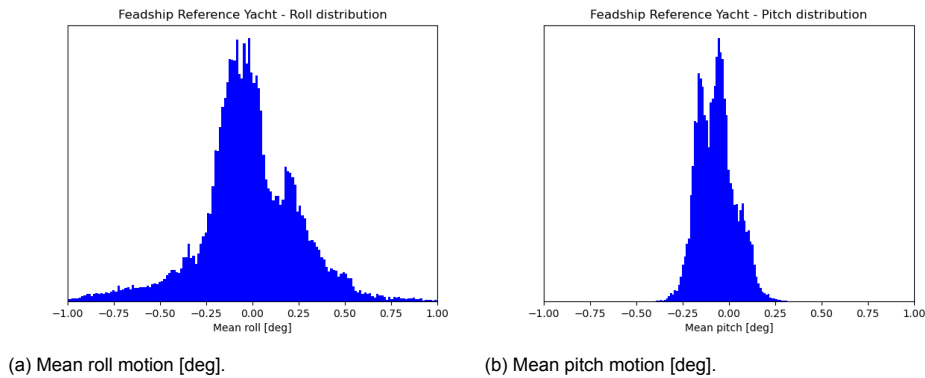
Figure 5.5: Most frequent roll and pitch motions.

Before further steps are taken, a first evaluation was done to check if biofouling growth trends are actually visible within the data. This was an important step to get insight in patterns that are tried to be captured. To do so, ship speed was filtered between 13.4 and 13.6 knots, with 13.5 knots as one of the most frequently sailed speeds. For this speed, it is visible in Figure 5.6 that there is a drift in power increase during operation. Furthermore, in periods of cleaning, as was performed in the beginning of 2020, it is visible that power again decreases back to lower values. This validates the assumption that speed increase visible is a result of marine biofouling, and not for example decrease of other propulsion system components.
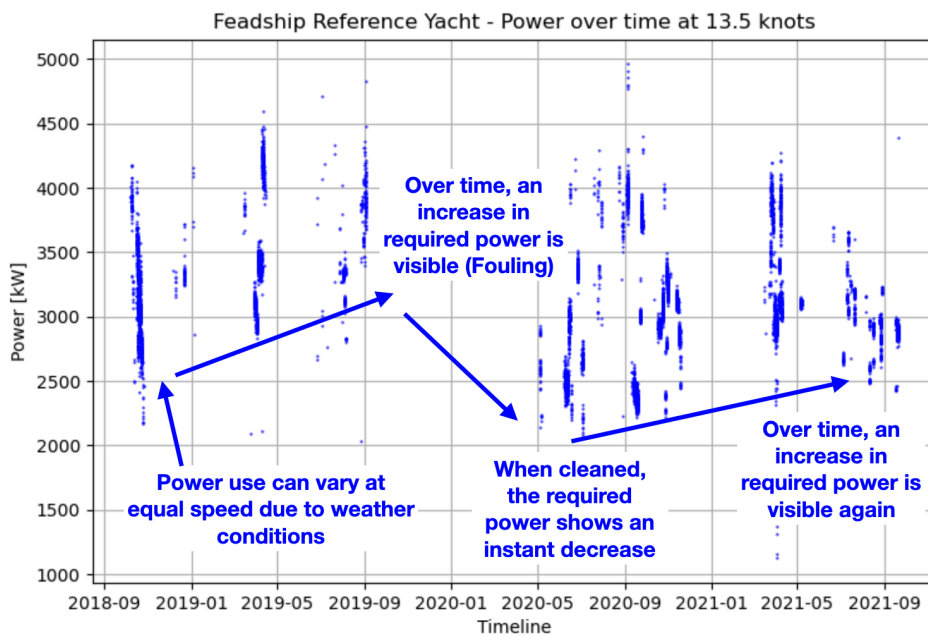
Figure 5.6: Power usage over time at a speed of 13.5 knots.

5.2.2. Data Integration

For the data integration, the different information sources must be combined. Note that Marin reports contain ship parameters, and are therefore independent of time. However, sensor data is acquired at different moments in time, which also applies for AIS data. Since the goal is to do power predictions and compare this to real power usage, the moments of power sampling are leading in the data integration. Note that sensor data also includes pitch and

roll motions, as well as wind speed and direction. In the AIS data, predictions for weather, waves and currents have been made based on ship location. Furthermore, ship speed over ground is also derived from AIS. Since wave and current predictions are not measured but based on calculations, these are predicted on 3 hour intervals and are interpolated over time. Here the ships location was taken at its point in time, together with near surroundings and weather conditions to compute the sea state and relevant parameters. This data is then integrated over the time spots with known ship sensor data to provide some information about sea state that the ship was currently in.

5.2.3. Data Filtering

As mentioned in the method exploration in subsection 3.1.2, the data will be filtered with help of Chauvenet's criterion. With this criterion, errors that have large deviation will be found, based on a Gaussian distribution and the standard deviation of each dataset column. In Equation 5.1, $erfc$ is the complementary error function, Δ_i represents the difference between the ith datum and the mean value over the dataset, σ is the standard deviation of the variable of interest, and N the size of dataset column (Chauvenet, 1863).

$$erfc\left(\frac{\Delta_i}{\sigma\sqrt{2}}\right)N < 0.5 \tag{5.1}$$

5.2.4. Combining Input Data

With the input data set filtered, the white box fouled ship power predictions are made, as was explained in detail in the previous chapter. To select data for which these predictions have been made, both ship speed and wind have played a role. For the ship speed, all data above 10 knots have been used, as these contain the most frequently sailed speeds and a fouling pattern should be clearly visible here (as was shown in Figure 5.2a). Furthermore, the change in speed was also taken into account, as a too large change in a rapid time would mean that the ship was accelerating or slowing down, which gives wrong predictions on the expected power and would result into bad analysis data. With data sampling every 3 minutes, the choice has been made to only analyse ship speeds where the previous speed was within a one knot range. This was first not implemented, but then inaccurate predictions were sometimes made, as a static approach is taken and previous ship motions are not taken into account. For the wind speed, only data with winds below 8 m/s have been used, as higher winds would mean bad weather conditions, where ship performance is hard to predict. This last approach was taken based on Coraddu et al. (2019). Last it can be noted that sufficient data was available, so that the chosen filtering does not affect the required level of data for the modeling.

To provide ship history leading to the current fouled situation, anchor & sailing time together with average speeds and anchor temperatures are provided. As main ship parameters, ship length and type of antifouling are added. This data can then be scaled to use in grey box training, testing and predictions.

5.2.5. Data Scaling

Data scaling is an import part of the data preparation. The machine learning algorithm must find relations between different values to predict the target outcome. However, when some values have a different magnitude than others and are far higher, the risk is present that the model cannot correctly learn the importance of these characters. With all values equally scaled, the model can give weight to more important variables and does not need to learn about invariance, speeding up training times. The normalization is done with the function below:

$$x_{i,norm} = \frac{x_i - x_{min}}{x_{max} - x_{min}} \tag{5.2}$$

This also means that the target variables will be scaled, and that the grey box will thus give scaled predictions. Therefore, grey box predictions can be transformed back to real values with the following function, taking the maximum and minimum value of the original used grey box dataset for the target vector:

$$x_i = x_{i,norm} \cdot (x_{max} - x_{min}) + x_{min} \tag{5.3}$$

Last it can be seen that only numerical values can enter the grey box to find relations, this means that words, terms or categories cannot be used directly. However, these can also be translated to standards values, so that the algorithm can learning relations with these categories. For example, to model the type of antifouling, each type of coating can be computed to a different number. With *One Hot Encoding*, categorical variables are represented as binary vectors. For the terms 'red', 'blue', 'green', the vector below would be translated as follows:

$$['green' \quad 'green' \quad 'red' \quad 'blue' \quad 'red' \quad 'green'] \tag{5.4}$$

$$\begin{bmatrix} 1 & 1 & 0 & 0.5 & 0 & 1 \end{bmatrix} \tag{5.5}$$

5.3. Deep Extreme Learning Machine

As part of the method exploration, the choice was made to build the data-driven model for marine biofouling growth with help of a Deep Extreme Learning Machine (DELM, subsection 3.2.1). With the information going into the grey box now clear, the formation of the DELM will be explained in detail. Extreme Learning Machines (ELM) have been developed for feedforward neural networks, which overcomes problems posed by backward-propagation training algorithm with potentially low convergence rates, critical tuning of optimization parameters, and presence of local minima that call for multi-start and re-training strategies (Huang, 2014; 2015; Ridella et al., 1997; Rumelhart et al., 1986). These are some of the advantages as outlined in the method exploration for feedforward training over backward-propagating training for the current research and environmental and physical phenomena that the model must simulate.

The goal of any black or grey box model is to configure the given input to output. By providing the model with data, it can be trained to find these relations. Between the input and output are neurons, in the DELMs case with weights and without any bias (Huang, 2014). This problem can be seen as a regression problem, as the goal is to predict a scalar / single value. A generalization approach is taken, where the goal is that the machine fits the data instead of memorizing it. The network is trained (slowly adjusting weights) with every piece of new information. The goal is that when we present the network with a new example, it can accurately predict its result. In this section, first in subsection 5.3.1 the background of the extreme learning machine is discussed. Next, in subsection 5.3.2 the working of a shallow extreme learning machine will be presented. After this, in subsection 5.3.3, the conversion from shallow to deep extreme learning machine is explained. Last, in subsection 5.3.4, the hyperparameters are selected.

5.3.1. Background of Extreme Learning Machines

Back-propagation (BP) learning algorithms have been playing dominant roles in training feedforward neural networks. However, it is well known that BP learning faces several challenges such as local minima, trivial human intervention and time consuming in learning (Huang, 2014). ELM was originally inspired by biological learning and proposed to overcome the challenging issues faced by BP learning algorithms, using features of the brain such as zero time and human intervention in learning. In the ELM, Extreme means to move beyond conventional artificial learning techniques and to move toward brain alike learning. ELM aims to break the barriers between the conventional artificial learning techniques and biological learning mechanism:

> 'Extreme learning machine (ELM) represents a suite of machine learning techniques in which hidden neurons need not be tuned. This includes but is not limited to random hidden nodes, it also includes kernels. On the other hand, instead of only considering network architecture such as randomness and kernels, in theory ELM also somehow unifies brain learning features, neural network theory, control theory, matrix theory, and linear system theory which were considered isolated with big gaps before' (Huang, 2014, p. 3).

5.3.2. Working of a Shallow Extreme Learning Machine

First, the working of a single layer ELM, a Shallow Extreme Learning Machine (SELM), will be discussed. In the ELMs case, the network consists of both an initial randomized weight matrix by the size of the input layer and the number of neurons. The weights and input data are entered into the activation function, so that the neural network can produce non-linear results based on non-linear activation functions. The type of activation function is a hyperparameter ($\mathcal{H}$) that must be selected. Next, the output weights must be fitted to the data to find answers closest to the desired output. Overall, this can be summarized as shown below, where β is the output weights, ϕ the activation function, w_j the random input weights, and x_i the inputs of the network (Akusok et al., 2015).

$$\sum_{j=1}^{L} \beta_j \phi(w_j x_i) \tag{5.6}$$

For the training procedure, the relation between the estimated outputs y_i, the target output t_i is shown below. Here the error ϵ summarizes the difference between the target and estimated output that contains both random noise and dependency on variables not present in the input variables X.

$$y_i = \sum_{j=1}^{L} \beta_j \phi(w_j x_i) = t_i + \epsilon_i \tag{5.7}$$

Next, the output weights β_j must be found to estimated the outputs y_i. The ELM solution will be found with help of the Moore-Penrose generalized inverse (†), also referred to as pseudoinverse (Radhakrishna Rao and Mitra,

1972). This basic implementation of ELM uses the minimal norm least square method, and can be summarized as follows:

$$H\beta = T \tag{5.8}$$

$$\beta = H \dagger T \tag{5.9}$$

Where:

$$H = \begin{bmatrix} \phi_1(w_1 x_1) & \cdots & \phi(w_L x_1) \\ \vdots & \ddots & \vdots \\ \phi(w_1 x_N) & \cdots & \phi(w_L x_N) \end{bmatrix} \tag{5.10}$$

$$\beta = \left(\beta_1^T \cdots \beta_L^T \right)^T \tag{5.11}$$

$$T = \left(y_1^T \cdots y_L^T \right)^T \tag{5.12}$$

To improve generalization performance, a regularization term can be added as introduced by Deng et al. (2009):

$$\beta = \left(H^T H + \lambda I \right)^\dagger H^T T \tag{5.13}$$

A model with good generalization ability will have the best trade-off between empirical risk and structural risk, so that overfitting by the algorithm is avoided. This is a hyperparameter that must be selected. Since the ELM only contains feedforward training, the error ϵ is not used for backward propagation. This means that with the found weight matrices and chosen activation functions, new data can be entered into the machine to make predictions. The prediction ability of the machine will be discussed in a later stage of this section.

5.3.3. From SELM to DELM

Between the input and output can be different amounts of layers, a group of neurons. Using more than one layer provides deep learning, which can be helpful to find more complex relations. The number of neurons per layer and number of layers are both hyperparameters ($\mathcal{H}$) that must be selected. Each hidden layer and its output weights will be trained to find the desired output of the system, by adding additional hidden layers.

Kasun et al. (2013) describe the process of adding extra layers to the ELM network and making deep-learning predictions, which is also used by others to use ELM-based autoencoder (AE) as its building block, resulting in a sort of DELM (Tissera and McDonnell, 2016; Coraddu et al., 2019). With this approach, each hidden layer generates an autoencoded version of the original data, with the last hidden layer computing the target variable. The autoencoded version of the original data can be seen as an intermediate vector in between two hidden layers, with similar size as the input data. This process is shown in the Figure 5.7. Once the network has been trained, the output weights of the first hidden layer (W_{o1}) and the random weights for the second hidden layer (W_{p2}) can be combined into one weight matrix ($W_{h12} = W_{p2} W_{o1}$).
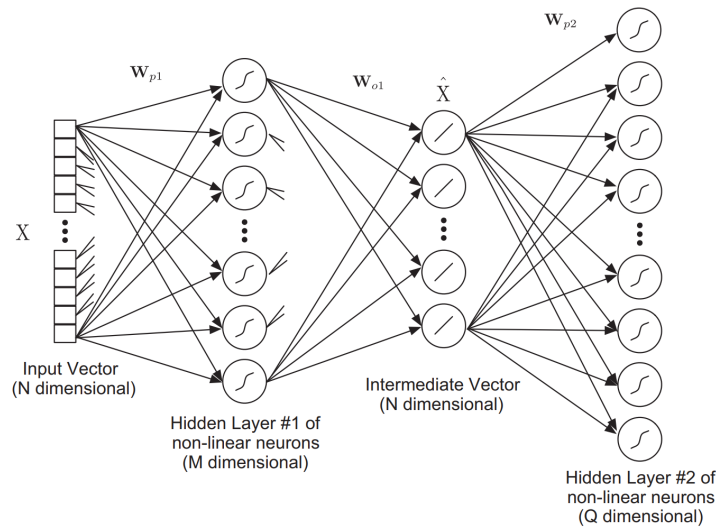

Figure 5.7: Configuration of multiple hidden layers in a DELM, from Tissera and McDonnell (2016).

To compute the so-called intermediate vectors, first the sizes of the input layer and the hidden layer have to be compared. When the layers have equal size, Equation 5.14 must be used to find the intermediate vector. It is important that the correct function is chosen for correct transformation from the feature space to input data. When the size is not equal, Equation 5.15 must be used. The output layer can be found with Equation 5.13 (Kasun et al., 2013). Without a regularization term, Equation 5.15 can be written as Equation 5.16.

$$\beta = H^{-1}T \tag{5.14}$$

$$\beta = \left(H^T H + \lambda I\right)^\dagger H^T X \tag{5.15}$$

$$\beta = H \dagger X \tag{5.16}$$

Overall, for a DELM neural network with 3 input vectors, 2 hidden layers of both 5 neurons, and 1 output vector the system could be summarized in a graphical overview as shown in Figure 5.8. It is important to notice that each hidden layer is a combination of incoming random weights and output weights. Furthermore, while the size of each hidden layer can differ, the intermediate vector will always be the size of the input vector.
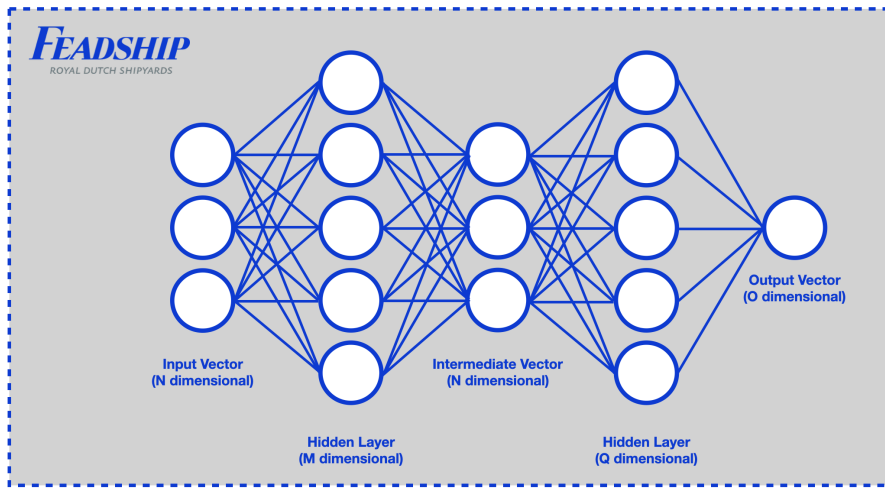
Figure 5.8: Neural network illustration for a DELM with 3 input vectors, 2 hidden layers of 5 neurons, and 1 output vector.

5.3.4. Hyperparameters

With the DELM now configurable and the mathematical computations behind it explained, the last step is to select the hyperparameters. This is part of the Model Selection process which includes choosing between different learning algorithms, setting the hyperparameters of a learning algorithm and choosing the structure of the learning algorithm. For the second, the goal is to find a set of hyperparameters that produce the best neural network, or other machine learning model. The hyperparameters include in this case the number of hidden layers, the number of neurons, but also the type of activation functions used. Note that an optimization function is not applicable as back-propagation training is not done. Unfortunately, there is no golden learning algorithm able to solve all data-related problems in an optimal way, and thus model selection is always required. This also means that it can be seen as a time consuming process, and has to be done with care, since even advanced practitioners and researchers sometimes fail to perform model selection in a correct way. (Oneto, 2018).

Number of Hidden Layers

As discussed in the method exploration, going beyond one hidden layers introduces a deep framework, which is able to understand complex relations. This improvement in relation capture with more then one layer is part of the selecting process for the number of hidden layers and thus the model architecture. Prior to deep-learning, problems that require more than two hidden layers were rare, as two or fewer layers were often sufficient for simple data sets. However, with complex data involving for example time series, additional layers can be helpful. Heaton (2015) summarized the capabilities of several common layer architectures as follows (van der Bos, 2021):

Number of Hidden Layers	Result
none	Only capable of representing linear separable functions of decisions.
1	Can approximately any function that contains a continuous mapping from one finite space to another.

2	Can represent an arbitrary decision boundary to arbitrary accuracy with rational activation functions and can approximate any smooth mapping to any accuracy.
>2	Additional layers can learn complex representations (sort of automatic feature engineering) for layer layers.

Table 5.2: Number of hidden layers and their capabilities, adapted from Heaton (2015).

With the provided information and comparable neural networks with marine engineering applications researched, a grid search for networks with 1, 3 and 5 hidden layers will be validation with help of cross validation. This will be done in section 6.3.

Number of Neurons per Layer

To select the number of neurons per layer, the most important thing to consider is the balance between the level of information and the amount of neurons. While not enough neurons will mean that not all patterns can be captured, to many neurons will result in neurons that cannot be trained due to lack of information. The first will result in an underfit, while the second will result in overfitting. The latter is not always visible since the machine might continue to perform better on training data. However, in this situation more unrealistic patterns will be found, and this will result in a poor result on testing / validation data. An overview of this process is found in Figure 5.9, where on the right the underfit, overfit, an optimal solution are illustrated for a data set. On the left, the optimal point is indicated with the vertical dotted line while the overfit becomes visible increase in validation error.
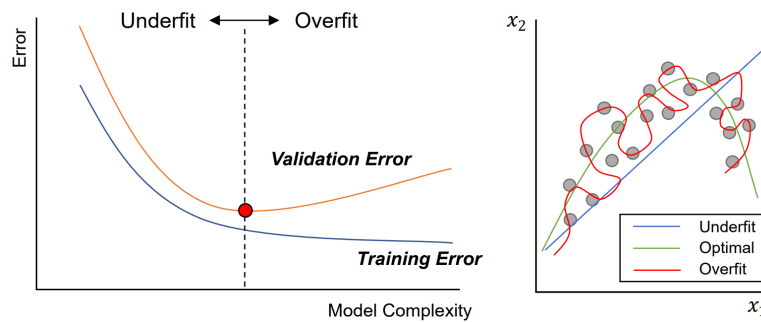
Figure 5.9: Model error comparison (left) and corresponding fitting relations (right), from Odendaal (2021), based on Da Silva et al. (2017).

Finding the optimal number of neurons comes down to a process of trial and error, using the grid search method. For this reason, neural networks can be studied to get a first impression on the number of neurons per hidden layer. However, it can be seen that little models are available with similar application. Therefore, neural networks with power prediction application are reviewed, something which is applied in ship design & marine engineering. Since the number of neurons must fit the amount of information available in the grey box and the ability to predict the target variable, the number of input and output vectors together with number of neurons and hidden layers are displayed in Table 5.3. These numbers will be taken as a starting point to get some identification of network size, and grid search will be used to find the optimal number of neurons.

Reference	Input Vectors	Output Vectors	Hidden Layers	Neurons
Pedersen and Larsen (2009)	9	1	1	12
Parkes et al. (2018)	6	1	3	50, 50, 50
Zwart (2020)	13	1	1	15
van der Bos (2021)	17	1	3	24, 12, 9
Odendaal (2021)	5	1	2	30, 40

Table 5.3: Neural network architectures with marine engineering applications.

For selecting the amount of neurons per hidden layer, it is important that there is a balance between the level of information provided and the models ability to process this information and capture it. In the validation of the model, a cross validation will be performed where different hyperparameters will be researched with help of a grid search method. This will be further explained in section 6.3. Here, performance will be evaluated with help of the mean absolute percentage error (MAPE), as shown in Equation 5.17. For the grid search 10, 25, 50, 75 and

100 neurons per layer will be validated over the learning dataset. Note that with more neurons there was a risk of overfitting, and thus the to be explored neurons per layer are not very extreme.

$$|\epsilon_{\%}| = \frac{100}{N} \sum_{i=1}^{N} |\frac{y_i - t_i}{t_i}| \tag{5.17}$$

Activation Functions
To make the network able to give non-linear output, the activation function was added. Since different functions could be used, this is a hyperparameter that must be selected. Below some of the more frequently used activation functions in ELM's and neural networks are shown. To introduce non linearity into the model, the Sigmoid function is advised as a frequently used activation function in ELMs and DELMs.

1. Sigmoid function:

$$f = \frac{1}{1 + \exp(-wx)} \tag{5.18}$$

2. Fourier function:

$$f = \sin(wx) \tag{5.19}$$

3. Gaussian function:

$$f = \exp(||w - x||^2) \tag{5.20}$$

4. Rectified linear activation function:

$$f = \begin{cases} wx & \text{if } wx \leq 0 \\ 0 & \text{else} \end{cases} \tag{5.21}$$

Regularization Coefficient
As mentioned, the regularization parameter allows to trade between a small training error and a small regularization term, which enforces smoothness and regularity, and is a hyperparameter that must be tuned. With a regularization term close to zero, emphasis is placed on a small training error and the model reduces to an empirical risk minimization (ERM) principle. With a regularization term approaching infinity, emphasis is placed on a small regularization term and the model reduces back to the problem as explained in Equation 5.9. The proposed mathematical model of Regularized ELM algorithm can be described as shown below, where $D\epsilon$ is a combination the model errors ϵ with their weight factor D (Deng et al., 2009):

$$\min \frac{1}{2}||\beta||^2 + \frac{1}{2}C||D\epsilon||^2 \tag{5.22}$$

As last hyperparamater and part of model selection, the regularization term will also be determined by cross validation in section 6.3. Here, research will be done into a regularization term of 0, 0.001, 0.01 and 0.1.

Summary of Hyperparameters Selected
In Table 5.4, the hyperparameters selected and to be researched in the cross validation in section 6.3 are shown.

Hyperparameter	Selection
Number of hidden layers	$\begin{bmatrix} 1 & 3 & 5 \end{bmatrix}$
Number of neurons per layer	$\begin{bmatrix} 10 & 25 & 50 & 75 & 100 \end{bmatrix}$
Activation function	Sigmoid function
Regularization term	$\begin{bmatrix} 0 & 0.001 & 0.01 & 0.1 \end{bmatrix}$
Input variables	17
Output variables	1

Table 5.4: Hyperparameters summary.

III
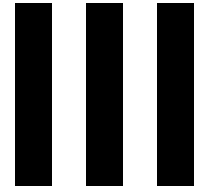
Validation & Business Case

In this part the outcome of the proposed model from Part I will be presented. In Part II, each part of the model was explained in detail. In chapter 6, the outcome of the model will be shown and the model will be verified and validated. Next in chapter 7, the questions set for the Feadship Business Case will be answered with the model. After this, in Part IV, results from the research will be discussed so that conclusions can be drawn.

6

Verification & Validation

In the previous chapters the methodology has been explained and a model was formed. In this chapter, first model outcome is shown in section 6.1. Next, in section 6.2, the verification steps taken in this research are discussed. After this insection 6.3, the model is validated. Last, in section 6.4, the final model is discussed.

6.1. Model Outcome
In this section the model outcome is presented. Here the results of the white box model as proposed in chapter 4 are presented. This process gives insight into application of the current model. With the current model outcome visualized, results can be validated and conclusions can be drawn. First in subsection 6.1.1 the marine biofouling growth and its resulting equivalent sand roughness height are presented. Next in subsection 6.1.2, the increase in frictional resistance and loss of propeller efficiency are presented based on the obtained roughness.

6.1.1. Marine Biofouling Growth
In section 4.2, the model to predict marine biofouling growth was explained. This model uses ships anchorage locations together with their time and water temperature. Based on this information, the ships fouling rating and calcareous surface coverage can be computed over the period of time since hull cleaning and antifouling application. As a result, the equivalent sand roughness height was formed, which represents the roughness present on the ship. In Figure 6.1, the development of the equivalent sand roughness height is presented for the studied Feadship yacht. It is visible that over a period of more than 400 days, the equivalent sand roughness height develops to a value over 500 micrometers.
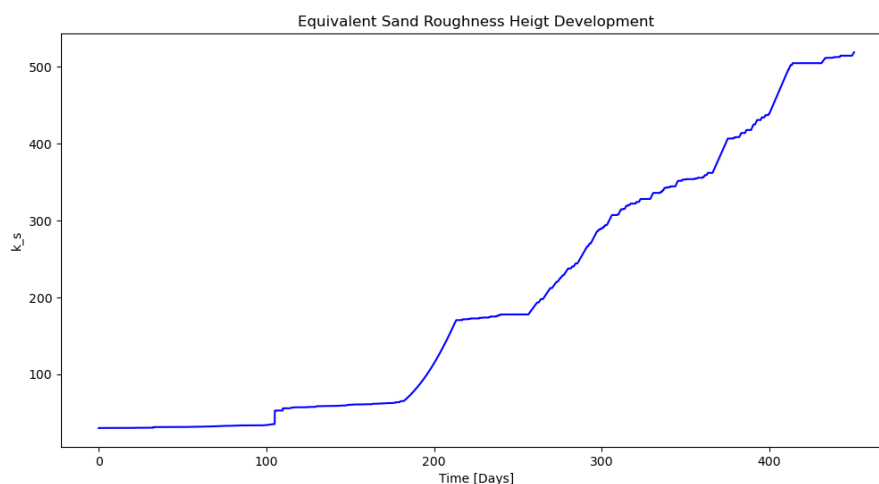
Figure 6.1: Equivalent sand roughness height development for Feadship yacht.

6.1.2. Added Sea Margin due to Biofouling

In this subsection, the model outcome for the added resistance and propeller efficiency loss is presented. This shows the performance of the white box model and will later be validated together with the data-driven model.

Added Resistance

In Figure 6.2, the increase in calm water resistance over time is presented as a result of biofouling and its roughness. The graph shows a similar development as shown in Figure 6.1. In the presented period, the ship resistance increase in calm water condition has increased from slightly above 255 kN to over 275 kN, an increase of more than 9%. This increase in resistance follows from an increase in frictional resistance due to biofouling, which was approximated by the function of Townsin as explained in subsection 4.3.1.
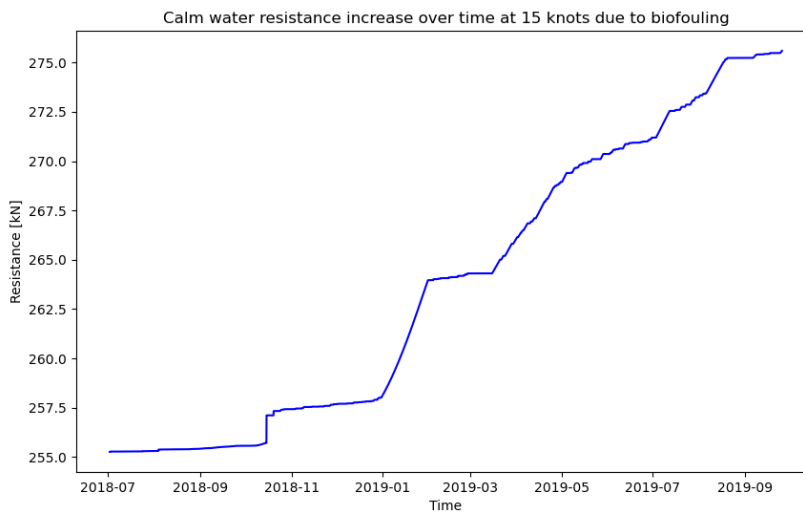
Figure 6.2: Resistance increase development over time for Feadship yacht.

Propeller Efficiency Loss

In Figure 6.3, the change in open water efficiency is displayed in the maximum fouling situation, which was derived from Figure 6.1. For the design speed of 15 knots, the open water efficiency at the operating point of the propeller reduces from 0.599 to 0.572, also visual by the distance between the purple and brown line around an advance ratio of 0.65. Overall, this can be seen as a reduction in the propeller efficiency of slightly less than 5%. Here, the frictional roughness on the propeller was used together with propeller parameters and performance characteristics for smooth condition, as explained in subsection 4.3.2. Together with the added resistance, this means that 14.3% more power is required in the latest fouled situation to reach the design speed.
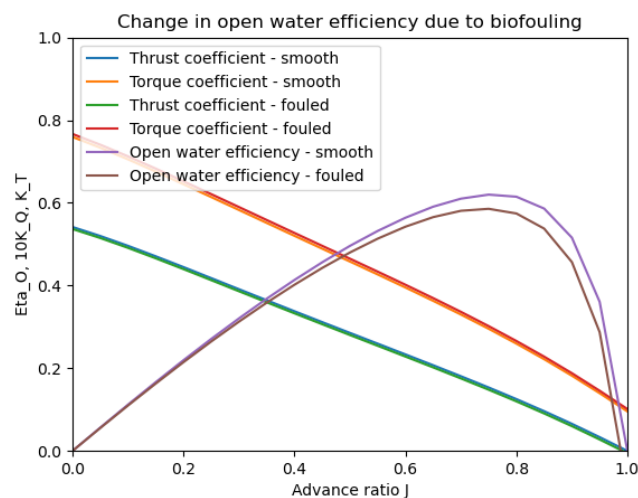
Figure 6.3: Open water efficiency change for Feadship yacht.

6.2. Verification

With white model outcome presented, the verification steps that have been taken are discussed to ensure proper modeling. This contains both verification steps for the physical model discussed in subsection 6.2.1, as for the data-driven model discussed in subsection 6.2.2. Here the main goal is to ensure that the model is implemented correctly (Sargent, 2010).

6.2.1. Physical Model

For the white box approach, the entire model has been checked to see if each part was implemented as supposed and gave outcome as expected. For the biofouling growth model, this meant that for the Equator and Mediterranean, the fouling curves were given as output as shown in section A.4. For all models, the verification mainly included debugging, making sure no errors are present, and using hand calculations to verify results. Last, the model was also tested with slightly different parameters as a continuity test, with extreme parameters as a degeneracy test, and with doubled or half values as a consistency check as explained by Sargent (2010). Even though proof of verification is impossible, it can be seen that efforts have been taken to ensure proper model implementation.

6.2.2. Data-Driven Model

For black box verification, an additional approach can be taken. First, it was checked if functions are entered correctly and worked as supposed to. However, with the neural network set, any pattern can be attempted to find. This also means that the model should detect clear pattern and predict with very high accuracy. This way it can be verified if the black box itself functions as expected, so that the fouling can be properly evaluated later, knowing the machine and neural network are working. To do so, the power prediction for smooth condition, which was discussed in section 4.1, will be reproduced with use of the black box in a proof of concept. Since this is all based on first principle modeling with given functions, it can be expected that with their variables given, the model should reproduce the results. The goal is perform these steps before hyperparameters are tuned with help of cross validation, so that it is verified that a working model was implemented. For this verification, number of hidden layers was set at 3, number of neurons per layer was chosen as 25, and the regularization term was chosen as 0.

The predicted power in smooth condition is a function of calm water, air drag, wave, and temperature difference resistance. The calm water resistance follows from the speed over water, which also provides the air drag resistance together with the wind speed and direction. For the current ship, variables that cause change in wave resistance are: ship & wave direction, wave height & period, and speed of the ship. In Figure 6.4 it is visible that when these variables are entered into the machine to predict the smooth power, an accuracy with an absolute error can be obtained of 0.9854 over a test dataset. Furthermore, when all separate resistance components are processed and entered into the black box, it can predict the smooth power with an accuracy of 0.9999.

(a) Based on ship speed & direction, wave height, direction & period, wind speed & direction, and sea temperature.

(b) Based on calm water, air drag, wave, and temperature difference resistance.
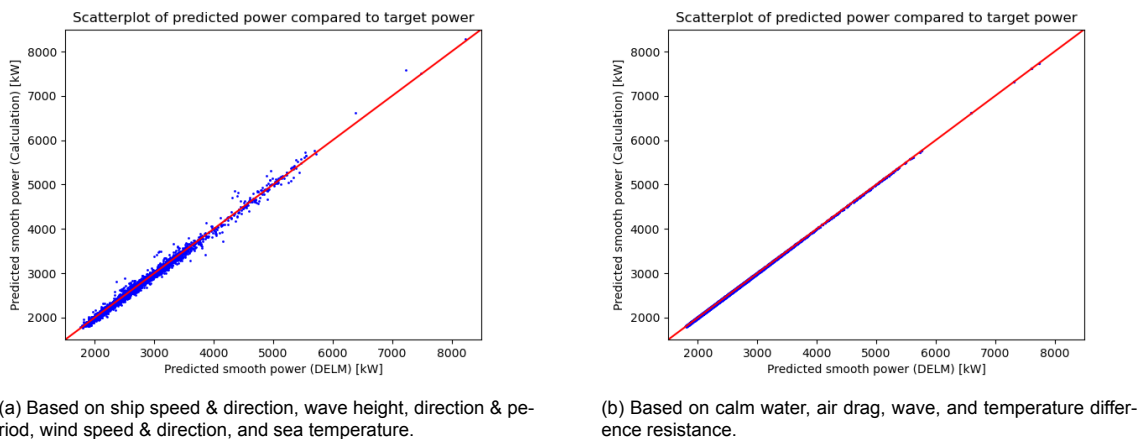
Figure 6.4: Test of DELM for smooth power prediction.

From Figure 6.4b it becomes clear that if all information is known, the black box can perfectly make predictions and draw relations. However, it is not yet assessed how the neural network predicts with a lack of information. For this purpose, the first prediction is used (Figure 6.4a) and the most dominant parameter, the ship speed, is left out of the equation. By doing so, the black box reduces its accuracy to 0.878 and increases variation, as shown in Figure 6.5. It should be noted that most of the researched data has a smooth power of around 2500 kW, if data for more different speeds were used, the prediction accuracy would be lower. By comparing Figures 6.4a & 6.5,

the difference when ship speed is and is not given, becomes clearly visible.
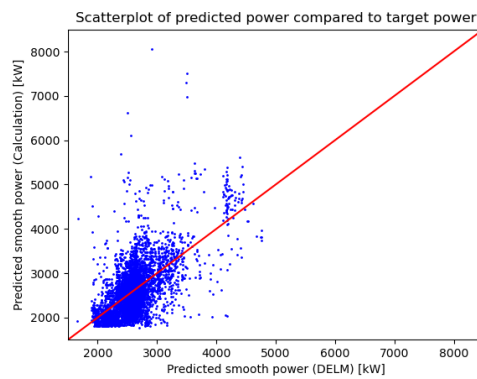
Figure 6.5: Test of DELM with similar input as in Figure 6.4a, except ship speed.

6.3. Validation

In this section the model will be validated to asses performance. In the previous section, verification was done to check if the model is implemented as supposed. However, this does not ensure if the model chosen is the correct model. For this section, the main goal is to ensure that the model is an accurate representation of the real system (Sargent, 2010). With the goal of predicting current and future power, taking into account biofouling development, the dataset that is available will be used to validate both the white and black box model.

As mentioned, the accuracy of the white box can directly be validated by testing it to the test dataset, and this will be done in subsection 6.3.1. Next, the developed grey box model, will be validated in subsection 6.3.2. After this, to properly evaluate the model, the data-driven model is worked out without a white box input in subsection 6.3.3, making it a black box model.

6.3.1. White Box

Ship sensors provide optimal data to validate the model. For the white box, this is a great option to evaluate its performance based on real ship data. In Figure 6.6, the white box predictions are shown over the dataset against actual power measurements. Here, each white box prediction was performed by combining the smooth ship prediction as explained in the previous chapter together with an increase in frictional resistance, a change in wave resistance and a loss of propeller efficiency as explained in chapter 4.
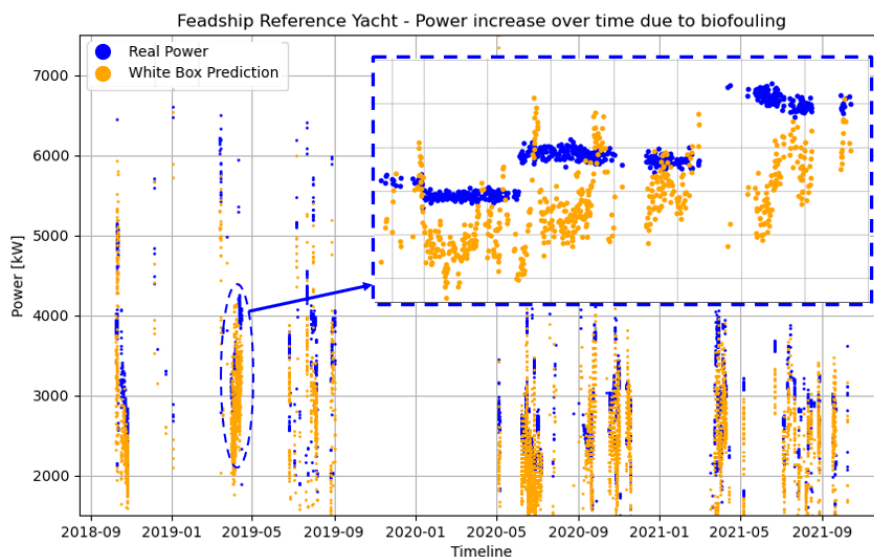
Figure 6.6: White box predictions over dataset.

In Figure 6.6 it is visible how white box predictions are most often lower than actual used power, and sometimes higher. Overall, the white box attains an accuracy with mean absolute error over the test dataset of roughly 85%.

With white box predictions also too low shorty after cleaning, the conclusion can be drawn that while an attempt has been made to incorporate all factors in the white box, it sometimes still misses an additional power factor. Overall fouling fits within the larger image of a so called sea margin, which can be described with the function below (Klein Woud and Stapersma, 2002).

$$\text{sea margin} = f(\text{fouling, displacement, sea state, water depth}) \tag{6.1}$$

For the white box approach, it can be seen that a part of the sea margin or a design margin is still missing. For this reason, the missing white box margin is researched based on the given data. In case clean ship data was available, the missing margin could best be found over this data. However, with only data available in already fouled situations, the choice is made to look for the margin which gives the white box the highest prediction accuracy over the dataset. In the figure below, the white box accuracy over the dataset is visualized for an additional margin from zero to twenty percent over smooth ship power. In this figure, it can be seen that when a 12.5% margin is applied over a ships power required in smooth condition (thus excluding added power due to fouling), prediction accuracy of the white box is the highest. For Figure 6.6, this would mean that all the white box predictions (orange) now predict slightly higher power (move up), with the result that they are closer to the real power measurements (blue).
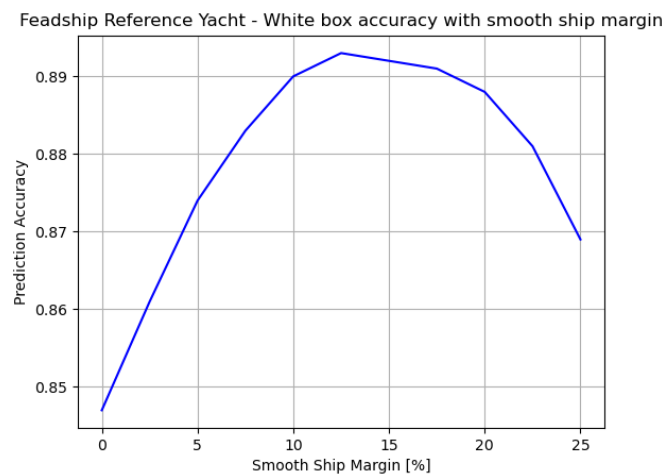
Figure 6.7: White box accuracy with additional margin over smooth ship power.

In Figure 6.8, the prediction accuracy of the white box with and without the found margin for smooth ship power. Here it is clearly visible how the additional margin moves predictions from predictions that are too low to more correct findings.
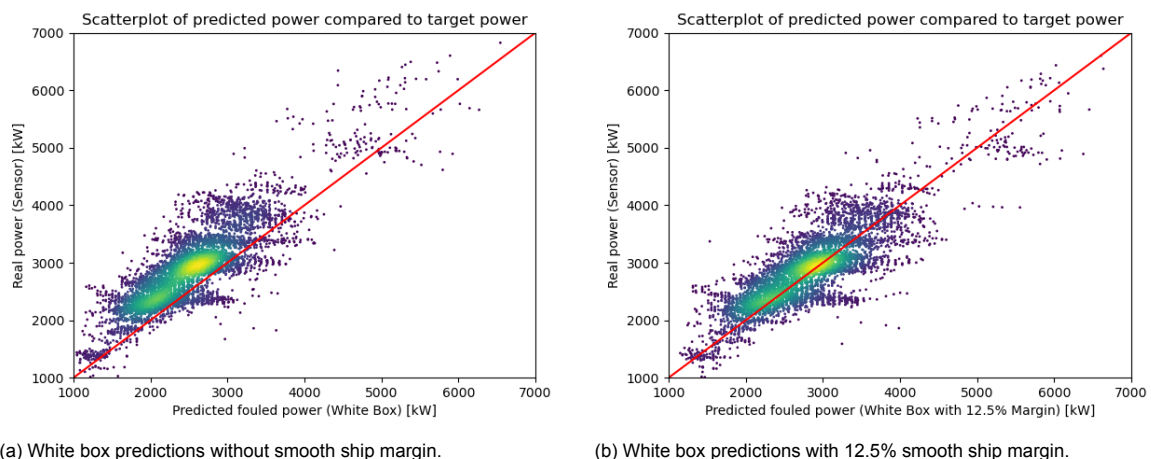
(a) White box predictions without smooth ship margin.

(b) White box predictions with 12.5% smooth ship margin.

Figure 6.8: White box predictions with and without smooth ship margin.

This would mean that for the most accurate white box prediction of required power at any moment in time, the function below can be used. Note that the margin is taken over the power prediction for smooth ship, after which the power contribution due to biofouling is added. This approach is taken since it is the believe that an additional

factor on ship propulsion itself is missing rather than a factor on biofouling contribution. This was derived from the fact that white box prediction accuracy was also considerably lower with low levels of biofouling.

$$P_b = P_{b,S} \cdot 1.125 + \Delta P_{b,R} \tag{6.2}$$

6.3.2. Grey Box

As part of model selection, a DELM was chosen as type of learning machine or the current application in the method exploration (subsection 3.2.1). Additionally, with this model selection, research has been done into different hyperparameters. This was performed in subsection 5.3.4, and next cross validation will be used to find remaining hyperparameters, together with error estimation. For this cross validation, a selection will be made between a time series cross validation, and a k-Fold Cross Validation. Time series cross validation could be done, since the problem involves a time-dependent problem. In this case, the dataset will be split into 5 samples of equal size, and forward validation will be used to asses model performance on a test dataset later in time (Shrivastava, 2020; Hjorth and Hjort, 1982). An overview of this is shown in Figure 6.9.
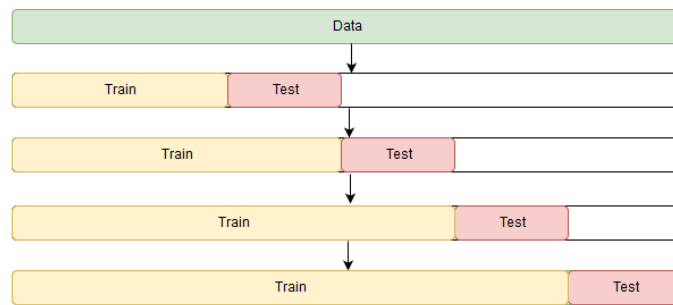
Figure 6.9: Cross validation in time series, from Shrivastava (2020).

However, it is also known that different types of fouling growth show a Gaussian type trend, and can change in time. Furthermore, when calcareous fouling settles, ship roughness increases more rapidly. Since the model is based on days since cleaning, its best to find the pattern within the days trainable, and not use the DELM for large extrapolation. Therefore, the choice will be made to find the remaining hyperparameters with help of k-Fold Cross Validation (KCV) (Kohavi et al., 1995; Anguita et al., 2009). First the dataset available is split into a training dataset and test dataset, where the test data is not used until model selection is done. Within model selection, the training dataset is split into k independent subsets (namely, the folds), each one consisting of n/k samples: $(k-1)$ parts are used, in turn, as a training set ($\mathcal{L}$), and the remaining fold is exploited as a validation set ($\mathcal{V}$). The procedure is iterated k times (Coraddu et al., 2015). An overview of this process is shown in Figure 6.10.
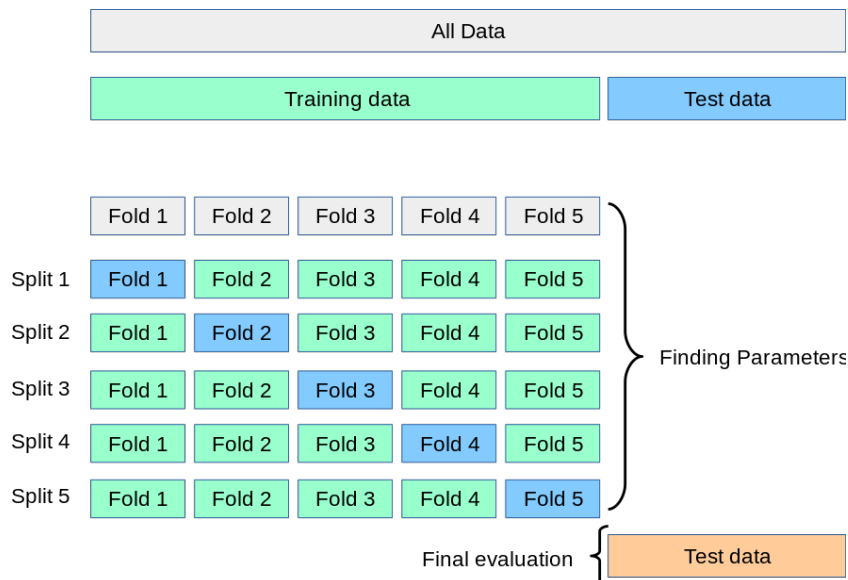
Figure 6.10: Example of a 5-fold cross validation, from Benner (2020).

As a last step of the model selection, a grid search was applied for tuning of the following hyperparameters:
- Number of hidden layers: $\begin{bmatrix} 1 & 3 & 5 \end{bmatrix}$
- Number of neurons per layer: $\begin{bmatrix} 10 & 25 & 50 & 75 & 100 \end{bmatrix}$
- Regularization term: $\begin{bmatrix} 0 & 0.001 & 0.01 & 0.1 \end{bmatrix}$

This meant that the model was run for a total of $3 \times 5 \times 4 = 60$ combinations, where each iteration contained the model being trained 5 times on the different possibilities in the validation and training folds. As a result, the best performance was found for a neural network with 3 hidden layers, 25 neurons per layer, and a regularization term of 0.01. Below, the vector with the results for the different validation folds and its average value is shown below. To give better insight into which extent this number is true, a 95% confidence level interval is applied. With the function below, this results into the average error on the validation sets of 87.9% $\pm$ 1.8%.

$$\begin{bmatrix} 87.8\% \\ 90.0\% \\ 88.1\% \\ 89.5\% \\ 84.3\% \end{bmatrix} \qquad\qquad 1.96\sqrt{\frac{\sigma^2}{n}}$$

$$\begin{bmatrix} \mathbf{87.9\% \pm 1.8\%} \end{bmatrix}$$

Last, the suggested hyperparameters can be used for the reserved test dataset. With the grey box only able to detect fouling patterns within the data range it was trained for, the choice was made to use the test set with random sampling, instead of at the end of the dataset. It is important to mention that this still means that the random 15% sampled points for this test were excluded from model training. Building the test dataset from random sampling was done to avoid that the model was trained until for example 150 anchorage days, and tested over 150-200 anchorage days, as other fouling patterns might occur. This is inline with the recommendation and goal only to use the grey box for data within its range, and not outside of trained data. It can be seen that the performance over the test set is equal to 91.4% $\pm$ 0.2%, with thus a mean absolute percentage error of 8.6% $\pm$ 0.2%. In Figure 6.11a, the scatterplot for grey box predictions compared to actual power measurements over the test set is shown, together with the error distribution.
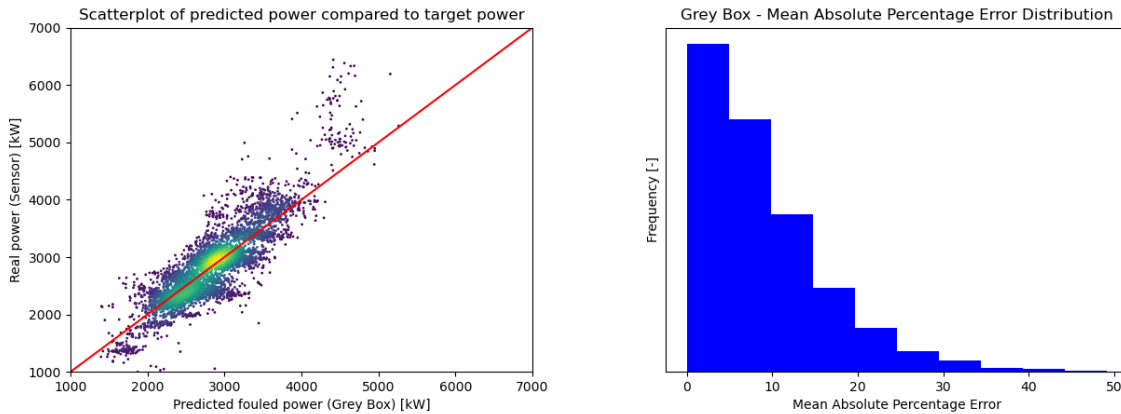
(a) Grey box predictions compared to real power measurements.   (b) Error distribution.

Figure 6.11: Grey box performance over test dataset.

Last, the model selection can be summarized as presented in Table 6.1.

Hyperparameter	Selection
Learning machine	Deep Extreme Learning Machine
Number of hidden layers	3
Number of neurons per layer	25
Activation function	Sigmoid function
Regularization term	0.01
Mean absolute errors estimated	12.1% $\pm$ 1.8% ($\mathcal{V}$), 8.6% $\pm$ 0.2% ($\mathcal{T}$)
Input variables	17
Output variables	1

Table 6.1: Model selection summary.

6.3.3. Black Box

Separate from the developed white box and grey box model, a black box model could be developed similar to the grey box model. In this case the only difference would be that the black box does not have the white box prediction as input, which made the model grey. An overview of this is shown in Figure 6.12, together with the input and output parameters for the black box model in Figure 6.2.

Input variables	Output variable
~~White box fouled ship power prediction~~	
Ship speed	
Ship direction	
Wave height	
Wave direction	
Wave period	
Wind speed	
Wind direction	
Average sea surface temperature	Fouled ship power
Anchorage days since clean ship	
Sailing days since clean ship	
Average ship speed	
Mean roll	
Mean pitch	
Roll deviation	
Pitch deviation	
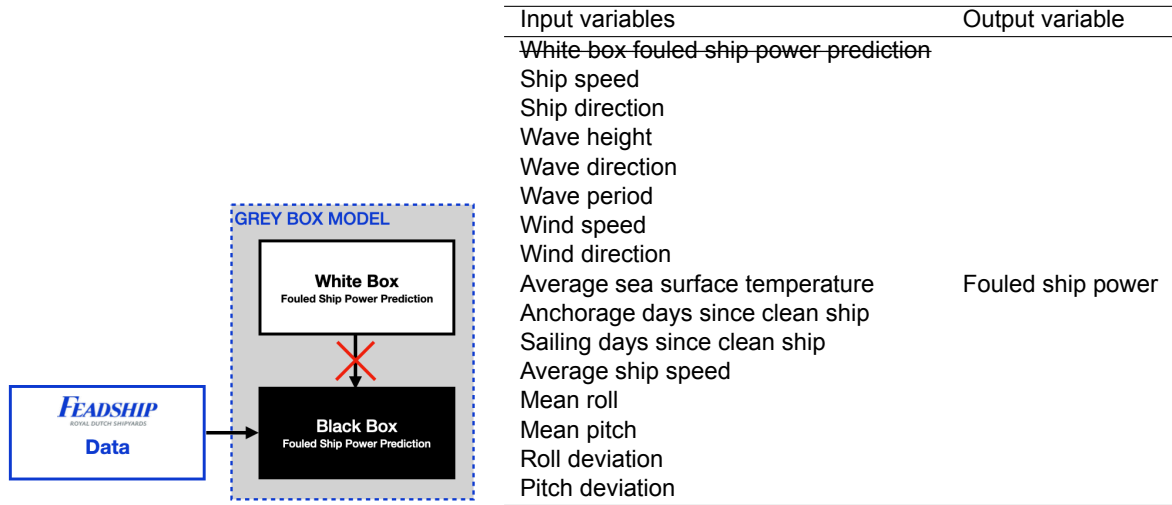
Figure 6.12: Black box model setup.

Table 6.2: Input and output variables for black box model.

For model selection, the same basis as the grey box model will be used to compare black box model performance. However, with different information available and processing of this information, the k-fold cross validation will again be applied in a similar way as for the grey box. This will make sure that both models are compared with their best set of hyperparameters. For the black box configuration, it was found that a model with 5 hidden layers, 25 neurons per layer, and a regularization term of 0.001 showed the highest accuracy over the validation sets. With mean absolute percentage accuracy's of 87.9%, 88.7%, 87.5%, 90.1% and 80.5%, an average error on the validation sets was found of $86.9\% \pm 2.9\%$. On the remaining test set that was not yet used in this learning process, an accuracy was found of $89.8\% \pm 0.2\%$. An overview of the predictions and error distribution over this test set for the black box is shown in Figure 6.13.
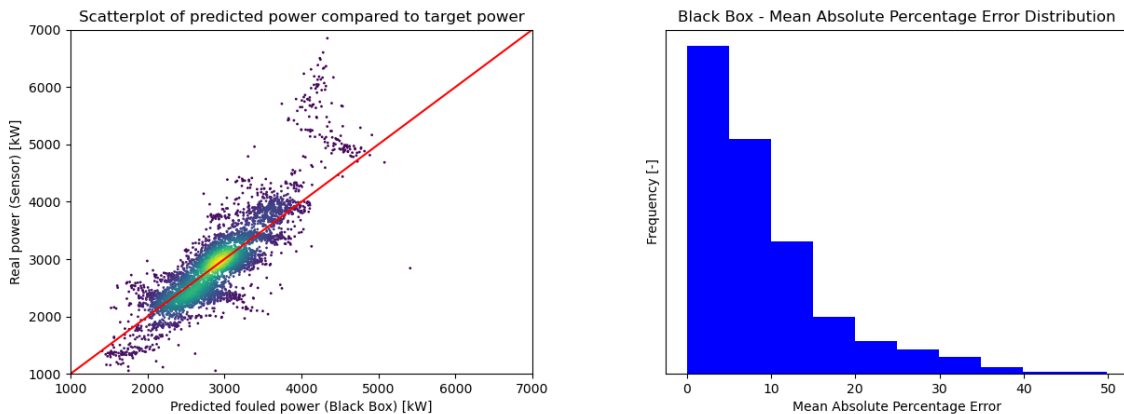
(a) Black box predictions compared to real power measurements.

(b) Error distribution.

Figure 6.13: Black box performance over test dataset.

It can be seen that the black box predictions and error distribution show a similar trend compared to the grey box predictions, as was shown in Figure 6.11. However, it as also found that performance was slightly better for the grey box predictions, outperforming the black box by several percentages. With the black box configuration for this model now worked out. Next, all models can be compared and evaluated in the following section. Developing the black box version of this model is an important step into assessing the added value of a white box prediction, and grey box modeling. After the models are compared, the final recommended model will be discussed in different situations.

6.3.4. Model Comparison

Last, the white box, black box and grey box models will be compared. This will first be evaluated over the dataset, and after this some insight will be given in performance outside the dataset. To evaluated performance over the dataset, a comparison will be made between prediction accuracy over the test dataset, that was not used in the learning process of both the grey and black box machines. In Table 6.3, an overview is shown for the different models and their mean absolute percentage accuracy, in addition with a 95% confidence level interval.

	Accuracy with Mean Absolute Percentage Error
White Box	85.3% ± 0.3%
White Box with 12.5% margin over smooth power	89.4% ± 0.3%
Black Box	89.8% ± 0.2%
Grey Box	91.4% ± 0.2%

Table 6.3: Performance comparison over test dataset.

Based on Table 6.3, it can be seen that the following conclusion can be drawn for performance over the test dataset: $GB > BB > WB$. However, it should be noted that when a missing margin on the smooth ship power is added for the white box, predictions come very close with accuracy compared to the black box predictions. Furthermore, when a 95% confidence interval is taken into account, model accuracy partly overlaps as white box predictions with margin can outperform black box predictions. Nonetheless, it can be seen that the additional information that the grey box model is provided with, helps this model to make the most accurate predictions within the data range it has learned from.

As a next step, some short evaluation will be done on model performance outside of trained data. While power measurements are not made here, model predictions can be compared and first assumptions on what is realistic and what is not can be made. In Figure 6.14, the model was applied over a longer period of time. To do so, all values expect anchorage days, sailing days, and the white box predictions were taken at their mean value within the dataset. For the combination of anchorage and sailing days, the activity of the yacht was used where sailing was done 16% of the time.

The model was ran a total of 30 times to give statistical meaningful results. Here, it should be reminded that deep learning models are stochastic models, making use of randomness while being fit on the data. In the figure, the mean predictions for the black and grey box are drawn with a line, while the prediction area between the average over the first 15 runs and the average over the last 15 runs is filled with shade. Here it is important to mention that the lines drawn are not the upper and lower bound of possible predictions. However, this simple but effective approach does give insight into where predictions are mostly equal, and where predictions show large variance. The author believes that this makes this figure more valuable as readers can better interpret where the model can be accurate, and where not.
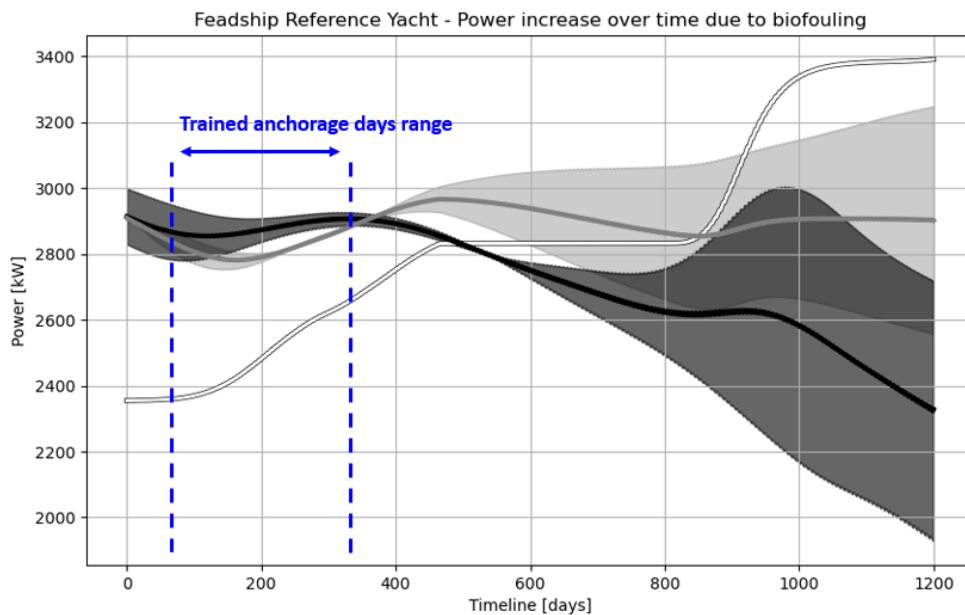

Figure 6.14: Comparison between white box, black box and grey box prediction for longer period of time.

Based on Figure 6.14, the following main points can be highlighted:
- Black box and grey box show similar trend within trained range. However, white box predictions are lower as smooth ship margin is missing, resulting in an under prediction compared to the measured data. It can be seen than when 12.5% margin is added over the smooth power, which is around 2350 kW in this situation (day 0), the white box line moves up 294 kW and follows the patterns found by the black and grey box.
- Outside of the trained data range, both the grey box model as the black box model show large variance in predictions, together with a often very different pattern than white box physical predictions.
- Points where the white box predictions show a large increase can be compared to grey box predictions. Here it becomes visible that the grey box predictions also shown an increases here, but a lot less than the white box model. This indicates that while the grey box uses the white box partly for its predictions, its mostly build upon the other variables.
- It is visible that within the data range that the grey box and black box model was trained for, it shows an increase in power with an increase in time and anchorage days. However, both before the known timeframe and after, it can be seen that the model often gives a decrease in power with the same input, while the white box model does not. This shows a poor extrapolation capacity, as it is also visible that model uncertainty becomes larger here.

6.4. Final Model

With the model validated and performance measured over actual ship data, the final model can now be proposed. In the previous section, it was found that a trained grey box has good performance for a ship and time range its trained for, and has poor extrapolation performance on a different ship. Based on this, the grey box should have a different configuration when its used for a ship where the grey box is not trained for. In subsection 6.4.1, the grey box model is further worked out for a ship with data for a grey box model. In subsection 6.4.2, the grey box model is worked out for a ship without data to train a grey box model. Last, in subsection 6.4.3 the final model will be summarized.

6.4.1. Ship with Data for Trainable Grey Box Model

As mentioned, a grey box should be trained on a ship to properly use it for this ships predictions. However, this is not the only variable that determines the applicability of the grey box for the situation. For the different parameters involved, their boundaries within the dataset are also important to determine applicability for new predictions. For the smooth power of the ship, it can be seen that the ship has sailed all speeds within its range during the given time period, this was already evaluated in section 5.1 where the given data was presented. Here in Figure 5.2, the most frequent speeds and output powers where shown. Besides this, it can be seen that also the average speed and temperature together with the number of anchorage and sailing days are variables the grey box was trained upon. For the latter two, Figure 6.15 shows the dataset for the given vessel and the trained anchorage and sailing days since cleaning. Based on this figure, it is advised to only use the grey box for the known time limit, in this case around one year. This is also important since fouling growth does not show a constant or linear pattern, and thus large extrapolation could result into inaccurate predictions, as was shown in Figure 6.14.
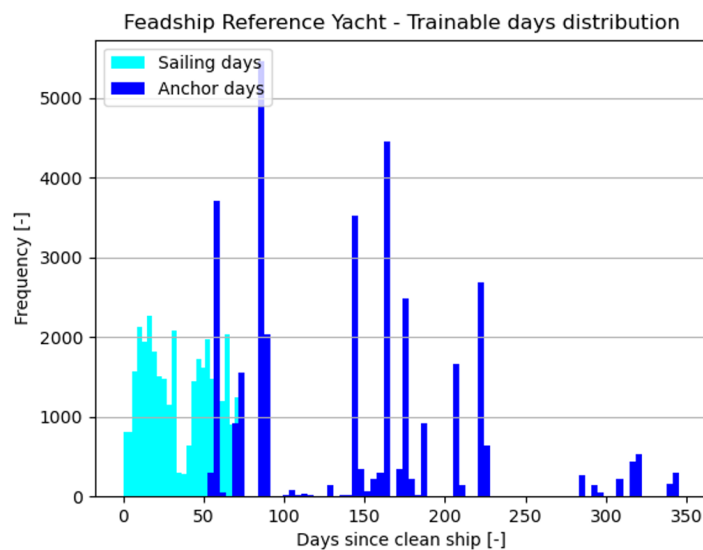

Figure 6.15: Trained days for anchorage and sailing days since clean ship.

Next, the average temperatures the ship encounters will be evaluated. Here it can be noted that this is the average temperature over ship anchorages since cleaning. The encountered sea water temperatures and average values since cleaning are shown in Figure 6.16. Here it can be seen that even though the network is trained with average temperatures ranging from around 15 to 26 degrees, still not all temperatures are covered. With yachts all around the globe, found patterns are not enough for all predictions that could have to be made. Despite the fact that the white box model fouling curves are also not based on cold water locations, it is expected that these could better be scaled and extrapolated than found grey box curves. For this reason, it would be good to not use the grey box for sea temperatures which do not fall within the range of the encountered ones.
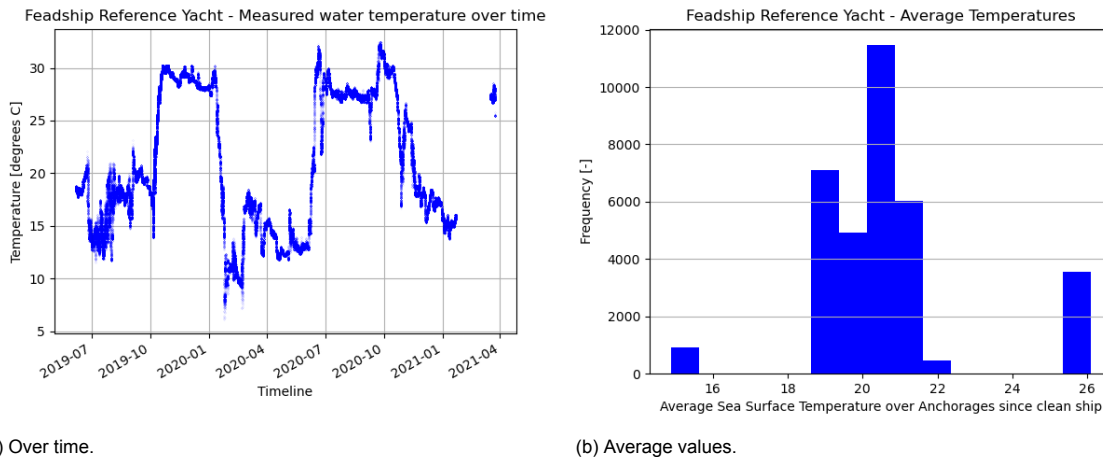
(a) Over time.   (b) Average values.

Figure 6.16: Average sea temperatures and sea temperature over time encountered.

With the data ranges known that the grey box is trained for, it can be determined if ship fouled power should be predicted with help of the grey box or not. Next, predictions for ships without data for a grey box model will be explained.

6.4.2. Ship without Data for Grey Box Model
In chapter 4, the white box model was explained to make biofouling growth predictions and compute its resulting added resistance and loss in propeller efficiency. In section 6.3 of this chapter, this model was validated against actual ship data. One of the things that stood out in this comparison was that the power predictions were often not high enough, which was also visible in situations shortly after cleaning. This gave the indication that some factor was still missing. Additionally, in the white box model, the following main limitations were found to be present:
- Fouling growth curves extrapolated based on measurements in Equator and Mediterranean, making it less applicable for regions colder than the Mediterranean.
- Fouling pattern when sailing was not taken into account.
- Model based on used type and thickness of antifouling and original measurements, meaning that it might not fully correspond for current ship antifouling system.

The fact that no additional measurements in colder regions are available is a limitation that cannot be overcome at this moment. However, the other limitations can be tried to minimize with the following efforts:
- **Missing margin:** Compute missing margin for smooth ship power, as proposed in white box model evaluation.
- **Fouling pattern when sailing:** Derive fouling pattern from real ship data / grey box model, as proposed in chapter 3.
- **Model based on used type and thickness of antifouling:** Find correction factor for antifouling system based on real ship data.

With the proposed steps as listed above, it can evaluated if these attempts to overcome some of the model limitations could help improve the white box model. The suggested improvements could then be tested and validated against the ship dataset available. To do so, first the changes during sailing will be worked out. Here, it must be mentioned that instead of computing differences due to sailing with the grey box, mean values for each input sample will be used together with a changing value for sailing days. With this approach, the goal is to find a general pattern in fouling change during sailing. From this, a sailing factor can be derived and implemented in the white box approach. This approach is taken in discussion with Feadship, were preference was to derive results

into a mathematical factor. It is expected with this only implemented, white box prediction model accuracy would at first be lower, as this value was already under predicted. However, it was already found that this is partly the case because of a missing margin. Furthermore, it is also mentioned that the antifouling system is not equal as modelled. Therefore, after implementing the sailing factor, different combinations of antifouling factor and smooth ship sea margin will be evaluated to find the best fit, and see if model accuracy can overall be improved.

On the ship investigated in this research, a SPC (Self Polishing Copolymeer) coating was used as antifouling system, comparable to a SPC coating used in the current white box approach (Uzun et al., 2019). However, eventhough more detachment is expected on a fouling release coating, ship speed is still the most important factor for fouling detachment, and some decrease in power due to fouling was visible in the dataset. Based on the patterns found within the grey box, the fouling power change during sailing was as shown in Figure 6.17.
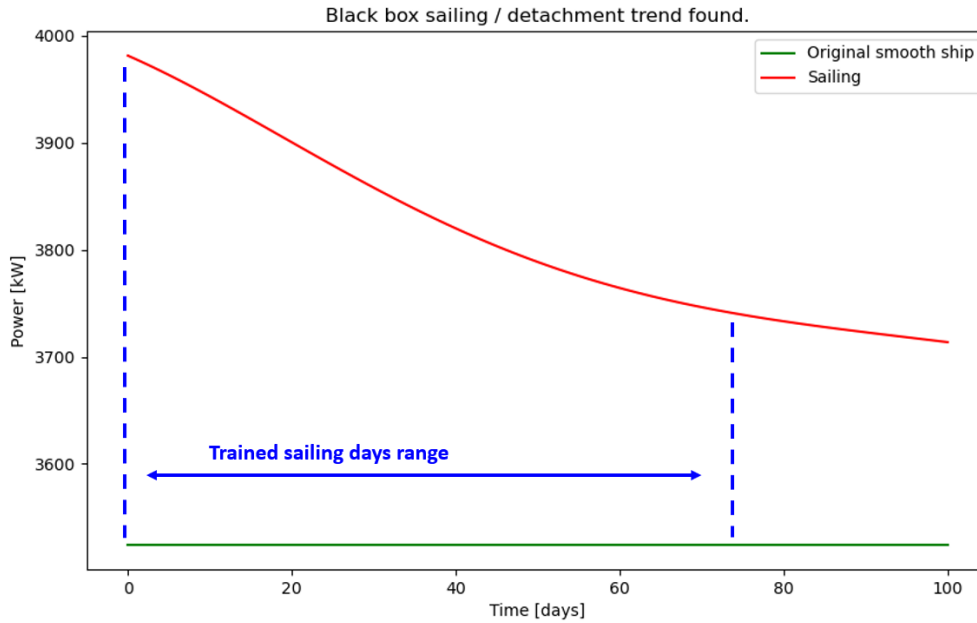
Figure 6.17: Detachment pattern captured in grey box model during sailing.

First it is important to mention that this pattern was found in between periods of anchorage, and that this is not a pattern that fits for a continuance of 75 days, but rather 75 within a maximum of 350 anchorage days encountered. This means that within this year, after periods of anchorage, the grey box captures some decrease when sailing. Note that this decrease in power means a decrease in roughness, which can either be the result of the antifouling polishing or fouling detachment. This also means that if longer periods would be sailed directly, this would not guarantee to result into the same phenomena. However, in a trained period of roughly 1 year, during 75 days of sailing this power decrease was found. Overall it can be seen that within these 75 days, the power goes from 3,980 kW to 3,750 kW, showing a reduction in required power of 230kW. Compared to the original smooth ship power, this is a percentage of around 6.5%. The reduction in added power from 455kW to 225kW can be seen as a reduction of -50.5% due to sailing. On average, the sailing factor (sf) for each day of sailing (t_{sail}) could be taken as follows:

$$sf^{t_{sail}} = 0.495 \tag{6.3}$$

$$sf = \sqrt[75]{0.495} \tag{6.4}$$

For the current case, this leads to a sailing factor of 0.99 on the added power due to biofouling per sailing day. With this approach, the believe is that always an equal fraction of the added power due to biofouling is lost due to when sailing. Furthermore, this also means that this factor can be applied and that it will never lead to a negative fouling contribution, which is important since it should only lower the fouling contribution. The power after a sailing ($P_{b,new}$) can now be found with help of the power before sailing ($P_{b,old}$), sailing days (t_{sail}), smooth ship power ($P_{b,S}$) and sailing factor (df):

$$P_{b,new} = (P_{b,old} - P_{b,S}) \cdot sf^{t_{sail}} + P_{b,S} \tag{6.5}$$

Overall, this simple derivation can be used to work out a sailing factor on the known fouling on the ship. In Figure 6.18, the suggested function is added to the found pattern to see the difference. It can be seen that some show equal flow, especially within the given data range.
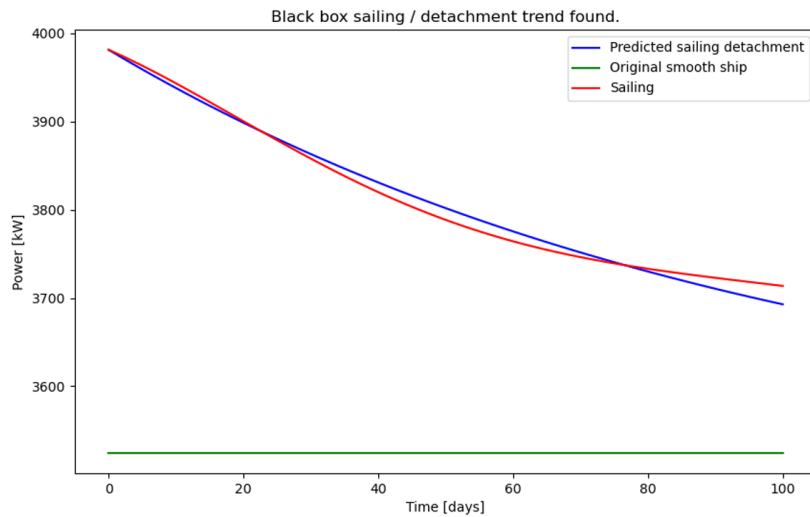
Figure 6.18: Detachment pattern and suggested sailing function.

With the new fouling pattern found for sailing, the proposed white box curves can now be corrected. Over a given period of a year, it can be seen that the found pattern is small but still visible in Figure 6.19. For a longer period with more sailing days, the fouling change in sailing plays a more significant role. However, it should be kept in mind that the pattern was found for a ship with a time period of a year after cleaning. With different stages of fouling growth, the detachment of some of the earlier fouling does not mean that other fouling like barnacles would also partly release. Furthermore, polishing effects of the antifouling also depend on lifetime of the product. Both could be seen as model extrapolation, where good results are not guaranteed.
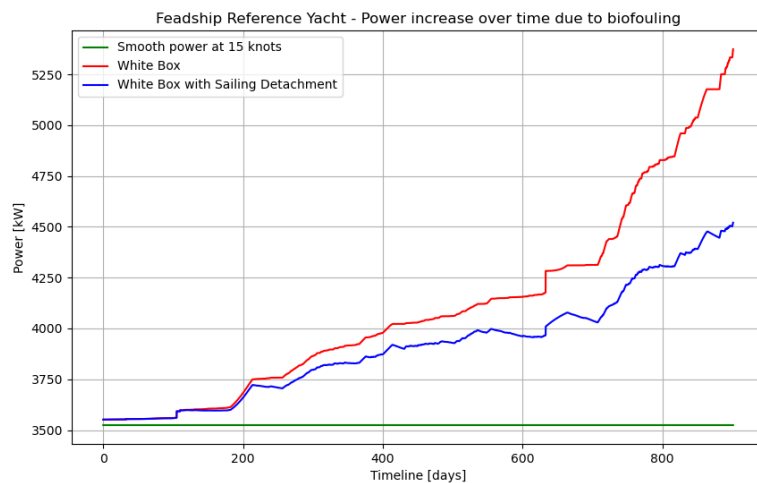
Figure 6.19: White box prediction with and without sailing detachment correction.

Last, the antifouling factor and the ship margin can be assessed. However, with only anchorage data for a little bit more then a year, measured and predicted white box fouling contributions are still relatively small. This means that correcting the antifouling factor only has a relative small effect on the given error, especially compared to the smooth ship margin. In the one year period, a smooth power use of around 3,500 kW has now gone up to 3,800 kW. Changing the antifouling factor on the maximum 300kW difference (and smaller earlier) does not have much effect compared to the changing the margin on the original 3,500kW smooth power. Furthermore, it was already noted that most differences come from instabilities in power compared to speed for the ship itself, rather than errors in fouling predictions. For this reason, the choice has been made to not apply an antifouling factor, as a solid basis for this could not be formed. However, if longer periods of data were available or antifouling curves for different types of coating, a more applicable curve could be selected. Overall, the conclusion is that the white box can still predict with high accuracy, which is the main goal. This also means that the overall margin for the ship will not be changed, and is thus taken as 12.5%.

6.4.3. Model Proposal

With the model now worked out for a ship with trainable data and a ship without trainable data, fouling predictions can be made for each ship. This means that the current tool can work for both design support as for planning future maintenance and predicting to be expected and current fouling. Overall, the grey box model can be summarized in as shwon in Figure 6.20 for a single ship.
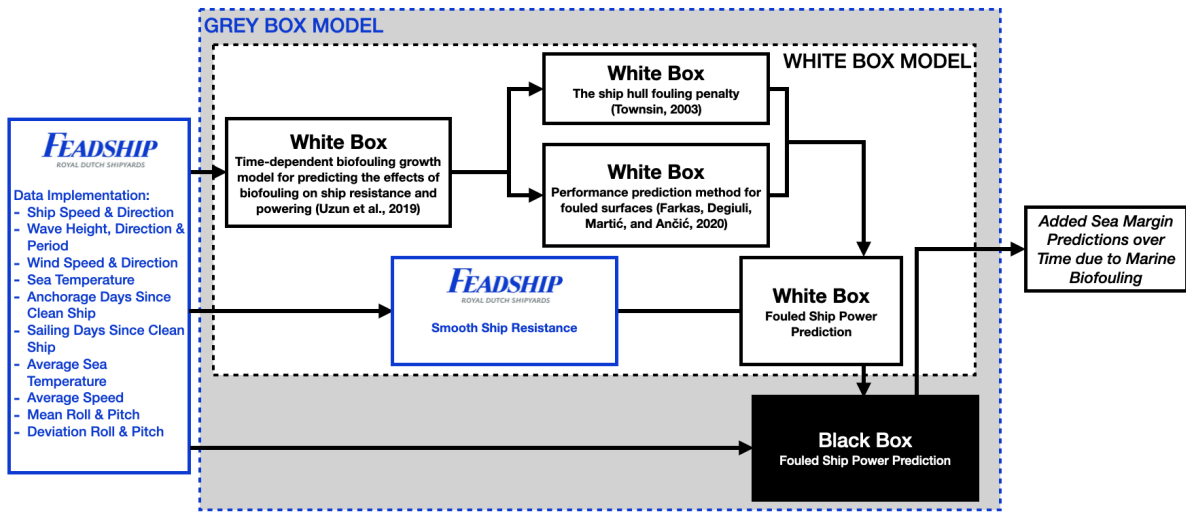
Figure 6.20: Final grey box model.

Once more ships are trained with a data-driven model and the relations for ship size and type of antifouling become familiar, ships without sensor data available can also make use of a data-driven prediction, on the condition that the desired output is within the range of the trained data. Last, it should be mentioned that when a ship has no sensor data, or desired output from the model falls outside of the trained data range, a full white box approach with data based improvements will be taken as shown in Figure 6.21.
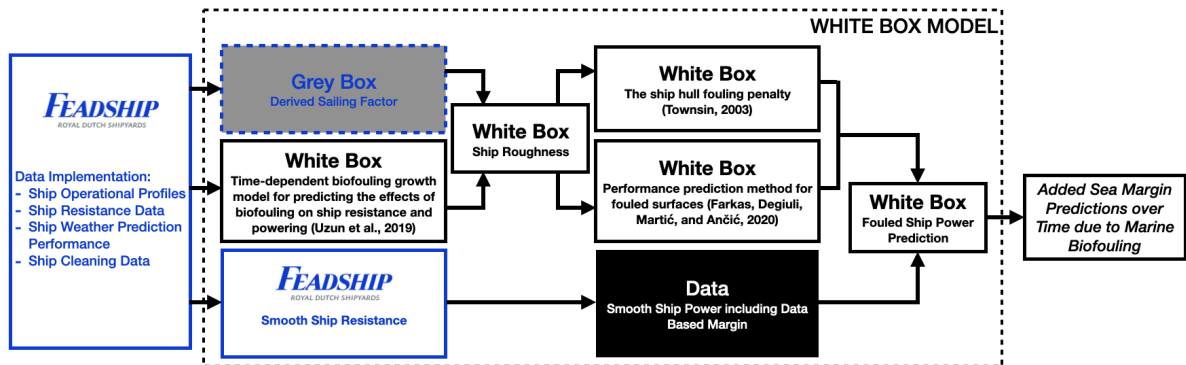
Figure 6.21: Full white box approach with data based improvements.

7

Business Case

In this chapter the Feadship Business Case will be discussed and presented. First, the model as validated in the previous chapter is applied to a part of the fleet in section 7.1. Next these curves are used to find changes in operation, which will be presented in section 7.2. After this, the model is used to study possible effects of different intervals of propeller cleaning and their effects section 7.3. To study local effects of fouling, section 7.4 will take a closer look at regions with higher and lower flow. As a last part of the business case, some additional attention is payed to different type of antifouling coatings. In section 7.5, antifouling coatings together with their effectiveness, roughness, and characteristics are discussed. Next in section 7.6, information is provided on how antifouling coatings can be tested and implemented into the developed model. With this done, the the questions as outlined in subsection 1.6.2 will be answered in section 7.7.

7.1. Fouling Growth Curves for Feadships

Based on the current model, different fouling growth curves can be developed for Feadships, which can be used for future maintenance and in early stage design. Along the Feadship fleet 3 profiles can be identified:

- Profile A: European sailing profile
- Profile B: Europe & Caribbean Ocean sailing profile
- Profile C: Worldwide sailing profile

Based on different ships in the profiles that are currently active and their data, predictions curves can be developed. Note that cleaning is not yet taken into account, as it needs to be studied when yachts must be cleaned. The European profile ships are mostly active in the Mediterranean Sea, and sail on average only 5% each year, with other time either spend in dock, anchored, or in harbour. As for profile A, the same can be done for the second profile, which contains ships operating not only in Europe but also in the Caribbean Ocean, sailing averagely around 10% of the time. As a reference, a yacht in this profile has been taken that was first anchored in the Caribbean, and later in Europe. Both ships are shown and labeled in Figure 7.1, where a 80 meter ship was used for profile A and a 60 meter ship for profile B.
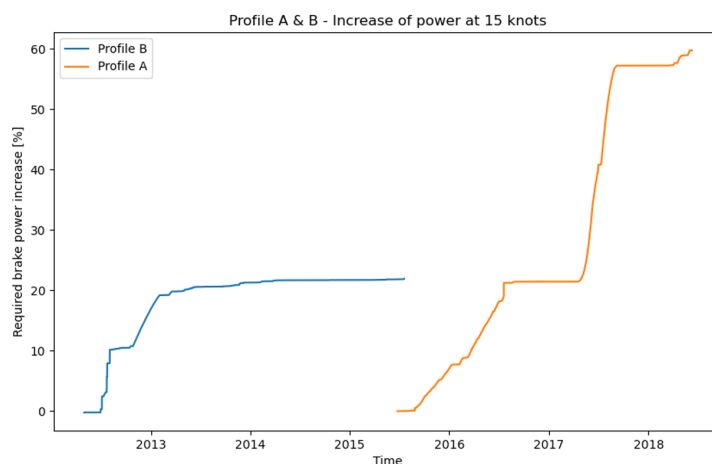
Figure 7.1: Fouling development on ship from profiles A & B.

Last, the same process has been done for profile C. Since this contains yachts sailing all across the globe, different fouling patterns can occur. Furthermore, these yachts are also again more active, sailing 15% averagely. For this reason, multiple profile C yachts and their fouling development are visualized in Figure 7.2. It can be seen that for the yacht that is shown over the longest period, a more rapid increase starts again in 2018, this is the case since after a longer time, barnacles and calcareous fouling starts to grow all over the ship if not cleaned. The different ships are labelled by their waterline lengths.
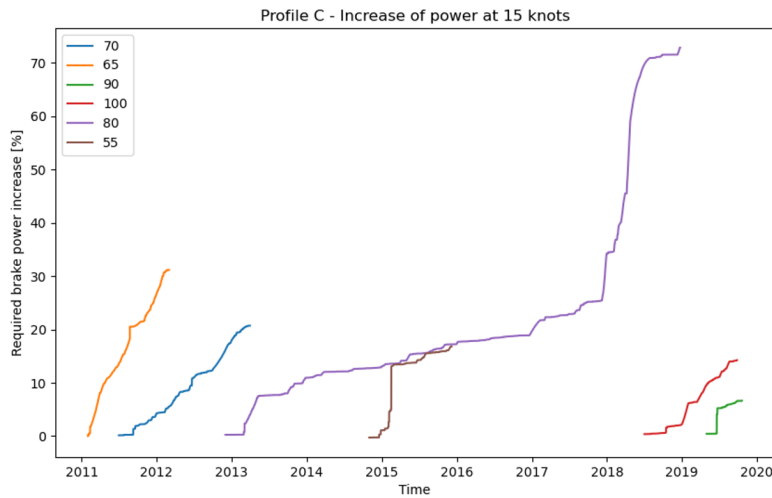
Figure 7.2: Fouling development on ships from profile C, labeled by waterline length of the ships.

For profile C, it becomes visible that different ships can have different fouling patterns. For this reason, as a next step general plots have been developed based on water temperature, ship activity, and ship length, based on Feadship yachts. As a reference a 55, 65, 80 and 100 meter Feadship have been taken. For each yacht, three figures are developed, containing five percent, ten percent and fifteen percent sailing, as these are the most common values within the fleet. In each figure, the expected brake power increase from fouling is presented. This is done over a 3-year period, for water temperatures of zero, ten, twenty and thirty degrees. First a five year period was chosen, with most products having a warranty for either 2 or 5 years and ships often going out of water for renewal surveys or even intermediate survey. However, it can be noted that within this period all maximum power increases are attained within the first 3 years, which was therefore chosen as the new timeline. As an example, one is presented in Figure 7.3, where the fouling curves are given for the studied 100 meter ship, sailing 15% of the time.
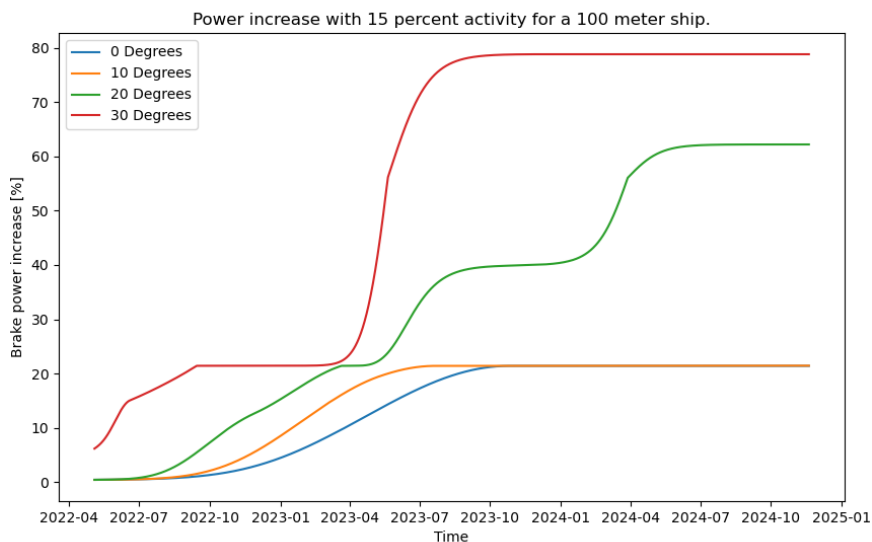
Figure 7.3: Fouling development for 100 meter yacht with 15% sailing, showing increases in power based on different sea surface temperatures.

With the following obtained fouling curves for Feadships, the following two goals can be achieved:
- Hull cleaning & antifouling application intervals can be determined for current and to be designed Feadships, together with type of antifouling.
- Based on antifouling choices, future additional power requirements are known, and a better choice for engine margin can be made.

For the second point it can be noted that currently, engines are selected based on fixed margins and fouling is only accounted very roughly, without any specific procedure. For Feadships, this is done by applying an average margin that was build upon a case study of 4 Feadships, as was presented in the introduction of this thesis (chapter 1). In general ship design, either the same approach is taken, or a yearly factor is applied. For example, Klein Woud and Stapersma (2002) propose a yearly factor of 1.07 to account for fouling.

With the current study applied to Feadships and results worked out across the fleet, the goal is that a more specific value can be used to calculate power requirements and find a better fit. In the following sections, more investigation is done into biofouling and its effects for the marine propulsion system.

7.2. Changes in Yacht Operation due to Biofouling

With added sea margin due to biofouling now predictable, next the changes as a result of this for ship operation can be found. In Table 7.1, it is presented how the fouling curve as shown in Figure 7.3 can be used. For the current table, the 20 degrees sea surface temperature curve was selected. Here, the average increase of power over 6 months is converted into increase of power, loss of speed, loss of range, increase of fuel consumption, and with that added cost. To perform this calculation, average power used when sailing was taken from the studied ship, together with an MGO price of 1,250.00 $/mt. This value is based on its average in the beginning of June 2022, while it is also visible that this was rapidly changing. As an example, the MGO price development in the six months prior to this number is shown for the Port of Rotterdam in Figure 7.4. For the fuel rate, the product sheet of the installed engine was used, where interpolation was done between the closest given power and respective fuel rates. This approach is inline with the performance diagram of the engine, as shown in Figure 7.5a. With this, it can also be seen that tables as below are an important evaluation, as the outcome of the model and the best decision accordingly is not fixed. Hence, it should continuously be checked whether current fouling management strategies are still optimal. Note that Feadship yachts often are in temperatures even higher than presented in this table, resulting in more severe consequences for yacht operation.

Time [months]	Average increase of power over year	New power use [kW]	Top speed [knots]	Fuel rate [L/h]	Total added fuel consumption [mt]	Loss of range [Nm]	Estimated added cost
Start	0%	2,215	20.0	544	0	0	$0.00
0-6	2%	2,259	19.9	554	3	182	$4,367.52
6-12	17%	2,592	18.0	623	30	1,279	$37,123.95
12-18	35%	2,990	16.2	707	61	2,325	$76,431.66
18-24	47%	3,256	15.2	762	82	2,885	$102,636.80
24-30	62%	3,588	14.1	832	108	3,491	$135,393.22

Table 7.1: Operational changes as a result of biofouling for 100 meter yacht at 20 degrees sea surface temperature and 15% sailing over 2.5 years.
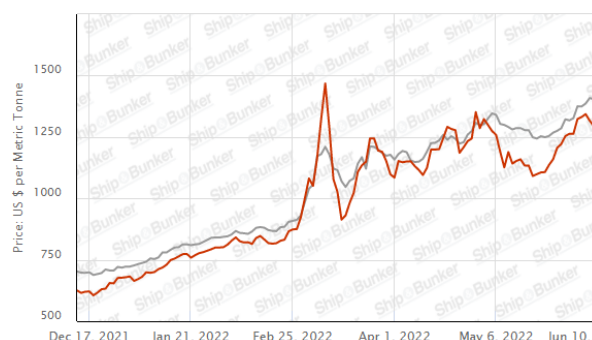
Figure 7.4: Development of price of MGO in Port of Rotterdam during period of current research, from Ship & Bunker (2022).

In the section above it was shown how the current model can be used to make scientific based estimates for changes of yacht operation. Here, it became clear that due to biofouling, more power is required to sail the same

speed. To increase the output power of the engine, the fuel rate ($\dot{m}_f$) is increased, as shown in the equation below (Stapersma, 2022). Here, it is visible that the increase in fuel rate results into an increase in engine cycles (f).

$$P_B = \frac{\dot{m}_f}{sfc} = \frac{m_f \cdot f}{sfc} \tag{7.1}$$

Each cycle requires heat input ($\dot{Q}_f$), the engine than transfers this thermal energy into mechanical energy, resulting in the work (W_e) provided by the engine. Here, the efficiency between the transfer of heat to work is noted as the engine efficiency (η_e). The more cycles the engine does in the same time frame, the more heat required, and the more work and power delivered.

$$\eta_e = \frac{P_B}{\dot{Q}_f} \tag{7.2}$$

$$P_B = W_e \cdot f \tag{7.3}$$

The exhaust flow rate of the engine ($\dot{m}_{out}$), is a combination of the air flow into the engine ($\dot{m}_{in}$) and the fuel rate, as shown below.

$$\dot{m}_{out} = \dot{m}_{in} + \dot{m}_f \tag{7.4}$$

Therefore, with increase in power, a greater mass and thus volume of exhaust gas passes through the exhaust valve in the same amount of time. As a result, the exhaust temperature increases, together with the temperature of the engine itself. This process is shown in Figure 7.5, where the engine performance diagram is also presented.
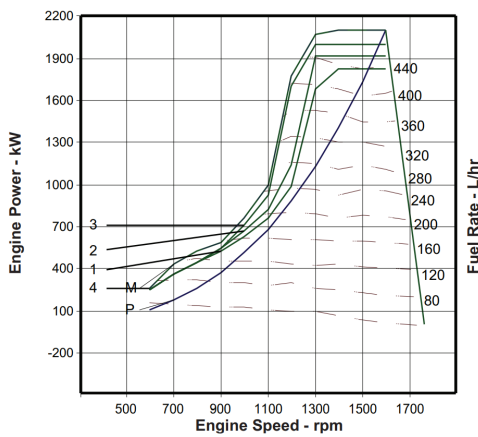
(a) Marine Engine Performance Diagram, from Caterpillar (2022a).
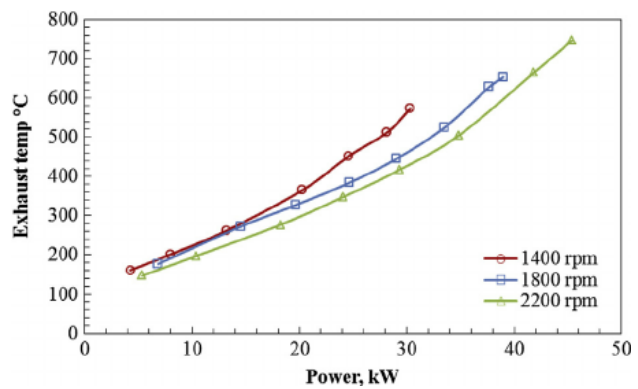
(b) Exhaust gas temperature variation with engine power, from Bari and Hossain (2013).

Figure 7.5: Relation between engine power, engine speed, fuel rate, and exhaust temperature.

However, fouling does not relate to just higher exhaust temperatures. Often marine engines make use of open cooling systems, using sea water as a refrigerant, as shown in Figure 7.6a, where the water intake is noted with 1. When fouling is present on the ship, it often also settles within the water intakes, as shown in Figure 7.6b. In this situation, the diameter of water intake becomes smaller and less sea water is available for the cooling system. The combination of both can lead to improper cooling of the propulsion system, where temperatures become too high. This can result into malfunctions, breakdowns, and with that downtime.
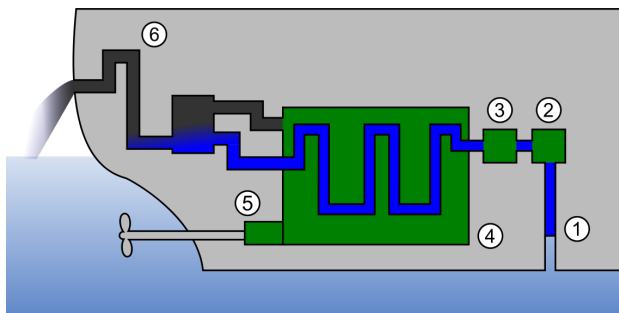
(a) Ship engine cooling system.

(b) Fouled sea water intake.

Figure 7.6: Marine engine open cooling system using sea water.

Not only does the problem described above increase the risk of engine breakdowns, it can also be seen that the increase in fuel use causes more required maintenance. In Table 7.2, the maintenance intervals are shown for the installed engine of the studied ship. From this it can be found that when more fuel is used, as shown in Table 7.1, the engines need maintenance faster and with that more regularly.

Interval	Maintenance task(s)
When required	Used filter inspection
Daily	Engine crankcase oil, cooling system, walk-around inspection, marine transmission oil, air starter lubricator oil, air tank, engine air cleaner, engine oil filter differential pressure, engine fuel filter differential pressure
Every 50 service hours or weekly	Zinc rods, engine air cleaner
Every 250 service hours or 121,375 L (32,030 gal) of fuel	Scheduled oil sampling, engine oil and filters, cooling system, batteries, alternator belts, fuel tank, initial valve lash and injector timing
Every 500 service hours or 242,750 L (64,060 gal) of fuel	Air cleaner elements
Every 1000 service hours or 485,500 L (128,125 gal) of fuel	Engine protective devices, crankcase breather, fuel filters
Every 2000 service hours or 971,000 L (256,250 gal) of fuel	Engine valve lash, vibration damper & engine mounts
Every 3000 service hours or 1,456,500 L (384,375 gal) of fuel	Performance analysis report
Every 4000 service hours or 1,942,000 L (512,500 gal) of fuel	Electric starting motor, fuel injectors, top end overhaul, cooling system
Every 6000 service hours or 2,913,000 L (768,750 gal) of fuel	Alternator, air starting motor, water pumps, thermostats
Every 7500 service hours or 3,885,000 L (1,025,000 gal) of fuel	Turbochargers, overhaul, after failure overhaul

Table 7.2: Maintenance Management Schedules for installed engine, from Caterpillar (2022b).

From this table the conclusion can be drawn that a fuel consumption of 485.5 L / hour is a critical value, as above this value most maintenance is done based on fuel consumption. This critical value is achieved when the engine uses 1,445 kW of power. With two of these engines installed, for the current yacht this would mean that when it sails around 14 knots or higher, required engine maintenance starts to increase. Furthermore, this situation is also met with the average speed of 13 knots, when the increase in power due to biofouling is 30% or higher. Thus, the conclusion can be drawn that engine downtime will occur more frequently due to biofouling.

An overview of this is shown in Figure 7.7, where both the studied increase in power and maintenance frequency are presented. In this figure, it is clearly visible that for the current ship, the critical fuel consumption is reached at an increase in brake power of 30%. Starting from this value, all major engine maintenance is now done on a fuel basis, resulting in more frequent service due to biofouling. At this point possible engine malfunctions and additional downtime due to biofouling are not yet taken into account.
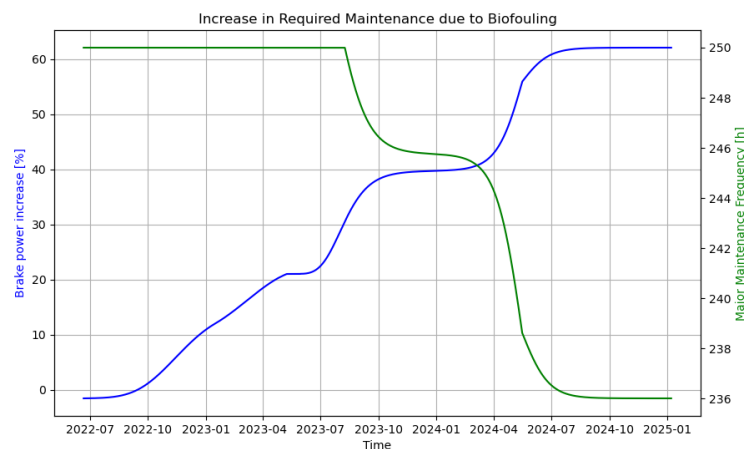
Figure 7.7: Increase in maintenance frequency due to biofouling fuel increase.

7.3. Propeller Cleaning

One of the questions outlined for the business case was how influential the propeller was when it comes to the problem of biofouling, and when or how it should be treated. In Figure 7.8, the total added power due to biofouling is visualized. Here, both the added power due to hull resistance and the added power due to loss of propeller efficiency, are shown.
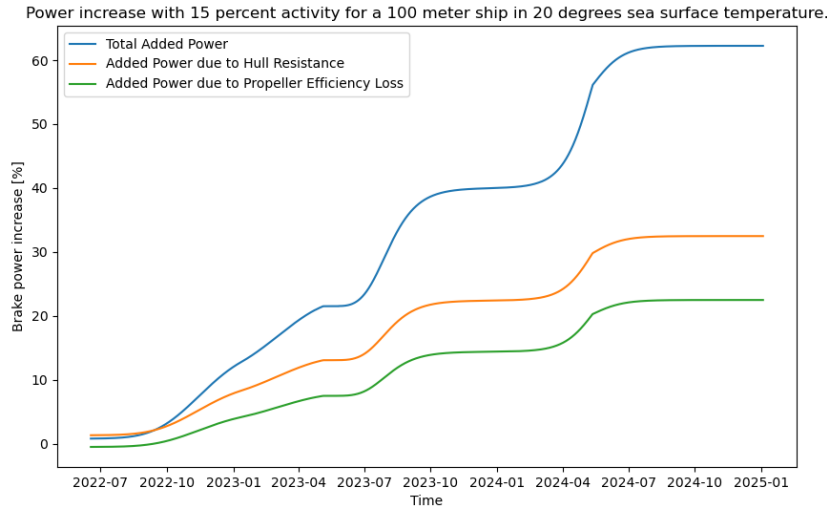
Figure 7.8: Propeller and hull contribution to total added power.

To minimize the added power due to biofouling, both the hull and propeller can be cleaned, so that the ship becomes smooth again, getting rid of the rough surface which causes friction. When the hull and propeller are compared, it can be seen that the hull has a far larger underwater surface than the propeller. However, their contribution to the added power due to fouling shows a far more even distribution. While cleaning both is optimal, it must be noted that cleaning the propeller also shows significant decrease in added power. Furthermore, propellers can also be cleaned underwater if the appropriate or no coating is applied. Note that underwater hull cleaning is also possible, both with divers as with robots. However, due to the curves of the Feadship yachts, cleaning robots perform less optimal on Feadships compared to for example container vessels. Furthermore, cleaning the full hull of these large yachts can be time consuming, while the propeller is cleaned faster with quick result. In the figure below, an overview of the total added power due to biofouling is given with different propeller cleaning intervals.
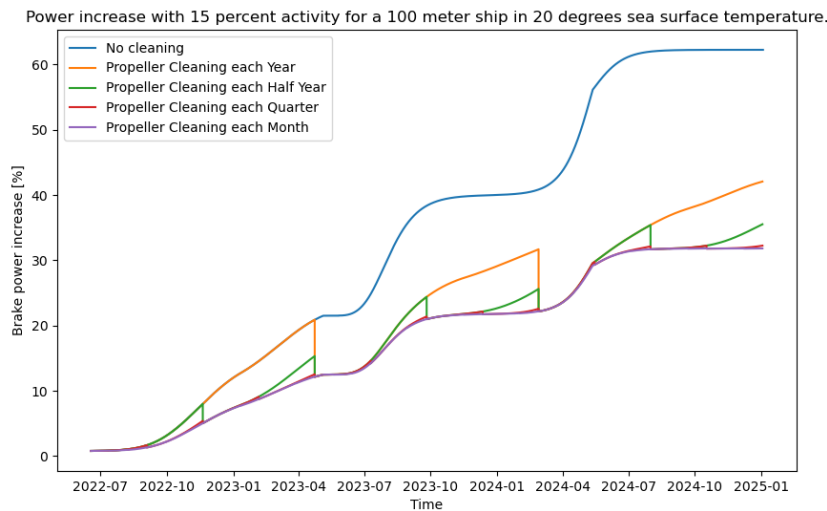
Figure 7.9: Effect of different propeller cleaning intervals on total added power.

7.4. Location Specific Antifouling

In subsection 4.3.3, a method was introduced to split the added resistance of a ship from fouling up per ship section. With this approach, the goal is to find how different ship sections each have their weight on added fouling resistance, and how location specific antifouling treatment might improve overall performance. At this moment, often the following antifouling treatment is applied for new build Feadships:

1. Ship hull is built and primer is applied, after which the yacht sails to yard within one week to go into dry dock again, as primer does not protect against fouling.
2. Two layers of antifouling are applied to the ship.
3. One additional antifouling layer is applied from the waterline to the first one meter of the ship, also referred to as a 'belly-band'.
4. At some time in the building process, the dock is filled with water. Around 3-6 months after antifouling had become active with water, ship is launched and starts sailing.

The current part of the business case dives deeper into a more specific and aware antifouling approach. Biocidal antifouling coatings are often only active for 2 years, as industrial parties recommend. For new build Feadships, this would sometimes mean that the ship should not go out of the water after 2 years, but already after 1.5 years, which is not always realized. Furthermore, regions closer to the surface can expect more sunlight and higher water temperatures, and thus more fouling growth. Additionally, fouling results into an even higher resistance where flow numbers across the ship are higher. All of this combined can lead to a region specific approach on antifouling application, which is discussed in this section.

(a) Oblique view aft body.

(b) Bottom view.
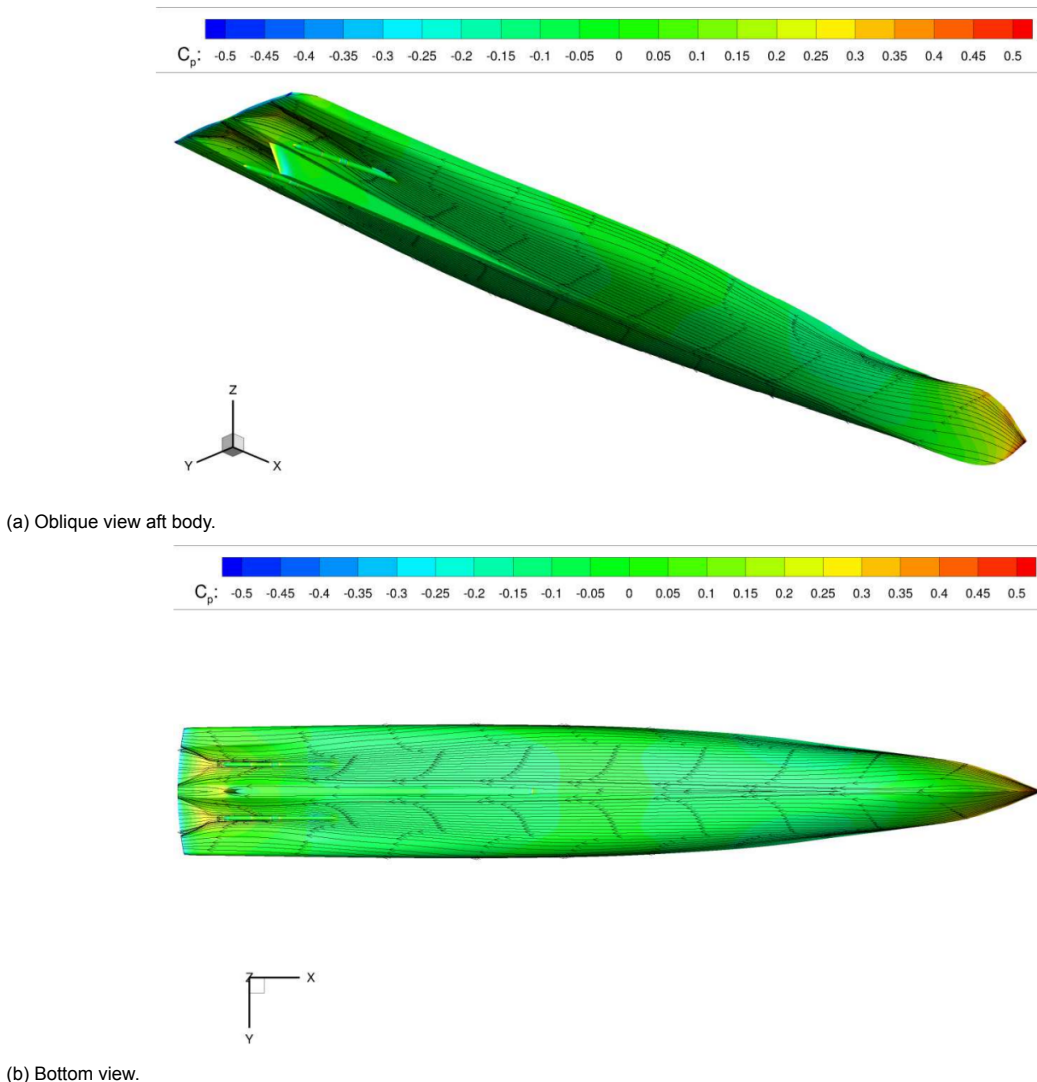
Figure 7.10: Streamlines and pressure distribution on the hull.

In Figure 7.10, the pressure coefficient is shown over the ship underwater hull, which can be described with the function as shown below:

$$C_p = \frac{p - p_\infty}{\frac{1}{2}\rho_\infty U_\infty^2} \tag{7.5}$$

It can be seen that the current function has both flow speed and pressure across the hull as input. However, with help of Bernoulli's equation and the assumption of incompressible flow, the function can be simplified as follows:

$$C_p|_{Ma\approx 0} = 1 - \left(\frac{u}{u_\infty}\right)^2 \tag{7.6}$$

For the stream line figures, C_p ranges from -0.5 to 0.5. For locations where $u = u_\infty$, it is visible that C_p = 0. Based on the figures, three main observations can be made:
- Pressure is equally distributed over the hull, with only small differences present in general
- Pressure is highest at the bow
- Pressure is lowest at the stern, indicating higher flow speeds here

Based on the current observations and the patterns found between hull friction due to biofouling and appropriate antifouling application, it can be seen that the stern is an important region. Not only is it more important to keep this section clean, fouling release coatings could also have more optimal working here, as fouling detachment will occur at lower speeds compared to the rest of the ship.

In subsection 4.3.3 the function of Townsin was worked out in more detail to find resistance per area. With this, both the influence of different levels of biofouling and different flow speeds can be found. When we want to break down the resistance between the low flow region of the bow, the midship with average flow, and the high flow region around the stern, the function can be written as follows:

$$\Delta R_F = \sum_{i=1}^{n} \left(\frac{1}{2}\rho S_i V_S^2 \left(0.044 \left[k_{s,i}^{\frac{1}{3}} \cdot \frac{1}{1.5/100 \cdot 100^{1/3}} - 10 \cdot Re_i^{-\frac{1}{3}} \right] + 0.000125 \right) \right)_i +$$

$$\left(\frac{1}{2}\rho S_{i+1} V_S^2 \left(0.044 \left[k_{s,i+1}^{\frac{1}{3}} \cdot \frac{1}{97/100 \cdot 100^{1/3}} - 10 \cdot Re_{i+1}^{-\frac{1}{3}} \right] + 0.000125 \right) \right)_{i+1} +$$

$$\left(\frac{1}{2}\rho S_n V_S^2 \left(0.044 \left[k_{s,n}^{\frac{1}{3}} \cdot \frac{1}{1.5/100 \cdot 100^{1/3}} - 10 \cdot Re_n^{-\frac{1}{3}} \right] + 0.000125 \right) \right)_n \tag{7.7}$$

Note that the function was written in such a way that if we took the normal function of Townsin, this would still result into the same sum of values as with the equation written above. However, in this case we want to reevaluate the weight of each fraction, we can find the new Reynolds number as shown below. For the high flow stern region, the equation can be solved as shown in Equations 7.9 and 7.10.

$$Re = \frac{u L_{WL}}{\nu} \tag{7.8}$$

$$\left(\frac{u}{u_\infty}\right)^2 = 1.3 \tag{7.9}$$

$$u = 1.14 u_\infty \tag{7.10}$$

In case Equation 7.7 is used with normal flow and a given fouling situation, the added frictional resistance for the aft section of the ship is 40.5 kN. When the real and higher flow speed is taken into account for this region, it can be seen that this value goes up to 52.7 kN, and is 23.2% higher. Note that the same approach can be taken for the front of the ship to find a similar lower resistance here. Based on these findings, it can be seen that biofouling effects across the hull can differ largely. Especially for ships with a less even distribution of flow, finding important regions could be valuable, with possible different antifouling approaches for these locations as a result.

Even with a rounded hull Feadship yacht and almost equal flow across the entire hull, at the studied locations it was already clear that a region with higher flow has a significantly higher biofouling resistance. This means that this is an interesting topic from both a ship design and operation point of view. If ships have larger differences in flow speed across the hull, attention could be given to applying different products for different locations. As mentioned, foul release coatings are characterized for their smooth application, compared to often more rough biocidal coatings, and can have optimal working in locations with high flow.

7.5. Antifouling Coatings

Within this research, it was already discussed that antifouling coatings are the primary protective measure to mitigate the problem of marine biofouling for ships. In section 1.2 an introduction was given into different antifouling solutions, while in section 1.3, the development of different antifouling measures was presented. Today's antifouling coatings can be classified into two main categories based on their compositions: biocidal and non-biocidal coatings (Demirel et al., 2013). To compare the different types of coatings, an overview of different type of biocidal and non-biocidal coatings is presented in Table 7.3.

Coating	Composition	Effectiveness	Characteristics
Controlled Depletion Polymer (CDP)	Biocidal	Up to 3 years (Van Rompay, 2012)	Use of hydration process and release of biocides. Mainly applied to ships with short drydock intervals operating in low fouling regions (Atlar, 2008).
Self-Polishing Copolymers (SPC)	Biocidal	Up to 5 years (Van Rompay, 2012)	Good initial hydrodynamic performance owing to their smooth surfaces and better antifouling ability. Preferred for vessels with longer drydock intervals (Taylan, 2010). Full recoating down to bare steel 2 or 3 times in 25 years. Not suitable for aluminium hulls.
Hydrid SPC	Biocidal	Life span between 3 and 5 years	Biocide release method regarded as hybrid, between hydrolysis and hydration.
Foul release (FR)	Non-biocidal	3-5 years before FR coat needs repair/reapplication	Prevent the attachment of marine species on hull owing to surface properties. Not appropriate for slow ships and for ships spending long time in ports, as coating requires shear force from higher speeds to detach the marine organisms. Full recoating required 1-3 times in 25 years.

Table 7.3: Antifouling coating comparison, adapted from Demirel et al. (2013).

Note that biocidal coatings as discussed consist of either soluble matrix biocide releasing coatings and insoluble releasing coatings, as shown in Figure 7.11. Both coatings rely on the release of biocide, and it is visible that loaded antifoulant is released to the environment over time. However, with the soluble matrix, the coating becomes more thin as the unloaded part of the paint is also detached during operational time. Therefore, the type of biocidal coating is also important for antifouling reapplication and cleaning at a later stage, as the level of coating thickness is important for durance of protection and the adhesion strength of the antifouling.
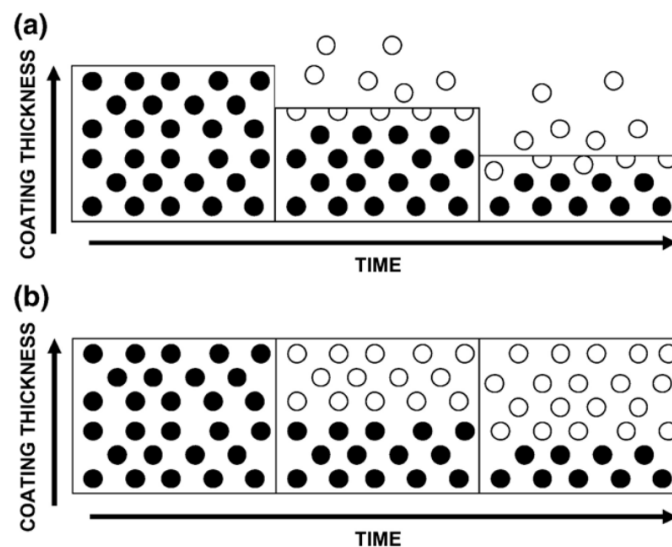

Figure 7.11: Schematic of (a) soluble matrix biocide releasing coating and (b) insoluble biocide releasing coating. ● Antifoulant loaded, ○ depleted antifoulant, from Chambers et al. (2006).

With the characteristics and basis of the different type of coatings explained in Table 7.3, next it is valuable to get insight into the performance of these different type of coatings. However, it can be seen that since these different types of coatings have different workings, coatings can be more or less effective for ships with certain applications. Nonetheless, it is important to get insight into the effectiveness in the coatings presented. Currently there is limited scientific data available on contributors to added drag of in-service ships, represented by modern-day coating roughness and biofouling, either separately or combined (Yeginbayeva and Atlar, 2018). For the prediction of biofouling growth, one of the first mathematical models by Uzun et al. (2019) was used to make fouling roughness predictions. For product comparison, very little information is available, and companies must mainly rely on supplier information. To give some insight into product comparison, in the table below the expected effective power increase is shown for a CDP, SPC and FR coating for clean, low and high hull roughness at 19 knots. Here it should be noted that this case study was worked out for a benchmark container vessel (KRISO Container Ship, KCS), which has different hull shape, and largely different operational profile than Feadship yachts. However, as this study only shows expected power with a given roughness situation, and not expected fouling growth, the second is less a problem. Even though increase of power might not be as expected for Feadships, this comparison does give good insight the roughness of products themselves, and their resulting added power.

Roughness Condition	CDP type	SPC type	FR type
Smooth	5.5%	3.5%	1.3%
Low hull roughness	13.6%	11.4%	4.7%
High hull roughness	14.8%	12.5%	6.1%

Table 7.4: Increase of effective power ($\%\Delta P_E$) for KRISO Container Ship (KCS) at 19 knots, adapted from Atlar et al. (2018).

In the table above, it can be seen that regardless of level of biofouling on the ship, FR type antifoulings are the most smooth, while CDP type coatings have the most rough texture. However, this does not give insight into how fast these levels of biofouling are being reached with these coatings. Even though it is known that this is dependent on a large number of variables, as was discussed in section 2.1, product comparisons in fixed conditions would help to do product choice on a more scientific basis. Furthermore, this would also help into translating the current developed model for different types of SPC coatings and possibly other antifouling paints. Nevertheless, the ship owners rely mostly on experience with products and advice from antifouling company experts. The only thing that is provided by these companies if any about product performance, is expected speed loss and fuel consumption over the product before docking. An overview of this is shown in Table 7.5. Note that fuel savings is not always provided, and thus only shown where available.

Product	Type	Speed loss over docking cycle	Fuel savings over docking cycle
Interswift 6800HS	Copper Acrylate SPC	3.3%	
Intercept 7000	Linear Polishing (LPP)	2.7%	
Intersmooth 7465HS	SPC	2%	
Intersmooth 7465Si	SPC	2%	
Intersmooth 7475Si	SPC	1.5%	
Intercept 8500	Linear Polishing (LPP)	1.3%	
Intersleek 1100SR	FR	1.2%	9%
Jotun HPS	Silyl methacrylate-based coating	1%	14.7%
Hempel Hempaguard X7	Silicone coating with biocide-activated hydrogel surface	1.4%	6%

Table 7.5: Antifouling speed loss and fuel savings over docking cycle based on International Marine (2022a; 2022b), Hempel (2022) and Jotun (2022).

For better insight into product choice, it would be optimal if antifouling suppliers either shared static and dynamic tests of their coatings, or if research is done into biofouling growth with different antifouling coatings applied. With this, the model as worked out throughout this research can be improved. As one of the industry leaders, Feadship wants to move from a stage of experience and trial & error to a more scientific approach were they can make an accurate assessment on the best products for their yachts. They want to look beyond antifouling marketing, supplier promises, and experts, and level in the conversation based on own knowledge and measurements from products. For this reason, the procedure for static antifouling panel testing and implementing results into the model is outlined in the following section.

7.6. Antifouling Panel Testing and Model Implementation

In this research a method was developed to make fouled power ship predictions with a physical model, and improve these predictions with a data-driven model. For the physical model, the prediction of biofouling growth is based on a SPC coating of which the exact type is unknown, together with growth measurements for this coating in the Mediterranean and Equator region. To improve the model and gain new insight from both an industry and research perspective, it would be optimal to gain insight into growth measurements for different coatings, at different locations. With antifouling applied to panels and static measurements, biofouling growth can be analyzed and captured. When more regions are captured, ship owners can give more accurate predictions for fouling growth and its effects. When more coatings are captured, ship owners can make more scientific based choices for antifouling coating, not only relying on supplier experts. With this added insight, a better trade-off can be made between costs of products and their effects.

To get an understanding of how this done, one can start with consulting ASTM D6990-05 (2011). In this document, the standard practice for evaluating biofouling resistance and physical performance of marine coatings is explained. Here, the testing and installation settings are discussed, together with safety hazards and materials to be used. In the different procedure steps, ASTM D3623-78a (2012) is highlighted, the standard test method testing antifouling panels in shallow submergence. This method is designed as a screening test in evaluating antifouling coating performance, where systems that provide positive comparisons with standard systems should be considered acceptable for use in protecting underwater marine structures. Since the degree and type of fouling relies heavily on the environment, as outlined in section 2.2, a fouling census on a nontoxic surface should be taken. For the exposure to be valid, the nontoxic surface should show heavy fouling, and the standard test should show significantly less fouling. In the test method, a clear procedure is given on required panels, how the panels need to prepared including pretreatment and antifouling, and how fouling should be evaluated/tested.

For application to the current model, Uzun et al. (2019) next explain how these analyses were supported with image processing, which enables obtaining colour contrast and having a more accurate quantification of the fouled area, number, and size of the attached fouling organisms. Note here that the image processing does not supply a fouling rate itself, but simply is a useful tool to better asses the fouled plate. Here biofouling accumulations on the test panels were categorised into three main groups:
- Slime, including absorbed inorganic and organic matter, trapped silt and detritus and other unidentified slimes (Rating 0–20).
- Non-shell organisms (shorter than 5 mm): Plants, soft-bodied organisms, weed, very isolated (limited) barnacle accumulation (Rating 0–50).
- Calcareous type fouling (higher than 5 mm): Barnacles, mussels, tubeworms, etc. (Rating 0–100).

The maximum rating of each biofouling group varies considering their hydrodynamics effect on frictional drag, for which the paper of Uzun et al. can be consulted for a clearer few on how these ratings were formed. To go from the processed images and their fouling patterns to the fouling rating for the three main groups, Uzun et al. use the Braun-Blanquet scale method, as shown in Figure 7.12. With this the surface coverage of each type of fouling can be converted to a fouling rating for this fouling, fitting in between the ratings as listed above.

Braun-Blanquet Score	Range of Cover (%)
5	75–100
4	50–75
3	25–50
2	5–25
1	<5; numerous individuals
+	<5; few individuals

Figure 7.12: Braun-Blanquet scale method, from Braun-Blanquet et al. (1932).

Uzun et al. identified a delay, growth and saturation phase within the fouling growth of each type, proposing a Gaussian function for proper fit, with a half-bell curve to satisfy the saturation phase. Note that for the surface coverage of calcareous fouling, an additional curve is made. Here, instead of transferring the numbers to a fouling rating, the surface coverage is captured throughout the period and fit with a logistic curve.

With this approach antifouling coatings can now be compared and modeled with static tests. Note that this does not include the more complex problem of biofouling changes during sailing, which is especially important for foul release coatings. In the current research, an attempt has been made to capture this phenomena with the grey box model. Dynamic tests could also be performed where panels are either tested on a drum or are placed under a ship. Nonetheless, it is important that these tests are performed for different levels of biofouling at different speeds, as adhesion strengths can differ largely. Once a pattern is captured, this can be taken into account to change either fouling rating and calcareous surface coverage, equivalent sand roughness height, or simply added power due to biofouling, depending on modeling fidelity.

7.7. Answers to Business Case

In this section the answers to the questions as outlined in subsection 1.6.2 will be answered, based on the information provided in this chapter and throughout the thesis report.

Which type of antifouling should be applied for which yacht?
With the developed model, fouling predictions can be made for all ships and trade offs can be made for the product which can best be applied. However, further research into comparisons of different products and their performance would help significantly. For this reason, the advice is to do antifouling coating tests for more product, with a detailed guideline given in section 7.6.

What is the difference between the influence of salt and fresh water on the marine biofouling growth?
In this research, it was found that salinity values are largely different for salt water as for fresh water. This means that fouling relations that are found in one do not fully apply in the other. Furthermore, some micro organisms can only live in either salt or fresh water, effecting ships moving in between both.

How does anchor location relate to the problem of biofouling?
In the developed model, it can be seen how anchorage location and its environmental conditions have a large influence on biofouling development. With figures, it was visualized how increase in brake power can differ largely as a result of sea surface temperature. Furthermore, these increases in power where then used to show changes for a largely variety of ship operational parameters.

How influential is the propeller to the problem of fouling and how/when should it be treated?
In the white box model outcome, it was found how ship resistance increased with 9% over the researched period, while the propeller efficiency decreased with 5%. With the propeller having a large effect on biofouling added power compared to its size, cleaning ship propellers during operation can be seen as a valuable step for efficiency improvements. This recommendation is trend with research performed on ship grooming as part of antifouling approach. Furthermore, insight was created into the potential effectiveness of propeller cleaning in section 7.3.

Should vessels be cleaned and provided with new antifouling prior to yacht transits?
This question can be answered case specific with the developed model together with docking and antifouling costs known from prior projects done within Feadship. In this chapter it became clear that added costs and decrease in operational performance due to biofouling can be very large, and that cleaning before transit can be a smart strategy. This is not only to minimize fuel cost and regular maintenance, but also to remain speed and range, and decrease risk of engine malfunctions.

Can it be useful to use more antifouling on some regions of the ship than others, e.g. regions with higher Reynolds numbers?
While flow is fairly equal distributed over the researched ship hull, it can be seen that even on small regions with higher and lower flow, differences in resistance due to fouling were clearly visible. While regions with high pressure might require more antifouling for proper adhesion strengths, for regions with high flow different products as foul release coatings can be applied. Foul release coatings showed that they were smoother compared to biocidal coatings, and the cleaning / detachment phenomena required for this coating is reached at lower speeds in these areas.

IV

Conclusion & Discussion

In the previous part of this report the model outcome was evaluated and the business case was produced based on the model. In this last part, conclusions based on the results will be drawn in chapter 8 and discussed in chapter 9. Based on this, model limitations will be summarized and recommendations will be given in chapter 10, together with main contributions made.

8
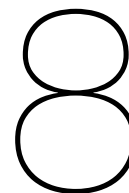
Conclusion

In this chapter the different research questions that were proposed in section 1.8 will be answered. First, in section 8.1 the sub questions regarding the methodology will be answered. Next, in section 8.2 the questions regarding the model results will be answered. Last, in section 8.3 the main research question will be answered.

8.1. Methodology

Different sub questions have been pointed out to find and develop an accurate prediction method. These questions have been answered in the problem analysis (chapter 2) and method exploration (chapter 3) and answers can be summarized as below.

What are the current methods to predict added sea margin due to marine biofouling?
Different methods exist to predict added sea margin from fouling, with the simplest methods advising to either use a constant yearly fouling factor or to use a standard factor for a one or two year period. However, these coefficients give large inaccuracy, as fouling is dependent on a lot of variables and can variate by large numbers. Even though many research has been done in marine biofouling, little models have yet been developed to predict the level of biofouling on ships. This is mainly due to the fact that we do not yet know how all fouling variables physically combine into types of biofouling growth. However, models have been developed that measure different types of fouling overtime, and build functions based on how this process develops and results into roughness. Then, roughness can be interpolated and extrapolated with sea surface temperature as the dominant fouling parameter. It can be seen that more research has been done into biofouling effects on hull resistance, ship performance in waves, and propeller efficiency loss. Here, both first-principle experimental based models can be used together with the use of Computational Fluid Dynamics (CFD). Last, together with an increasing trend in the full maritime research field, first attempts have been made to use data-driven modeling to derive added sea margin as a result of marine biofouling growth.

What are the method requirements to model the effects of fouling?
The methods requirements are set in section 2.6, and are assessed in section 3.4 to verify that all requirements are met in the worked out methodology. This contains white box requirements for the modeling of biofouling, added hull resistance and propeller efficiency loss. Furthermore, requirements have also been set to overcome white box limitations with help of black box modeling, turning the delivered model into a grey box model. Last, errors should be filtered out of voyage data to obtain accurate and realistic results.

What methods are suitable to meet the method requirements, and if suitable how can machine learning and grey box modeling assist in solving the problem?
Based on the method requirements, a grey box model has been proposed to deal with the problem. With this model, the option is given to predict biofouling with both a data-driven model as with a more mathematical formulated model. This means that when large amounts of data are available, it can be used to derive fouling patterns for the studied ship. However, either when this data is not available, or when predictions must be made for new conditions, it can be seen that it is better to use a white box approach, as the grey box model will have less accuracy due to extrapolation. The proposed model can be found back in section 3.3, while the final model and its use is shown in subsection 6.4.3.

8.2. Model Results

With the methodology worked out in chapter 4 and chapter 5, model outcome was worked out and is validated in chapter 6. Furthermore, in chapter 7, additional information was derived from the model to answer relevant questions. As a result, the sub questions lined out regarding model results can now be answered.

Does the model show difference in added sea margin for different antifouling systems, and can this form a basis for antifouling system selection?
First, it can be seen that the current model does not yet have different antifouling systems configured. The model build from white box predictions contains a SPC type antifouling coating. Differentiation into types of SPC and other antifouling coatings is not yet made, as the authors of the biofouling growth model recommend this for future research. Not only is it in this research not included, to the authors knowledge there is little research available yet into antifouling performance of different products available on the market. While pros and cons are known and highlighted, it is often not known how well products actually perform compared to each other, or how much fouling growth they can prevent at all. When it comes to fouling change during sailing, it can be seen that little information is available on this either. Nonetheless, a first attempt was made to predict change in fouling when sailing with help of the data-driven model for the researched Feadship yacht, which resulted into some detachment present when sailing. It can be seen that for coatings that rely on fouling detachment as fouling release coatings, this phenomena will be even more strongly visible. Overall, the model gives insight into the predicted fouling in the future for a SPC coating. Considering this together with the profile of the yacht, the fuel penalty can be calculated together with cost of antifouling, docking and cleaning. Based on that, a decision can be made on the optimal antifouling system. Last, it can be seen that when sensor data is available, the data-driven model can be trained to find patterns in the data. While this is now done for one ship, researching this for multiple vessels can give insight into performances of different antifouling systems. With little to no calculations and predictions now involved in antifouling system selection and maintenance intervals at Feadship, the conclusion can be drawn that the model is a big step towards a more scientific approach for these problems. With possibility of processing different ships in a data-driven model and labeling antifouling systems, patterns can be learned directly from to be collected ship data.

How much do vessel parameters, operational profile and location influence marine biofouling growth?
Since the data-driven model was currently only developed for one ship, multiple vessels with different parameters can in this model not yet be compared to asses differences. However, in the white box model large attention was given to the effects of roughness on ship performance. The friction coefficient resulting from biofouling roughness is dependent on the length of the ship, while this constant can then be applied over the hull wetted surface to find added resistance. This means that with an increase in ship length and ship underwater area, marine biofouling effects will be larger. It is expected that biofouling growth is larger along the waterline, as this area gets more light and has higher sea temperatures. However, from a study in the business case, it can also be seen that differences from ship parameters are relatively small on the percentage of added power required compared to the effects of water temperature and the amount of ship sailing. It was found that ship location and thus water conditions have the largest influence on biofouling growth, with sea temperature as the strongest parameter. Especially in waters with high temperatures, the accumulation of barnacles on the ship can start at a fast point in time, with high roughness and sea margin as a result. Regarding the operational profile, it can be seen that marine biofouling can best settle on the ship in anchoring profile. While it is expected that biofouling cannot settle on the ship above a certain speed, a detachment phenomena was even found over sailing data. Overall, this means that the more active the ship, the less fouling will be on the ship, and vice versa.

How accurate is the model compared to the current sea margin predictions used in Feadship and general ship design, and if required should adaptions be made?
From a ship design perspective, fouling sea margin predictions are either not made, or often with very simple approximations. Overall, powering calculations and ship speeds assessments are made for clean hull, as the problem of biofouling is more dealt with in ship maintenance and production than in the design stage. However, even in early stages of ship design, often already a lot of relevant information is known to make first predictions on biofouling development, and this thesis has been an attempt to support doing so. In the business case, fouling curves have been developed based on parameters of different Feadship yachts together with different levels of sailing and encountered sea temperatures. This together with incorporation of the obtained model in Feadships 7SEAS portal should give the Naval Architects from De Voogt more insight into the problem of biofouling, from a ship design perspective. In agreement with Feadship, it is currently being worked out how now known margins can be better incorporated in the ship design process, to make better decisions for both antifouling systems and desired engine margin / propulsion lay-out. In the different design stages, discussions can be made with clients on proposed antifouling systems and engines margins, together with predictions on future biofouling growth and their desired operational profile. With the model developed, additional insight is gained and information shared will not only be based on experience but also accompanied by research and science.

8.3. Main Research Question

For this research, the main question was formulated as follows:

> *"How can Feadship use in-house & onboard sensor data to accurately predict the added sea margin as a result of marine biofouling over time for yacht design, operation & maintenance?"*

By answering the outlined sub questions, it has been described how a grey box model has been worked out to process sensor data and use neural networks to make predictions of fouling sea margin within the boundaries of the dataset. Furthermore, a white box approach has been worked out to obtain results and get a deeper understanding of settlement of slime, micro organisms, and calcareous on the hull resulting in hull roughness. This information can then be used to find increase in frictional resistance over the hull and loss of propeller efficiency. With implementation of the proposed grey box model, predictions can be made for ships varying in all ranges of available data. This means that even in the earliest stages of design, once ship parameters are estimated and insight in operational profile is obtained, predictions can be worked out at a more accurate level then currently available. These predictions are specific for selected profile and dependent variables as water temperatures and time, instead of constants, improving ship design. With the development of this tool for Feadship and their fleet, and contributions made to this field of research, the main goals of this thesis have been met.

9

Discussion

In this chapter the main results and conclusions drawn from the research are discussed. This is first done from a scientific and economic point of view in section 9.1, and then from social and ethical point of view in section 9.2. After this, recommendations for ship design and operation are given based on these in section 9.3. Last, in section 9.4 additional recommendations are given for yacht design and operation in specific.

9.1. Findings from Scientific & Economic Point of View

With the current research, a model has been worked out to get a deeper understanding of the problem of marine biofouling, and make ship and situation specific calculations for the level and effects of it. With this, the problem is translated from a largely unpredictable problem which was lacking interpretation to something that is better captured. With this, additional information is provided for yachts based on their profile. For the design process this includes the assessment for better engine margins, and clearer expectations on possible outcomes. For operational use of the yacht, information is now available on added fuel use, loss of range and loss of speed, and increase in maintenance for a better cost-benefit analysis on ship cleaning and antifouling application. Shipowners often rely on ways how things are always done, while it was found this can continuously change. For example, the prices of MGO more than doubled within time of this thesis, having a large effect on operational costs of the ships. Therefore, having a model with predicted fouling growth supports quick assessments on when ships should be docked. With the use of a physical model together with use of ship data, an attempt has been made to best capture the problem in a scientific way, so that an optimal trade-off from an economic point of view can be made.

9.2. Findings from Social & Ethical Point of View

In this research, it was found that marine biofouling is one of the major problems in the maritime world. This is not limited to added cost for ship owners, but also includes the increase in greenhouse gasses and balance of the world oceans. To minimize biofouling accumulation, ship owners often use toxic antifouling coatings, and kill organisms to try and mitigate the problem. Nonetheless, biofouling still accumulates and ships sail around with fouled hulls and propellers. Not only is this a problem for sailing in the region where the biofouling attached, transferring invasive aquatic species around the world threatens the ecological balance of our seas. As a result, countries as New Zealand and Australia have already set rules for ships entering their country, requiring ships to clean prior to arrival and avoid entrance of new biogrowth organisms. However, each country follows different guidelines and procedures, and not each place is as strict in their policies. In most countries, these rules are not yet effective, and in some countries in water cleaning is not even a problem, regardless of whether toxic antifouling coatings are released directly into the water or not. Summarized, it can be seen that both the detachment of antifouling products and fouling itself comes with both risks and responsibilities, so that the quality of our waters and the life of aquatic species is maintained. Furthermore, the decrease of ship efficiency currently results into large additional fuel use and greenhouse gas pollution by ships.

To fulfill the goals set in this research, a grey box approach was chosen, which makes use of machine learning principles. Here, benefit was taken from data available to improve physical model predictions and learn more on this problem. Nevertheless, the use of machine learning principles and their ethical and social concerns should also be taken into account when applying these practices. For artificial intelligence, three major areas of ethical concern for society include: privacy and surveillance, bias and discrimination, and the role of human judgement. These are important to take into account, as the extensive use of artificial intelligence is a fast increasing trend, without many regulation yet around the development on this technology. For Feadship and this research the first

is most applicable, as the privacy of ship owners who provide sensor data should always be in the best interest. Therefore, it is important that this process remains as disclosed as possible, and that the data is handled with great care. Nonetheless, it can be seen that the application of artificial intelligence also gave great new insight into this model, and the decision process is always done by humans in combination with the interpretation of more understandable and transparent physical models. Concluding, users should always be aware of ethical and social concerns to machine learning principles, and weigh of ethical concerns when developing new algorithms.

9.3. Recommendations for Ship Design & Operation

Based on the findings discussed above for both points of view, for new ships that are designed it is first advised to improve fouling growth predictions. When these are made for the to be designed ship with suggested operational profile, proper engine margins can be selected which cover for example a 2 or 3 year period. Furthermore, more attention can be given to choice of antifouling coating, frequency of ship cleaning and care of collecting toxic substances and biogrowth when cleaning. Also from a economic point of view, it was found that more frequent ship cleaning can improve total ownership cost, not yet discussing otherwise negative effect in also loss of range. Furthermore, the benefits of more frequent propeller cleaning were also outlined in this thesis. If owners wish to use ships in an even more responsible way, it would be advised to use non-toxic products such as fouling release coatings. Here, instead of killing organisms, focus is put on making the surface of the ship hard to settle on, and stimulate a natural cleaning phenomena when sailing. Next to this, for warmer waters, yearly full ship cleaning would be advised to use the ship in a more efficient way, and avoid large increases in power due to biofouling. In case the ship operates in a colder region, cleaning at least every two years is advised. However, not only does this depend on water temperature, also other factors have a significant role, including frequency of ship use and sailing. In general, the author advises to look into relevant literature mentioned in the current report and figures developed within this research, to draw some first approximated conclusions on when ships could be cleaned to improve performance. Last, the advice is given to clean the ship if it was first in one place for a longer time and is then prepared for a long transit. This would avoid the travel of aquatic species, and will also improve the range in this transit and fuel use. Last, it can be seen that fouling not only results into increases in power, but can also settle around the sea water intakes, and thus reduces effectiveness of the onboard cooling systems. Requiring more power from the ship propulsion system in combination a cooling system lacking optimal performance can result into engine malfunctions and possible downtime, with high costs as a result.

9.4. Recommendations for Yacht Design & Operation in Specific

Next to the points addressed above, it can be seen that yachts sail far less than most ships, and are often stationary in warm waters and during daytime. Therefore, the problem of biofouling is an even larger problem for yachts. From a yacht owners perspective, it can be seen that economic is not the main driver, and that the yacht quality and performance is most important. Therefore, separate from the economic incentive to clean the ship, more value should be considered at ships reaching design speed, having a long range, and experiencing minimal downtime. In this research, it was found that yacht owners only sail their ship 15% of the time or even lower. This short time that is available to sail the yacht is very valuable for owners, and comes at the high yearly costs of maintaining the ship. This means that downtime when yachts are wished to be used, is very undesirable. For the problem of biofouling, this puts additional importance for yacht owners to not only invest in crew, maintenance and proper quality of the ship above the waterline, but also below the waterline of the yacht. Based on the current research, the advise is therefore to clean yachts on a yearly basis and incorporate sufficient engine margin in the design process. Furthermore, with the yacht industry being a leader in innovation and progress towards more sustainable shipping, it is advised to move towards non-toxic antifouling coatings. With clients becoming more interested in green shipping alternatives, recommendations given for propulsion should come inline with additional advice for proper antifouling systems and ship cleaning. Hence, the recommendation is also added to clean ships before large transits, such as sails from the Caribbean to the Mediterranean, or back to one of the yards in Holland. When fouling release coatings are used, it should be kept in mind that the yacht should not be stationary too long, as the desired detachment process of fouling would not be as good as desired with adhesion strengths becoming too strong. Inline with the fact that also for ship propulsion systems it is important to function regularly, it is thus advised to sail ships at least shortly every month, sailing a speed of at least 12 knots for proper fouling detachment, depending on applied product. With trends fouling trends that were identified in the current research, it can be seen that a desired future state and an expected one is a situation where ships are applied with non-toxic products, and are cleaned regularly. Next to this, it is expected and desired that ships only make large transits with a clean hull, reducing the environmental footprint of the yacht. This is not only something that is desired from a social or ethical point of view, but also something which is inline with a desired state for yachts and superyachts, taking optimal care of the ship. In conclusion the recommendations above are something were the yacht industry and Feadship can take the lead, and give better and more suited advise for their clients.

<div align="right">

10

</div>

Limitations, Contributions & Recommendations

In this chapter, first the models that formed the basis for the current model and are most applicable for biofouling predictions, are presented together with their limitations in section 10.1. Next, it is assessed how some of these limitations have been overcome, and how new insight was created in the current model in section 10.2, which can be seen as the research contributions of this research. Based on current and remaining modeling limitations, some future recommendations will be given for both Feadship to improve in-house modeling and for the field of research in marine biofouling in section 10.3.

10.1. Model Limitations

In the table below, the main models used together with their limitations an applicability are presented.

Model	Main Limitations	Applicability to Model
Time-dependent biofouling growth model for predicting the effects of biofouling on ship resistance and powering (Uzun et al., 2019)	• Derived fouling patterns based on Equator and Mediterranean and inter- and extrapolated. • Model based on one type of SPC coating. • Model based on static measurements, fouling changes when sailing not yet predicted. • Experimental based model, derived from physics but without full understanding yet.	This model forms the basis for the white box model, and thus the limitations to the single coating and limited fouling locations are also present in the current model. However, when ship data is available, the data-driven model can be used so that current coating is taken into account and the model can also work for regions where this method is less accurate.
The ship hull fouling penalty (Townsin, 2003)	• Added frictional coefficient derived from experimental study for large number of surfaces with roughness. • Found frictional coefficient used with pattern over flat plate found to model resistance over round ship. • Experimental based model, derived from physics but without full understanding yet.	Limitations of the model are present in the current study, as all alternatives have similar limitations. Model was used for its practical use and simplicity. Furthermore, limitations not applicable for data-driven model
Performance prediction method for fouled surfaces (Farkas et al., 2020b)	• Changes in thrust and torque coefficients due to fouling derived from open water tests. • Open water tests for roughness heights up to 500 micrometers, less accurate on higher levels.	Most applicable method to the authors knowledge where obtained roughness can be used to predict changes in propeller characteristics for fouled conditions and thus changes in propeller performance and open water efficiency. Furthermore, limitations not applicable for data-driven model.

Data-driven ship digital twin for estimating the speed loss caused by the marine fouling (Coraddu et al., 2019)	• Variance that occurs in ship sensor data makes it more difficult to derive patterns. • Speed loss was not always positive, as input of perfect clean state was missing for digital twin. • Linear robust regression for capture of fouling capture, only time-dependent with no distinction between anchorage or sailing. • Method requires non-indifferent amount of data.	For the data-driven approach taken in the current grey box, difference can be seen in smooth ship power prediction, where a white box approach is used rather than a trained ship digital twin. Limitations as variance in data and requirement of large and long period data were also experienced in the current data-driven problem. Instead of deriving a time-dependent linear pattern for biofouling speed loss, in the current data-driven model the choice was made to train a DELM on anchorage days, average anchorage temperatures, and sailing days for more insight in the biofouling problem.

Table 10.1: Main models used, limitations, and applicability to final grey box model.

10.2. Research Contributions

Next to mentioned limitations, it can be seen that while many research is performed into either biofouling or roughness effects on ships, little practical models currently exist to predict biofouling growth for a ship and calculate effects for ship propulsion. Most research is focused on given fouling situations and given ships, with then measured effects on ship performance with CFD or in a towing tank, making models very specific and less suitable for different situations. Especially the hard to capture biofouling problem is very difficult to describe. For this reason, the author is grateful for more practical developed models as used in the table above, and their usefulness to make predictions for ships based on input parameters, trying to become as accurate as possible. This thesis has been a work trying to combine the effects that are known and available, and improving where possible. Summarized, the main research contributions can be listed as follows:

- First proposal for use of grey box to model biofouling and its effects.
- Proposal to use smooth ship power with white box prediction for black box predictions, and model fouling based on anchorage days and average temperature, together with sailing days as second time-dependent variable, including all sensor data available and used for white box predictions.
- First proposal for determining fouling changes during sailing from data-driven model, leading to sailing factor that showed detachment trend in the current data-driven model.
- Combination of different available white box models, complimented with additional data-derived design / sea margin and sailing fouling changes to come to biofouling predictions for all ships.
- Research into different combinations of white box predictions and sensor measurements for optimal black box model performance.

10.3. Future Recommendations

With the model still containing limitations and new insight gained during the thesis, the following recommendations can be given for future research:

- Expansion of current biofouling growth model with measurements in new locations and for different types of antifouling coatings, including both biocidal and foul release coatings, as outlined in section 7.6.
- More research into fouling changes during sailing. Currently data-derived pattern was taken as a first estimate. However, more research and dynamic test for antifouling paints and fouling changes would help to provide choice in different types of systems.
- Gathering of additional data from different ships from data-driven model. Can give additional insight in influence on both type of antifouling and ship parameters for problem of biofouling. Here capture of speed over water instead of speed over ground would help to minimize noise in processed data.
- Research into improvement on antifouling systems, with biocidal and toxic products that can experience increasingly though legislation's, the demand is clear for optimization of antifouling systems that are environmental friendly and provide protection for clean and smooth sailing during a longer period of time.
- Monitoring and measurements of biofouling for yachts arriving back at the yards, together with evaluation of locations visited and time spend since last cleaning.
- Monitoring of ship hull and fouling development during last months of ship construction in water, gives insight in fouling levels already obtained. Good for information on when yacht should come back into dock, together with trade-off for possible in dock or underwater cleaning before launch.

Personal Reflection

Working on the master thesis for the past months has been a fun and challenging experience. Personally, I was really looking forward to the kick-off for this project. With many courses followed, reports delivered, and exams done during my period in Delft I was ready to start with something different at Feadship. Planning some time in advance to look for a nice research option with a company that excites you is something I could advise everybody. Your thesis for is for a longer period of time so its important that you like what you do, and this also gives the opportunity to still work in a company, with no internship in the master program.

During the master thesis I learned a lot of new things, not only about my subject, but also about how to handle a larger project together with overall communication and work skills. In general, I am happy with the result of the project and the work delivered. During my thesis, I got valuable personal feedback from my supervisors at TU Delft and Feadship. Sometimes I already think, before I listen to what they have to say, which is something I can improve. Even though I can be energized to talk about the subject, its always important to listen to what others say with care, as they often share new knowledge and bring important points. Next to this, I also experienced that everything is very time consuming, and that it is important to be careful with what you promise to deliver, as there is the tendency to wanting to do everything even though time is limited. Below you find an attempt to summarise some of my main experiences during the master thesis, which I hope are valuable to other students.

- **Project start:** The literature study is at the beginning of the project, and at times you are not sure what to work on. Even though there is a large project ahead of you that you know should take much time, at the beginning you will not always have a clue on where to start. During the literature study, I found that paper introductions are a great way to familiarize yourself with a research topic. While a paper itself is often about a very specific topic within a research field which is still new, the paper introduction or abstract covers work done within this field of research. Not only is important work cited, a summarized story is given on what is currently known and unknown, and what the main challenges are. Reading this gives you better background on the topic, which is valuable for the understanding of the problem.
- **Literature study:** At first I was not sure what the literature study was all about, and saw this mostly as book of knowledge and sum up of the performed research close to your topic. However, I found that this part of the project is much more about laying the ground work and making a research plan. The goal is to identify the gap and propose a method for your research, together with a plan on how to do this and relevant questions to be answered. You also have the false impression that the project takes forever and that there is a lot of time after the literature study, but this is shorter than expected. Therefore, I found that everything that I had worked out in detail in the literature study was very valuable. On the contrary, I realized that less time was available then expected with stuff I did not work out yet.
- **Modeling and writing:** Writing takes time, so for me it worked best to write what I have modelled once a clear part or section of the model was finished. While writing everything after the model will mean that you can get in problem with time, waiting until you can write full sections helps with spending not to much time on writing alone, and putting your focus on the model. For me it always works best to do all writing first, and then reread and check everything after, instead of worrying to much on each sentence when writing. However, I also found that rereading everything done can be a lot of work, and should not be underestimated.
- **Planning and keeping focus:** With a big project as a master thesis, it really helps to plan stuff out and get a sense of where you are in the project. When I had the sense that I had forever to finish the project, planning from the next deliverable back to when I should have a concept, to when I should have finished a certain chapter or section, and what this means for now usually helped with getting a sense of where I was in the project. Not only is it good to be on planning, this also helps with keeping your focus. Doing research requires a lot of attention and effort, and it can be challenging to keep focus on your work. This is something I also experienced, as a lot of things you are working on are new and require a lot of attention and energy. For me it always helped when I knew what to do, so I could have goals for each day on what to finish, even if they were small. Also, I try not to worry to much if my head is not in there for a day or two. Relaxing is also important together with doing fun things, not putting to much pressure on yourself helps, and keeps a good balance.
- **Results vs conclusions:** From the master thesis and some peoples approach towards this, you can get the expectation that you should deliver ground breaking research, fixing all problems found in the literature study. However, this is unrealistic and can lead to bad decisions or too much pressure on yourself. The goal is not to get the best or perfect results, but to draw the best conclusions based on your results and research. Its far more important to be critical, this includes your own work as well as work of others. You and everyone

involved in the project agreed on the approach taken, with a hypothesis on the outcome. This is something I experienced throughout the project, as I first was not sure on where the main emphasis was. However, from this thesis I learned that doing the research in the best way and sharing outcomes and experiences in a clear and critical way is more valuable than just showing good results. After this you can draw conclusions and give the best recommendations. While good results would be beneficial, you need to prove yourself as a researcher and work out your research gap. Either if its a good result or a bad result, if you do this, you can still make real contributions to your research field, which is worth more than results that no one can replicate or are not realistic.

- **Working with data:** This is something that should not be underestimated, and can be misleading. While we often work with physical modeling, where output is always as expected, this is not the case for data-driven models. Not only does it require a lot of work to clean a dataset and get everything working as supposed, results that are supposed to be found are not always visible right away. Everyone can expect some of the standard hurdles when it comes to data science and handling larger datasets, and enough time should be saved to reach the desired goals. Personally, I learned a lot from a data science oriented project. I did underestimate parts of it, and sometimes had to make big changes to get things working or stay on track. It was also realized that especially data-driven modeling, is very different than what I was used to as a marine engineer. You start almost from scratch again, and I even had trouble just reading papers, as I was not used to the language and terms used throughout. In this case its very helpful to ask for advice. The latter I did not do in the beginning, but having this certainly helps to make improvements and do things as they are supposed to be done.

- **Being on top of your project:** Yes it is your own project, so you are in charge and in the lead during the project. However, this is not the reason that I wrote this. Being on top of your project, together with its planning, communication, and work, gave me an overall good feeling. Being aware of when meetings should be planned, being in the lead with your project and on time, taking responsibility overall, gives yourself a good and confident feeling. On the contrary, I also found that when I was lacking with something, or when I did not know things, this was a less nice experience. With this I found that being actively involved costs energy, but also feels more rewarding. Even planning the next meeting with your thesis or company supervisor or making a presentation and preparing questions, can sometimes be a way more simple task than your research, but with a lot more satisfaction.

- **TU Delft repository:** I found using the TU Delft repository to be very helpful. You can access all other work by students and each thesis before you. Look at different projects to get inspiration and a general sense of what is expected. With each supervisor having a slightly different view of what is desired in a thesis, it also really helps to look at projects of students that were also supervised by the same person as you. I found that recommendations given to me where often already given to others, and this just safes a lot of work and thinking for both you and your supervisor. Not only is the repository useful for your final thesis, it is also a great support for your literature study, as each persons first chapters or part of the thesis still contain the work done in the literature study. Overall, seeing what is expected and the way its done saves time and is of great help.

Concluding I really enjoyed the thesis project and learned a lot, but was also relieved when at the end, which I hope and think is normal. For the people that read this, I hope my experience and recommendations are helpful to you, and good luck with your own project.

Bibliography

26th ITTC Specialist Committee on Uncertainty Analysis. (2011). Fresh Water and Seawater Properties. *ITTC - Recommended Procedures*.

Abarzua, S., & Jakubowski, S. (1995). Biotechnological investigation for the prevention of biofouling. i. biological and biochemical principles for the prevention of biofouling. *Marine Ecology-progress Series - MAR ECOL-PROGR SER*, *123*, 301–312. https://doi.org/10.3354/meps123301

ABS. (2011). *Fall 2011* (Surveyor, Ed.). Retrieved May 25, 2022, from http://www.eagle.org/eagleExternalPortalWEB/ShowProperty / BEA % 5C % 20Repository / News % 5C % 20& % 5C % 20Events / Publications / Quarterly/Surveyor/2011/Surveyor_2011Fall

Aijjou, A., Bahatti, L., & Raihani, A. (2020). Wind energy for shipboard electric power needs. *International Journal*, *9*(1.5).

Akusok, A., Björk, K.-M., Miche, Y., & Lendasse, A. (2015). High-performance extreme learning machines: A complete toolbox for big data applications. *IEEE Access*, *3*, 1011–1025. https://doi.org/10.1109/ACCESS.2015.2450498

Alghamdi, S. A., & Quijada Cordova, R. A. (2019). The impact of biofouling on marine environment: A qualitative review of the current antifouling technologies.

Alzieu, C., Sanjuan, J., Deltreil, J., & Borel, M. (1986). Tin contamination in arcachon bay: Effects on oyster shell anomalies. *Marine pollution bulletin*, *17*(11), 494–498.

Anguita, D., Ghio, A., Ridella, S., & Sterpi, D. (2009). K-fold cross validation for error rate estimate in support vector machines. *DMIN*, 291–297.

ASTM D3623-78a. (2012). *Standard Test Method for Testing Antifouling Panels in Shallow Submergence*.

ASTM D6990-05. (2011). *Standard Practice for Evaluating Biofouling Resistance and Physical Performance of Marine Coating Systems*.

Atlar, M., Yeginbayeva, I., Turkmen, S., Demirel, Y., Carchen, A., Marino, A., & Williams, D. (2018). A rational approach to predicting the effect of fouling control systems on" in-service" ship performance. *GMO Journal of Ship and Marine Technology*, *24*(213), 5–36.

Atlar, M. (2008). An update on marine antifoulings. *25th ITTC Group Discussions 3–Global Warming and Impact on ITTC Activities*.

Babin, M., Roesler, C., & Cullen, J. (2008). *Real-time Coastal Observing Systems for Marine Ecosystem Dynamics and Harmful Algal Blooms: Theory, Instrumentation and Modelling*.

Bakker, M. (2021). *A Reference-based Design Approach: in Preliminary Ship Design*. Retrieved December 22, 2021, from http://resolver.tudelft.nl/uuid:3b4f713f-13f2-45c8-9fed-f3ab7e1ac8f7

Bansal, H. (2019). *AI, ML & Deep learning overview.* Retrieved January 15, 2021, from https://becominghuman.ai / how - to - get - the - perfect - start - in - ai - ml - as - newbie - learn - the - art - in - just - 5 - mins - cba28d2705e4

Bari, S., & Hossain, S. N. (2013). Waste heat recovery from a diesel engine using shell and tube heat exchanger. *Applied Thermal Engineering*, *61*(2), 355–363.

Benner, J. (2020). *Cross-Validation and Hyperparameter Tuning: How to Optimise your Machine Learning Model*. Retrieved May 30, 2022, from https://towardsdatascience.com/cross-validation-and-hyperparameter-tuning-how-to-optimise-your-machine-learning-model-13f005af9d7d

Boat International. (2022). *Feadship Yachts*. Retrieved December 17, 2021, from https://www.boatinternational.com/profiles/feadship--21859

Braun-Blanquet, J. et al. (1932). Plant sociology. the study of plant communities. *Plant sociology. The study of plant communities. First ed.*

Bressy, C., & Lejars, M. (2014). Marine fouling : An overview. *Journal of Ocean Technology*, *9*, 19–28.

Burger, R. (2017). *Improving the Predictions of Ship Speed and Fuel Consumption for Heavy Lift Vessels*. Retrieved April 20, 2022, from http://resolver.tudelft.nl/uuid:dd79c53c-9e9f-44f9-8d71-f981eba12798

Calder, N. (1992). *Marine diesel engines: Maintenance, troubleshooting, and repair*. International Marine.

Castro, M. C. (2013). *International Maritime Organization (IMO) for the Control and Management of Ship's Biofouling to Minimize the Transfer of Invasive Aquatic Species*.

Caterpillar. (2022a). *Commercial Propulsion Engines - 3516C IMO II*. Retrieved June 14, 2022, from https://www.cat.com/en_US/products/new/power-systems/marine-power-systems/commercial-propulsion-engines/18408926.html#

Caterpillar. (2022b). *Operation & Maintenance Manual - 3516 High Output Marine Engine*. Retrieved June 18, 2022, from https://catpublications.com/

Chambers, L., Stokes, K., Walsh, F., & Wood, R. (2006). Modern approaches to marine antifouling coatings. *Surface and Coatings Technology*, *201*, 3642–3652. https://doi.org/10.1016/j.surfcoat.2006.08.129

Chauvenet, W. (1863). Manual of spherical and practical astronomy ii, 4.

Coraddu, A., Oneto, L., Baldi, F., & Anguita, D. (2015). Ship efficiency forecast based on sensors data collection: Improving numerical models through data analytics. *OCEANS 2015-Genova*, 1–10.

Coraddu, A., Oneto, L., Baldi, F., Cipollini, F., Atlar, M., & Savio, s. (2019). Data-driven ship digital twin for estimating the speed loss caused by the marine fouling. *Ocean Engineering*, *186*, 106063. https://doi.org/10.1016/j.oceaneng.2019.05.045

Da Silva, I. N., Spatti, D. H., Flauzino, R. A., Liboni, L. H. B., & dos Reis Alves, S. F. (2017). Artificial neural networks. *Cham: Springer International Publishing*, *39*.

Delft University of Technology. (2022). *Library*. Retrieved September 26, 2021, from https://www.tudelft.nl/library

Demirel, Y., Khorasanchi, M., Turan, O., & Incecik, A. (2013). On the importance of antifouling coatings regarding ship resistance and powering. *3rd International Conference on Technologies, Operations, Logistics and Modelling for Low Carbon Shipping*.

Demirel, Y., Khorasanchi, M., Turan, O., Incecik, A., & Schultz, M. (2014). A CFD model for the frictional resistance prediction of antifouling coatings. *Ocean Engineering*, *89*, 21–31. https://doi.org/10.1016/j.oceaneng.2014.07.017

Demirel, Y., Song, S., Turan, O., & Incecik, A. (2019). Practical added resistance diagrams to predict fouling impact on ship performance. *Ocean Engineering*, *186*. https://doi.org/10.1016/j.oceaneng.2019.106112

Demirel, Y., Turan, O., & Incecik, A. (2017). Predicting the effect of biofouling on ship resistance using CFD. *Applied Ocean Research*, *62*, 100–118. https://doi.org/10.1016/j.apor.2016.12.003

Deng, W., Zheng, Q., & Chen, L. (2009). Regularized extreme learning machine. *2009 IEEE symposium on computational intelligence and data mining*, 389–395.

Evans, J. (2009). Basic design concepts. *Journal of the American Society for Naval Engineers*, *71*, 671–678. https://doi.org/10.1111/j.1559-3584.1959.tb01836.x

Farkas, A., Degiuli, N., & Martić, I. (2018). Towards the prediction of the effect of biofilm on the ship resistance using cfd. *Ocean Engineering*, *167*, 169–186. https://doi.org/https://doi.org/10.1016/j.oceaneng.2018.08.055

Farkas, A., Degiuli, N., & Martić, I. (2020a). The impact of biofouling on the propeller performance. *Ocean Engineering*, *219*, 108376. https://doi.org/10.1016/j.oceaneng.2020.108376

Farkas, A., Degiuli, N., Martić, I., & Ančić, I. (2020b). Performance prediction method for fouled surfaces. *Applied Ocean Research*, *99*. https://doi.org/10.1016/j.apor.2020.102151

Feadship. (2015). *Savannah*. Retrieved December 13, 2021, from https://www.feadship.nl/fleet/savannah

Feadship. (2020). *Moonrise*. Retrieved December 13, 2021, from https://www.feadship.nl/fleet/moonrise

Feadship. (2021a). *Feadship Royal Dutch Shipyards*. Retrieved December 7, 2021, from https://www.feadship.nl/

Feadship. (2021b). *Viva*. Retrieved December 13, 2021, from https://www.feadship.nl/fleet/viva

Fleet Cleaner. (2022). *Keep your fleet clean without operational impact using safe and sustainable robot technology*. Retrieved May 28, 2022, from https://www.fleetcleaner.com/

Flemming, H.-C., Murthy, S., Venkatesan, R., & Cooksey, K. (2009). *Marine and industrial biofouling*. https://doi.org/10.1007/978-3-540-69796-1

Gibbs, P., & Bryan, G. (1986). Reproductive failure in populations of the dog-whelk, nucella lapillus, caused by imposex induced by tributyltin from antifouling paints. *Journal of the Marine Biological Association of the United Kingdom*, *66*(4), 767–777.

Google. (2022). *Scholar*. Retrieved September 26, 2021, from https://scholar.google.nl

Granville, P. S. (1987). Three Indirect Methods for the Drag Characterization of Arbitrarily Rough Surfaces on Flat Plates. *Journal of Ship Research*, *31*(01), 70–77. https://doi.org/10.5957/jsr.1987.31.1.70

Grin, R. (2015). On the prediction of wave-added resistance with empirical methods. *Journal of Ship Production and Design*, *31*(03), 181–191.

Hasselmann, K., Barnett, T. P., Bouws, E., Carlson, H., Cartwright, D. E., Enke, K., Ewing, J., Gienapp, A., Hasselmann, D., Kruseman, P., et al. (1973). Measurements of wind-wave growth and swell decay during the joint north sea wave project (jonswap). *Ergaenzungsheft zur Deutschen Hydrographischen Zeitschrift, Reihe A*.

Heaton, J. (2015). *Artificial Intelligence for Humans, Vol 3: Neural Networks and Deep Learning*.

Hempel. (2022). *Hempaguard X7*. Retrieved June 19, 2022, from https://www.hempel.com/en-us/products/brand/hempaguard/hempaguard-x7

Hjorth, U., & Hjort, U. (1982). Model selection and forward validation. *Scandinavian Journal of Statistics*, 95–105.

Huang, G.-B. (2014). An insight into extreme learning machines: Random neurons, random features and kernels. *Cognitive Computation*, *6*(3), 376–390.

Huang, G.-B. (2015). What are extreme learning machines? filling the gap between frank rosenblatt's dream and john von neumann's puzzle. *Cognitive Computation*, *7*(3), 263–278.

Huang, G.-B., Zhu, Q.-Y., & Siew, C.-K. (2006). Extreme learning machine: Theory and applications. *Neurocomputing*, *70*(1-3), 489–501.

HullWiper. (2022). *Revolutionising Underwater Hull Cleaning*. Retrieved December 16, 2021, from https://www.hullwiper.co/

IBM Cloud Education. (2020). *What is deep learning?* Retrieved January 16, 2021, from https://www.ibm.com/cloud/learn/deep-learning#:~:text=Deep%5C%20learning%5C%20is%5C%20a%5C%20subset,from%5C%20large%5C%20amounts%5C%20of%5C%20data.

IMO, I. (2001). International convention on the control of harmful anti-fouling systems on ships. *Entry into force: 17 September 2008, AFS/CONF/26*.

Institution, W. H. O., & of Ships, U. S. N. D. B. (1952). *Marine fouling and its prevention*. United States Naval Institute.

International Marine. (2022a). *Biocidal Antifoulings*. Retrieved June 19, 2022, from https://www.international-marine.com/in-focus/antifouling

International Marine. (2022b). *Foul Release*. Retrieved June 19, 2022, from https://www.international-marine.com/in-focus/foul-release-coatings

International Marine. (2022c). *The industry's most environmentally sustainable hull management package*. Retrieved December 16, 2021, from https://www.international-marine.com/

ISO 19030-2. (2016). *Ships and Marine Technology Measurement of Changes in Hull and Propeller Performance - Part 2: Default Method*. International Organization for Standardization.

ITTC. (2011). Recommended Procedures and Guideline Practical Guidelines for Ship CFD Applications. *ITTC - Recommended Procedures and Guidelines*.

ITTC. (2014). Analysis of Speed/Power Trial Data. *ITTC - Recommended Procedures and Guidelines*.

Jotun. (2022). *Jotun HPS*. Retrieved June 19, 2022, from https://www.jotun.com/ww-en/industries/news-and-stories/news/regulatory-and-commercial-advantage-easily-unlocked-for-owners-with-the-right-antifouling-says-jotun/

Kanninen, P., Peltonen, P., & Vuorinen, V. (2022). Full-scale ship stern wave with the modelled and resolved turbulence including the hull roughness effect. *Ocean Engineering*, *245*, 110434.

Kasun, L. L. C., Zhou, H., Huang, G.-B., & Vong, C. M. (2013). Representational learning with elms for big data.

Kjær, L., Pigosso, D., McAloone, T., & Birkved, M. (2018). Guidelines for evaluating the environmental performance of product/service-systems through life cycle assessment. *Journal of Cleaner Production*, *190*. https://doi.org/10.1016/j.jclepro.2018.04.108

Klein Woud, H., & Stapersma, D. (2002). *Propulsion and Electric Power Generation Systems*. The Institute of Marine Engineering, Science; Technology.

Kohavi, R. et al. (1995). A study of cross-validation and bootstrap for accuracy estimation and model selection. *Ijcai*, *14*(2), 1137–1145.

Korkut, E. (2012). An experimental investigation of the effect of foul release coating application on performance, noise and cavitation characteristics of marine propellers. *Ocean Engineering*, *41*. https://doi.org/10.1016/j.oceaneng.2011.12.012

Lam, J. S. L., & Lai, K.-h. (2015). Developing environmental sustainability by anp-qfd approach: The case of shipping operations. *Journal of Cleaner Production*, *105*, 275–284. https://doi.org/10.1016/j.jclepro.2014.09.070

Leifsson, L., Sævarsdóttir, H., Sigurdsson, S., & Vésteinsson, A. (2008). Grey-box modeling of an ocean vessel for operational optimization. *Simulation Modelling Practice and Theory*, *16*, 923–932. https://doi.org/10.1016/j.simpat.2008.03.006

Letschert, M. (2020). *A Process Design Towards the Yacht Environmental Transparency Index*. Retrieved December 10, 2021, from http://resolver.tudelft.nl/uuid:e49b703f-07ab-4d9d-8ce5-dee5150ef016

Lindstad, H., Verbeek, R., Blok, M., van Zyl, S., Hübscher, A., Kramer, H., Purwanto, J., Ivanova, O., & Boonman, H. (2015). GHG emission reduction potential of EU-related maritime transport and on its impacts. *TNO*.

Marine Travelift. (2022). *Yacht in 1000MT Marine Travelift*. Retrieved December 7, 2021, from https://www.marinetravelift.com/

Mavris, D., & DeLaurentis, D. (2000). Methodology for examining the simultaneous impact of requirements, vehicle characteristics, and technologies on military aircraft design.

MEPC. (2018). *Meeting Summary of the Marine Environment Protection Committee (MEPC), 72nd Session*. Maritime Environmental Protection Committee (MEPC), Part of the Internation Maritime Organization (IMO), London, United Kingdom.

Morrisey, D., & Woods, C. (2015). *In-water cleaning technologies: Review of information*.

Odendaal, K. (2021). *Enhancing early-stage energy consumption predictions using dynamic operational voyage data*. Retrieved December 20, 2021, from http://resolver.tudelft.nl/uuid:949882f3-60c4-484b-8268-40ce38f43830

Okay, O. (2004). Antifouling içeren gemi boyalarının uluslararası kurallar çerçevesinde kirletici etkilerinin incelenmesi. *Gemi Mühendisliği ve Sanayimiz Sempozyumu*, 24–25.

Oliveira, D., & Granhag, L. (2016). Matching forces applied in underwater hull cleaning with adhesion strength of marine organisms. *Journal of Marine Science and Engineering*, *4*(4), 66.

Oliveira, D., Larsson, A. I., & Granhag, L. (2018). Effect of ship hull form on the resistance penalty from biofouling. *Biofouling*, *34*(3), 262–272.

Oneto, L. (2018). Model selection and error estimation without the agonizing pain. *Wiley Interdisciplinary Reviews: Data Mining and Knowledge Discovery*, *8*(4), e1252.

Owen, D., Demirel, Y., Oguz, E., Tezdogan, T., & Incecik, A. (2018). Investigating the effect of biofouling on propeller characteristics using cfd. *Ocean Engineering*, *159*. https://doi.org/10.1016/j.oceaneng.2018.01.087

Parkes, A., Sobey, A., & Hudson, D. (2018). Physics-based shaft power prediction for large merchant ships using neural networks. *Ocean Engineering*, *166*. https://doi.org/10.1016/j.oceaneng.2018.07.060

Pedersen, B., & Larsen, J. (2009). Prediction of full-scale propulsion power using artificial neural networks. *COMPIT '09*, 537–550.

Petersen, J. P., Jacobsen, D. J., & Winther, O. (2012). Statistical modelling for ship propulsion efficiency. *Journal of marine science and technology*, *17*(1), 30–39.

Pielke, R. A. (2012). Sea Surface Temperature Trends as a Function of Latitiude Bands by Roger A. Pielke Sr. and Bob Tisdale. *Climate Science*.

Pierson Jr, W. J., & Moskowitz, L. (1964). A proposed spectral form for fully developed wind seas based on the similarity theory of sa kitaigorodskii. *Journal of geophysical research*, *69*(24), 5181–5190.

Propulsion Committee of the 27th ITTC. (2014). 1978 ITTC Performance Prediction Method. *ITTC - Recommended Procedures and Guidelines*.

Propulsion Committee of the 28th ITTC. (2017). 1978 ITTC Performance Prediction Method. *ITTC - Recommended Procedures and Guidelines*.

Radhakrishna Rao, C., & Mitra, S. K. (1972). Generalized inverse of a matrix and its applications. *Proceedings of the Berkeley Symposium on Mathematical Statistics and Probability*, *1*, 601–620.

Ridella, S., Rovetta, S., & Zunino, R. (1997). Circular backpropagation networks for classification. *IEEE transactions on neural networks*, *8*(1), 84–97.

Rumelhart, D. E., Hinton, G. E., & Williams, R. J. (1986). Learning representations by back-propagating errors. *nature*, *323*(6088), 533–536.

Sargent, R. G. (2010). Verification and validation of simulation models. *Proceedings of the 2010 winter simulation conference*, 166–183.

Schultz, M. (2007). Effects of coating roughness and biofouling on ship resistance and powering. *Biofouling*, *23*, 331–41. https://doi.org/10.1080/08927010701461974

Ship & Bunker. (2022). *World Bunker Prices - MGO*. Retrieved June 1, 2022, from https://shipandbunker.com/prices#MGO

Shrivastava, S. (2020). *Cross Validation in Time Series*. Retrieved May 18, 2022, from https://medium.com/@soumyachess1496/cross-validation-in-time-series-566ae4981ce4

Song, S., Demirel, Y., & Atlar, M. (2020a). Penalty of hull and propeller fouling on ship self-propulsion performance. *Applied Ocean Research*, *94*. https://doi.org/10.1016/j.apor.2019.102006

Song, S., Demirel, Y., De Marco, C., Tezdogan, T., & Atlar, M. (2020b). Fouling effect on the resistance of different ship types. *Ocean Engineering*, *216*, 107736. https://doi.org/10.1016/j.oceaneng.2020.107736

Stapersma, D. (2022). *Diesel Engines Volume 1 Performance Analysis, Lecture notes MT44100 (Internal Combustion Engines A)*. Retrieved June 14, 2022, from https://onlinereaders.tudelft.nl/index.php?orderableObject=301077

Stevens, E. (1937). The increase in frictional resistance due to the action of water on bottom paint. *Journal of the American Society of Naval Engineers*, *49*(4), 585–588.

Sui, C., de Vos, P., Stapersma, D., Visser, K., & Ding, Y. (2020). Fuel consumption and emissions of ocean-going cargo ship with hybrid propulsion and different fuels over voyage. *Journal of Marine Science and Engineering*, *8*, 588. https://doi.org/10.3390/jmse8080588

Superyacht Times. (2022). *100m+ Yachts Worldwide*. Retrieved December 13, 2021, from https://www.superyachttimes.com/yachts/100m+

SuperyachtNews. (2019). *Discovering the YETI*. Retrieved December 10, 2021, from https://www.superyachtnews.com/fleet/discovering-the-yeti

Taylan, M. (2010). An overview: Effect of roughness and coatings on ship resistance. *Internatonal Conference on Ship Drag Reduction*, 20–21.

Tissera, M. D., & McDonnell, M. D. (2016). Deep extreme learning machines: Supervised autoencoding architecture for classification. *Neurocomputing*, *174*, 42–49.

Townsin, R. (2003). The ship hull fouling penalty. *Biofouling*, *19*(S1), 9–15.

United Nations. (2016). *Decisions Adopted by the Conference of the Parties: Adoption of the Paris Agreement.* Framework Convention on Climate Change.

United States Naval Academy. (2022). *Principles of Ship Performance*. Retrieved April 13, 2022, from https://www.usna.edu/NAOE/academics/en400.php

Uzun, D., Demirel, Y., Coraddu, A., & Turan, O. (2019). Time-dependent biofouling growth model for predicting the effects of biofouling on ship resistance and powering. *Ocean Engineering*, *191*. https://doi.org/10.1016/j.oceaneng.2019.106432

van der Bos, J. (2021). *Towards energy efficient shipping*. Retrieved April 20, 2022, from http://resolver.tudelft.nl/uuid:4d0ae29f-3534-420e-91c5-88d12574451f

Van Rompay, B. (2012). Surface treated composites white book. *Hokapress* (pp. 243–262).

Yang, L., Chen, G., Rytter, N. G. M., Zhao, J., & Yang, D. (2019). A genetic algorithm-based grey-box model for ship fuel consumption prediction towards sustainable shipping. *Annals of Operations Research*, 1–27.

Yebra, D., Kiil, S., & Dam-Johansen, K. (2004). Antifouling technology - past, present and future steps towards efficient and environmentally friendly antifouling coatings. *Progress in Organic Coatings*, *50*, 75–104. https://doi.org/10.1016/j.porgcoat.2003.06.001

Yeginbayeva, I., & Atlar, M. (2018). An experimental investigation into the surface and hydrodynamic characteristics of marine coatings with mimicked hull roughness ranges. *Biofouling*, *34*(9), 1001–1019.

Zwart, R. (2020). *Trim optimization for ships in service: A grey-box model approach using operational voyage data*. Retrieved December 22, 2021, from http://resolver.tudelft.nl/uuid:599cfbd1-489f-406f-8ddf-64416fd7a53b

A
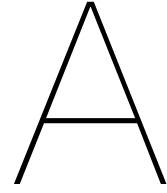
Marine Biofouling Growth

In this chapter, the model by Uzun et al. (2019) is explained in detail. To get an overview of where the model fits in the full methodology, chapter 4 can be reviewed. In section A.1, the fouling rating is explained. Next, in section A.2, the calcareous surface coverage is determined. Based on both, the equivalent sand roughness height is computed in section A.3. Last, in section A.4, the relevant biofouling growth curves are displayed.

A.1. Fouling Rating

In Equation A.1, the formula for the fouling rating is shown, where FR is the rated biofouling growth, a is the maximum rating, t is the sum of idle time, t_0 is the time that rating reaches to the maximum point and τ is the half-width of the bell curve (Uzun et al., 2019). Here, the authors mention that t_0 and τ are taken as coating performance parameters. In Table A.1, the variables used to compute the fouling rating are presented. It can be noted that in the method exploration (subsection 3.1.1), the calcareous fouling rating curves for the Mediterranean and the Equator were shown. An overview of all marine biofouling time-dependent curves can be found in section A.4

$$FR = ae^{\left[-\left(\frac{t-t_0}{\tau}\right)^2\right]}$$

(A.1)

Type of fouling	Location	t_0	τ	a
Calcareous fouling	Equatorial	379.4	187.2	100
	Mediterranean	726.4	129.7	100
Non-shell organisms	Equatorial	271.4	73.11	50
	Mediterranean	383.5	124.4	50
Slime	Equatorial	87	37.08	20
	Mediterranean	271.9	99.31	20

Table A.1: Antifouling coating performance parameters for each type of fouling (Uzun et al., 2019).

With the functions above, the fouling rating for a single anchorage can be computed. By repeating this process for each time and region, the accumulative fouling rating over a period of operation can be written as given below in Equation A.2. Note that interpolation and extrapolation can be used to find fouling growth in regions other than the Equator and Mediterranean, as explained in section 4.2.

$$FR_{tot} = \sum_{i=0}^{n} \left(\frac{\partial FR}{\partial t}\right)_i t_i + \left(\frac{\partial FR}{\partial t}\right)_{i+1} t_{i+1} + \left(\frac{\partial FR}{\partial t}\right)_n t_n$$

(A.2)

A.2. Surface Coverage

For the calculation of the surface coverage, Uzun and others propose a logistic growth model to predict calcareous type fouling surface coverage (SC) as a function of time, as shown in Equation A.4. The logistic function curves were fitted on field test data with help of logistic curve constants. In Table A.2, the constants for both the Equator

and Mediterranean region are presented. The accumulative surface coverage can be computed with a similar equation as the accumulative fouling rating over time, as shown in Equation A.3.

$$SC_{tot} = \sum_{i=0}^{n} \left(\frac{\partial SC}{\partial t} \right)_i t_i + \left(\frac{\partial SC}{\partial t} \right)_{i+1} t_{i+1} + \left(\frac{\partial SC}{\partial t} \right)_n t_n \tag{A.3}$$

$$SC = \frac{P - p}{1 + (exp^{b - ct})} + \frac{d}{1 + (exp^{f - gt})} \tag{A.4}$$

Constant	Equator	Mediterranean
P	100	0.00517
b	16	10
c	0.0407	40
d	3.5	50
f	10.32	32.81
g	0.7759	0.04715
p	3.101	0

Table A.2: Constants for calcareous surface coverage logistic curves (Uzun et al., 2019).

A.3. Equivalent Sand Roughness Height

As a last step of the marine biofouling determination, the equivalent sand roughness height will be computed. This parameter will be determined in micrometers, and represents the roughness thickness present on the ship surface. The equivalent sand roughness height is often used in marine biofouling studies to quantify the biofouling present on the ship, and translate this to added hull roughness.

When the total calcareous surface coverage (SC_{tot}) is below or equal to 5%, the equivalent sand roughness height (k_s) is determined with help of the total fouling rating (FR_{tot}) with Equation A.5. Calcareous surface coverage becomes the dominant parameter when this value is above 5%, in which case k_s will be determined with help of function Equation A.6. Last, it can be seen that with this a gap can be present between a fouling rating of 70 and surface coverage of 5%. section 4.2 can be consulted for a suggested interpolation of results in between both curves.

$$k_s(t) = \begin{cases} 0.007143 FR_{tot}^2 + 13.36 FR_{tot} + 30 & \text{if } 0 < FR_{tot} \leq 70 \\ 30 & \text{if } FR_{tot} = 0 \end{cases} \tag{A.5}$$

$$k_s(t) = \begin{cases} 2.4669 SC_{tot}^2 - 24.84 SC_{tot} + 1065.7 & \text{if } 5 < SC_{tot} \leq 50 \\ 80 SC_{tot} + 2000 & \text{if } 50 < SC_{tot} \leq 100 \end{cases} \tag{A.6}$$
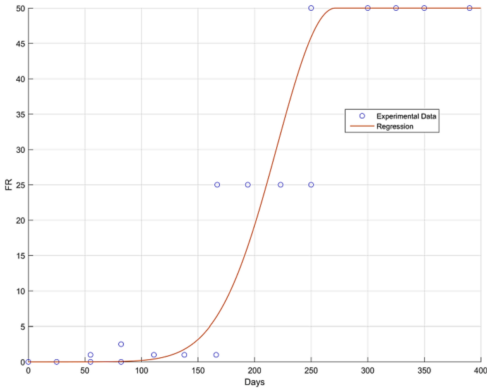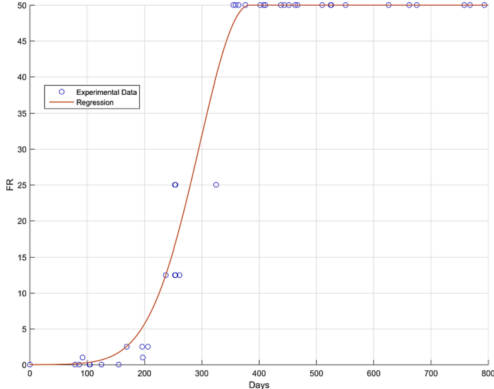
A.4. Resulting Growth Curves
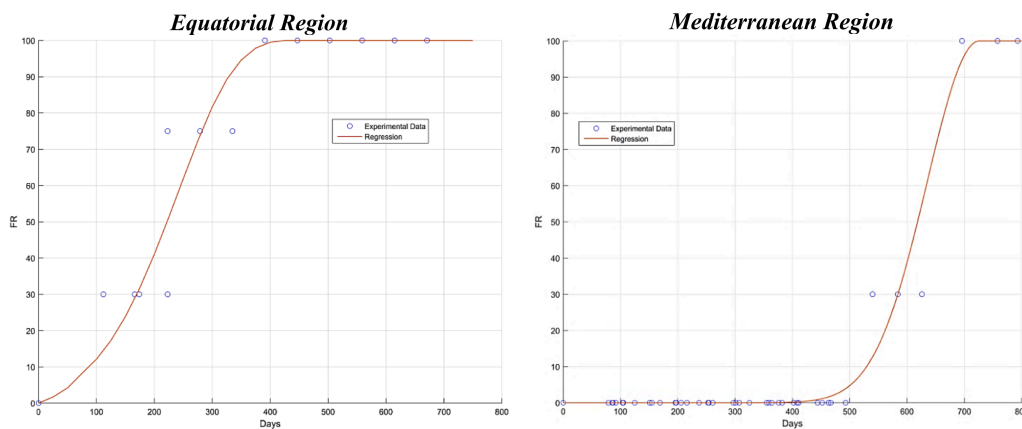
(a) Equator region.

(b) Mediterranean region.

Figure A.1: Calcareous fouling growth with a maximum fouling rating of 100.
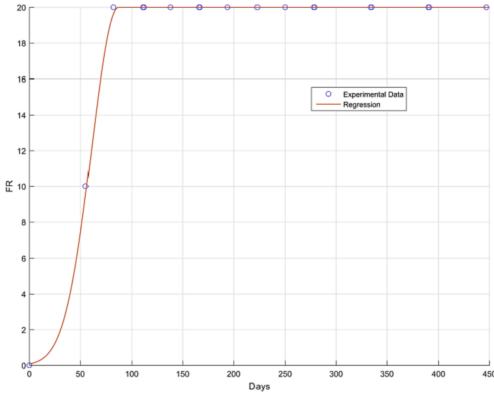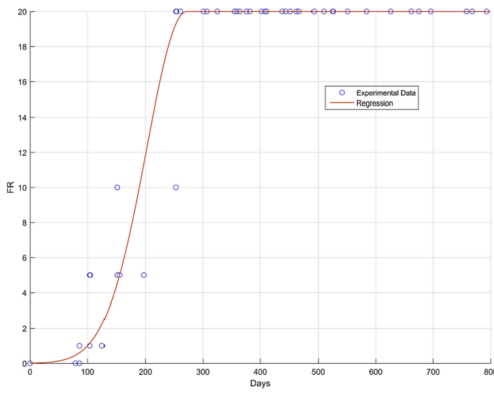
(a) Equator region.

(b) Mediterranean region.

Figure A.2: Non-shell organisms growth with a maximum fouling rating of 50.
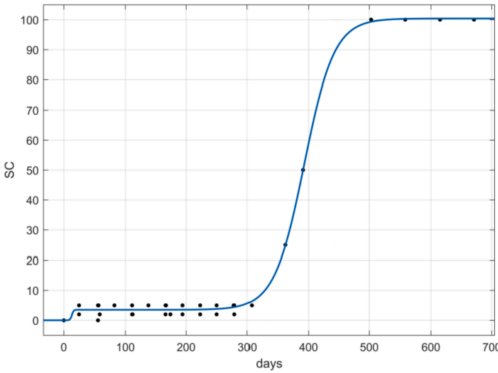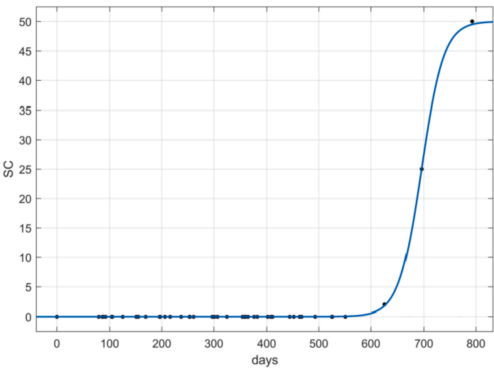

(a) Equator region.

(b) Mediterranean region.

Figure A.3: Slime growth with a maximum fouling rating of 20.

(a) Equator region.

(b) Mediterranean region.

Figure A.4: Calcareous type fouling surface coverage development.